AUBURN UNIVERSITY
Samuel Ginn College of Engineering

Final Report for ALDOT Project 931-101

EFFICIENT METHODS FOR DETERMINING SEISMIC SITE CLASS FOR ALABAMA BRIDGES

Submitted to

The Alabama Department of Transportation

Prepared by

Joshua McLeod

Chukwuma Okafor

Alok Kumar Saha

Jack Montgomery

Robert Barnes

Maria Emilia Clavijo Calderon

Final Report
MAY 2026

Highway Research Center
Harbert Engineering Center
Auburn, Alabama 36849

www.eng.auburn.edu/research/centers/hrc.html

1. Report No. 931-101	**2. Government Accession No.**	**3. Recipient Catalog No.**
4. Title and Subtitle Efficient Methods for Determining Seismic Site Class for Alabama Bridges		**5. Report Date** May 2026
		6. Performing Organization Code
7. Author(s) Joshua McLeod, Chukwuma Okafor, Alok Kumar Saha, Jack Montgomery, Robert Barnes, Maria Emilia Clavijo Calderon		**8. Performing Organization Report No.** 931-101
9. Performing Organization Name and Address Highway Research Center Department of Civil Engineering 238 Harbert Engineering Center Auburn, AL 36849		**10. Work Unit No. (TRAIS)**
		11. Contract or Grant No.
12. Sponsoring Agency Name and Address Alabama Department of Transportation 1409 Coliseum Boulevard Montgomery, AL 36130-3050		**13. Type of Report and Period Covered** Technical Report
		14. Sponsoring Agency Code

15. Supplementary Notes
Project performed in cooperation with the Alabama Department of Transportation.

16. Abstract

Shear wave velocity (V_S) profiles are critical inputs for seismic design of bridges because they influence the amplitude and frequency content of predicted ground motions. Site class, determined using the time-averaged shear wave velocity of the upper 30 meters (100 feet) of a site (V_{S30}), is used in the AASHTO Guide Specifications for LRFD Seismic Bridge Design to define seismic demand through the Seismic Design Category (SDC). This study developed a flexible and efficient approach for determining seismic site class at bridge sites in Alabama. Updated SDC maps were created for the state using the 2023 AASHTO Guide Specifications and gridded seismic hazard values from the USGS. Direct measurements of V_S were collected at 15 sites across Alabama using Multichannel Analysis of Surface Waves (MASW) and seismic refraction surveys. Passive Horizontal-to-Vertical Spectral Ratio (HVSR) measurements were also collected. The direct measurements were then used to evaluate a range of V_S and V_{S30} estimation methods, including SPT-based correlations, RQD-based correlations for rock, HVSR-based correlations, and geospatial correlations. Of the correlations evaluated, geospatial methods performed best overall. The model presented in Geyin and Maurer (2023) is recommended for general use across the state, while the model presented in Gann-Phillips et al. (2024) provided the most accurate estimates for sites within the Atlantic and Gulf Coastal Plains. SPT-based correlations tended to underpredict V_S for stiffer materials, which can lead to conservative SDC estimates and unnecessary design effort. Recommendations are provided to determine SDC, including guidance on when direct V_S measurements are likely to be beneficial.

17. Key Words Shear wave velocity; Seismic design category; Site class;		**18. Distribution Statement** No restrictions.	
19. Security Classification (of this report) Unclassified	**20. Security Classification (of this page)** Unclassified	**21. No. of Pages** 131	**22. Price** None.

Research Report

EFFICIENT METHODS FOR DETERMINING SEISMIC SITE CLASS FOR ALABAMA BRIDGES

Submitted to

The Alabama Department of Transportation

Prepared by

Joshua McLeod

Chukwuma Okafor

Alok Kumar Saha

Jack Montgomery

Robert Barnes

Maria Emilia Clavijo Calderon

Final Report
May 2026

DISCLAIMERS

Jack Montgomery, Ph.D.

Research Supervisor

ACKNOWLEDGEMENTS

Material contained herein was obtained in connection with a research project, "Efficient Methods for Determining Seismic Site Class for Alabama Bridges," ALDOT Project 931-101, conducted by the Auburn University Highway Research Center. Funding for the project was provided by the Alabama Department of Transportation (ALDOT). The funding, cooperation, and assistance of many individuals from each of these organizations are gratefully acknowledged. The authors particularly acknowledge the contributions of the following individuals for serving on the project advisory committee and assisting with the data collection and processing:

Scott George	ALDOT, Materials and Test Engineer, Montgomery
Kaye Chancellor Davis	ALDOT, Deputy State Materials and Tests Engineer, Montgomery
Bradley Williams	ALDOT, State Bridge Engineer, Montgomery
Ramy Abdalla	ALDOT, Assistant State Bridge Engineer, Montgomery
Nick Walker	ALDOT, Assistant State Bridge Engineer, Montgomery
Eric Christie	ALDOT, State Maintenance Engineer, Montgomery
Kristy Harris	FHWA
Desirae Carlton	ALDOT, Materials and Tests Bureau, Montgomery
Kwaishawn Albritton	ALDOT, Materials and Tests Bureau, Montgomery
Tim Colquett	Former ALDOT, State Bridge Engineer
Sam Sternberg	Formerly, Dan Brown and Associates and Auburn University

ABSTRACT

Shear wave velocity (V_S) profiles are critical inputs for seismic design of bridges because they influence the amplitude and frequency content of predicted ground motions. Site class, determined using the time-averaged shear wave velocity of the upper 30 meters (100 feet) of a site (V_{S30}), is used in the AASHTO Guide Specifications for LRFD Seismic Bridge Design to define seismic demand through the Seismic Design Category (SDC). This study developed a flexible and efficient approach for determining seismic site class at bridge sites in Alabama. Updated SDC maps were created for the state using the 2023 AASHTO Guide Specifications and gridded seismic hazard values from the USGS. Direct measurements of V_S were collected at 15 sites across Alabama using Multichannel Analysis of Surface Waves (MASW) and seismic refraction surveys. Passive Horizontal-to-Vertical Spectral Ratio (HVSR) measurements were also collected. The direct measurements were then used to evaluate a range of V_S and V_{S30} estimation methods, including SPT-based correlations, RQD-based correlations for rock, HVSR-based correlations, and geospatial correlations. Of the correlations evaluated, geospatial methods performed best overall. The model presented in Geyin and Maurer (2023) is recommended for general use across the state, while the model presented in Gann-Phillips et al. (2024) provided the most accurate estimates for sites within the Atlantic and Gulf Coastal Plains. SPT-based correlations tended to underpredict V_S for stiffer materials, which can lead to conservative SDC estimates and potentially unnecessary design effort. Recommendations are provided to determine SDC, including guidance on when direct V_S measurements are likely to be beneficial.

TABLE OF CONTENTS

List of Tables

List of Figures

1 INTRODUCTION

1.1 Background

Shear wave velocity (V_S) profiles (Figure 1) are critical inputs for seismic design of bridges because they influence the amplitude and frequency content of predicted ground motion (e.g., Abrahamson et al., 2008; Garofalo et al., 2016; Teague & Cox, 2016). This influence of the V_S profile at a site has been incorporated into seismic design codes through site class estimates, which act as a proxy for these local site effects. These site classes range from A to F depending on V_{S30} (average of V_S of the upper 100 ft or 30 m) with A being the stiffest rock condition and F being sites with very weak soils that require special analyses (Table 1).

V_{S30} values can be obtained from direct measurements performed at the site (i.e., using surface or borehole tests) or correlated with other in situ measurements, such as the Standard Penetration Test (SPT), Cone Penetration Test (CPT), shear strength, or other geotechnical parameters. Direct measurements of V_{S30} values are more reliable (e.g., Garofalo et al., 2016) than correlations, but in regions with relatively low seismic activity, such as Alabama, V_S testing is less common.

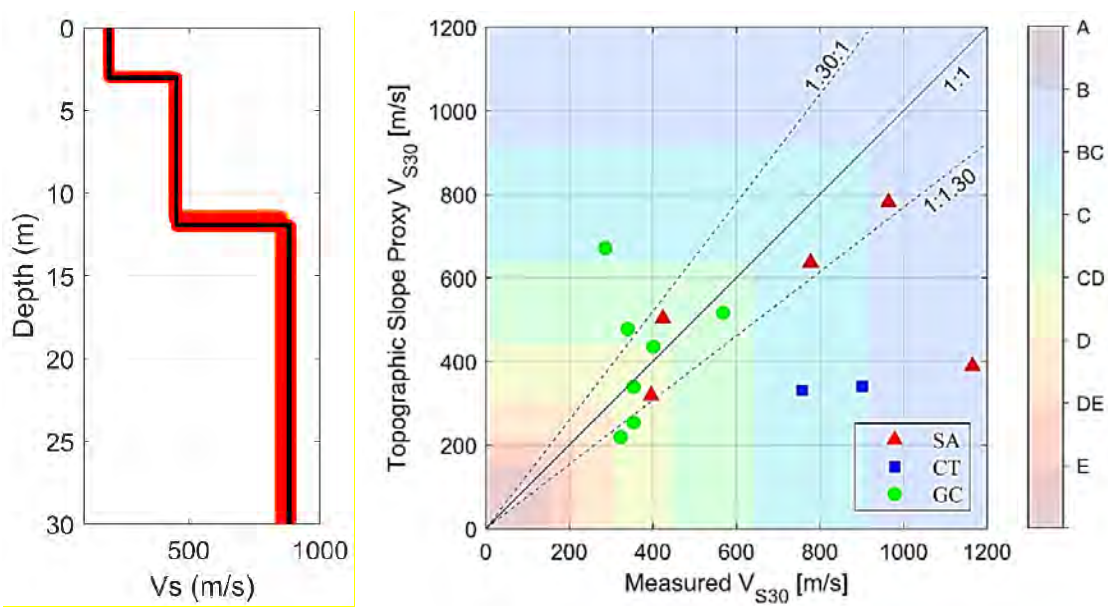

(a) (b)

Figure 1: (a) Shear wave velocity profile from a seismic station near Hartselle, Alabama and (b) comparison of V_{S30} values from a correlation with direct measurements (Carcamo, 2022). The background colors in Figure 1b indicate site class and the symbols show values from the southern Appalachan, central Tennessee, and gulf coast physiographic provinces.

Carcamo (2022) compiled a database of 15 V_{S30} profiles in Alabama as part of an Auburn University Highway Research Center (AUHRC) project. She concluded that existing correlations can provide preliminary V_{S30} estimates in Alabama, but have significant uncertainty (Figure 1) and may require updating before the correlations can be implemented for design.

The objective of this study was to create a flexible and efficient characterization approach for determining site class at bridge sites in Alabama. This study has incorporated the latest seismic hazard maps for Alabama and updated seismic design categories from the 3rd edition of the AASHTO Guide Specifications for LRFD Seismic Bridge Design (AASHTO 2023). Shear wave velocity data was collected at 15 sites across Alabama to compare with in-situ test results and other correlations in order to understand how these correlations perform in our state. These findings were then used to develop guidance to allow ALDOT engineers to differentiate between sites where correlations can be applied safely and sites where collecting direct measurements may be helpful to improve designs.

The findings from this work highlight the importance of testing correlations in the regions where they will be applied. Many of the correlations tested in this study were conservative relative to direct measurements collected at sites in Alabama. While this is likely to yield conservative design parameters, it may also result in unnecessary design effort and construction costs. The maps created in this study can help engineers and geologists identify which sites may benefit from direct

Table 1. Site class definitions (NEHRP, 2020)

Site Class	**V_{S30} (ft/s)**
A. Hard Rock	> 5,000 ft/s
B. Medium hard	3,000 ft/s to 5,000 ft/s
BC. Soft rock	2,100 ft/s to 3,000 ft/s
C. Very dense sand or hard clay	1,450 ft/s to 2,100 ft/s
CD. Dense sand or very stiff clay	1,000 ft/s to 1,450 ft/s
D. Medium dense sand or stiff clay	700 ft/s to 1,000 ft/s
DE. Loose sand or medium stiff clay	500 ft/s to 700 ft/s
E. Very loose sand or soft clay	< 500 ft/s
F. Soils requiring site response analysis	

V_S measurements. The study also found that geospatial correlations for V_{S30} perform as well as SPT-based correlations in terms of accuracy, but are simpler to apply and can be used to screen sites even before borings have been completed. Recommendations for implementing this research into current ALDOT practice are discussed. Topics related to this study that could benefit from future research are also discussed.

1.2 Project Objectives

The overall purpose of this research was to develop a flexible and efficient characterization approach for determining site class at bridge sites in Alabama. Updated seismic design category (SDC) maps were created for the state that are ready to be implemented in design practice. Correlations for estimating V_S and site class were tested, and recommendations were developed on which correlations provide the best estimates for Alabama. The study's findings were used to develop guidance for determining which bridge projects are likely to benefit from direct V_S measurements to optimize designs rather than relying on correlations. Specific objectives for this project include:

1. Evaluate current approaches to estimate site class in lower seismicity regions
2. Collect direct measurements of V_S at sites around the state.
3. Evaluate correlations for V_S and V_{S30} for use in Alabama.
4. Develop new seismic design category maps for Alabama.
5. Develop guidance for ALDOT engineers on how to estimate site class for future bridge projects

1.3 Scope of Work

The following tasks were performed to accomplish the research objectives of this project:

- Task 1: Complete a detailed review of existing practices for determining site class in other low seismicity regions in the US
- Task 2: Update maps of SDCs in Alabama considering the latest seismic hazard maps and AASHTO design procedures
- Task 3: Collect shear wave velocity profiles, along with existing geotechnical and geological information from selected bridge sites (existing and planned projects)
- Task 4: Develop correlations between shear wave velocity, site class, and geotechnical and geological data

- Task 5: Develop guidance to help ALDOT engineers select the best procedure for determining the site class based on the expected impacts on design
- Task 6: Prepare a final report documenting the characterization plan and SDC maps along with recommended training to implement the results

2 LITERATURE REVIEW

2.1 Seismic Hazard in Alabama

The eastern United States is generally considered a region of moderate seismic activity, but earthquakes still occur and can affect infrastructure. Alabama is influenced by several seismic zones, including the New Madrid and Southern Appalachian Seismic Zones (Figure 2). Most of the earthquake activity in Alabama comes from the Southern Appalachian Seismic Zone. While large earthquakes are rare, critical infrastructure like bridges must account for even potentially rare hazards.

Ground motion from earthquakes can affect bridges by inducing forces and movements in both the structure and the foundation. Seismic loading can also reduce soil strength, increase deformation, and alter the interaction between the soil and the foundation. In some cases, these conditions may lead to liquefaction, which can affect the stability and performance of bridge foundations. Therefore, it is important to consider the potential for seismic loading and strength loss when designing and evaluating bridges. The way this is considered depends on the hazard level.

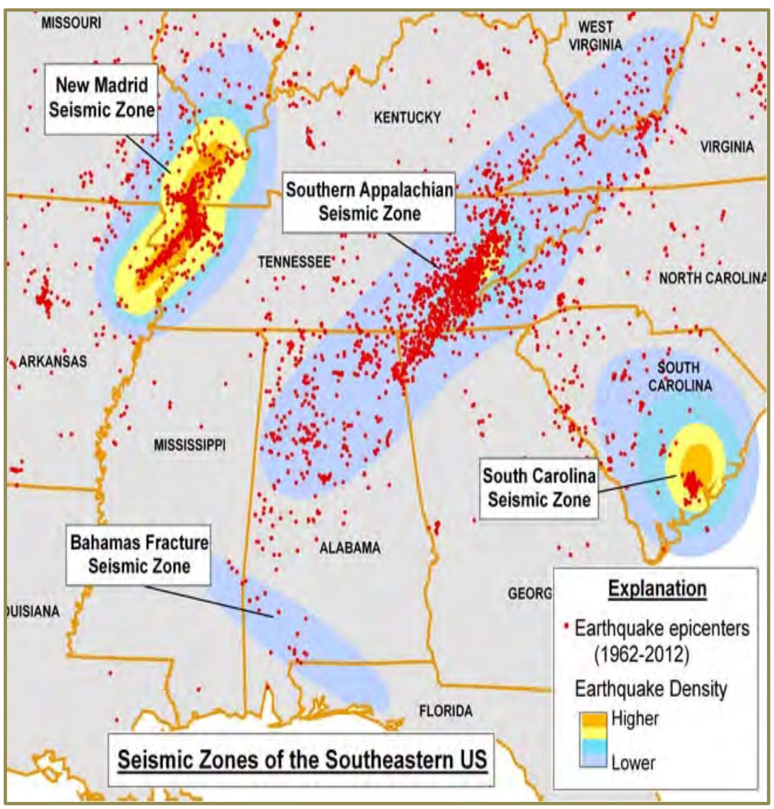

Figure 2: Seismic zones near Alabama (Source: Geological Survey of Alabama)

2.2 AASHTO Guide Specifications for Seismic Bridge Design

The latest guidance for seismic design of highway bridges in the United States is covered in the *AASHTO Guide Specifications for LRFD Seismic Bridge Design (3rd Edition, 2023)*. These specifications adopt a performance-based and displacement-based design philosophy to achieve a life-safety performance objective corresponding to a target collapse probability of approximately 1.5% in 75 years. The third edition of the guide specifications adopted risk-targeted ground motions, derived from the 2018 United States Geological Survey (USGS) National Seismic Hazard Model (NSHM), which replaced the previous uniform hazard approach. It also adopted an expanded set of site classes (Table 1) and removed previous recommendations for estimating V_{S30} from in-situ or strength data.

The level of design required for a bridge in the Guide Specifications is determined by the Seismic Design Categories (SDC). The SDC defines the hazard level at a site based on the ground motion parameter S_{D1}. S_{D1} is calculated by taking the response spectra for a given site and multiplying the period (T) by the spectra acceleration (S_a). The response spectrum depends on both location and site class, with softer sites generally exhibiting greater amplification and, consequently, higher seismic loading. S_{D1} is then defined as 90 percent of the maximum value of the product, TS_a, for periods from 1 to 2 s for sites with $V_{S30} > 1450\ ft/s$ and for periods 1 to 5 s for sites with $V_{S30} \leq 1450\ ft/s$, but not less than 100 percent of the value S_a at 1 s. The partitions of SDC are shown in Table 2 with SDC A representing the lowest hazard and SDC D representing the highest hazard.

Table 2: Partitions of Seismic Design Categories A, B, C and D

Value of S_{D1}	**SDC**
$S_{D1} < 0.15$	A
$0.15 \leq S_{D1} < 0.30$	B
$0.30 \leq S_{D1} < 0.50$	C
$0.50 \leq S_{D1}$	D

To guide the design process, the AASHTO (2023) specifications provide structured flowcharts that define the applicability of seismic design provisions and outline the required analysis procedures based on SDC and bridge characteristics. Figure 3 presents the seismic design procedure flowchart for bridges classified under SDC A and single-span bridges. In this category, seismic effects are minimum and simplified design approaches may be used. Figure 4 illustrates the seismic design procedure flowchart for bridges classified under SDC B, where seismic considerations become more significant. The flowchart provides the sequence of decisions needed to determine the appropriate analysis and design approach. This demonstrates the importance of obtaining an accurate SDC to ensure that the level of design work is consistent with the expected hazard.

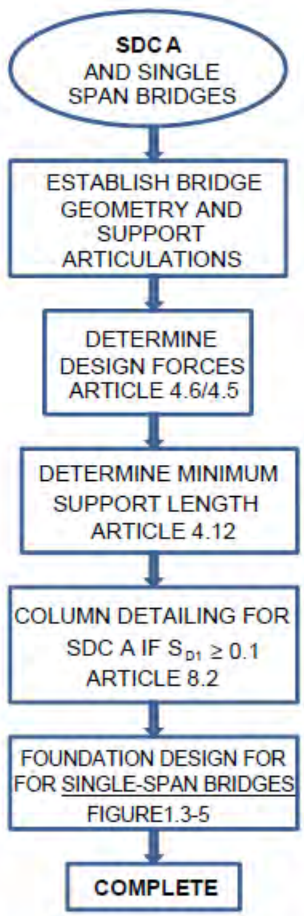

Figure 3: Seismic Design Procedure Flowchart for bridges in SDC A (AASHTO 2023)

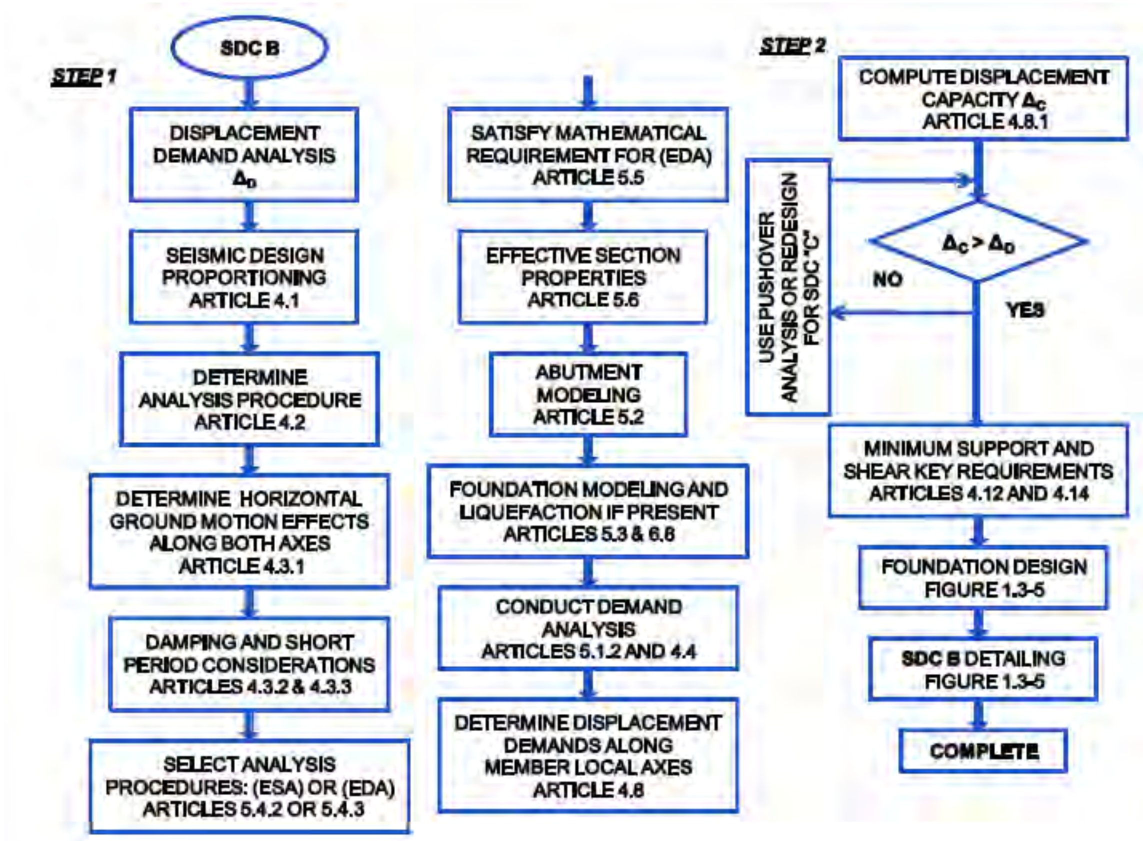

Figure 4: Seismic Design Procedure Flowchart for Bridges in SDC B (AASHTO 2023)

2.3 V_S Measurement Methods

Due to the importance of V_{S30} as input for seismic hazard analyses and site amplification, researchers worldwide have developed different techniques to estimate and measure this parameter. The studies have been performed at specific locations for site characterization and across large areas to develop V_{S30} maps for specific regions or even countries. Several methods can be used to develop V_S profiles and, therefore, to calculate V_{S30}.

2.3.1 Direct Methods

Direct methods involve taking a direct, physical measurement of V_S at a given site. Direct methods can be classified as invasive or non-invasive. Discussion of invasive and non-invasive methods is provided in the following sections of this report.

2.3.1.1 Invasive Methods

Invasive methods for measuring V_S involve placing the seismic source and/or receiver at different depths below the surface which requires either a borehole to be drilled or for some system of sensors to be placed into the ground using a penetrometer. Some examples of invasive methods for measuring V_S are borehole-based methods such as downhole logging (McDonald et al., 1958, Raikes and White 1984), cross-hole logging (Ballard, 1976, Butler and Curro, 1981), and P-S suspension logging (Kaneko et al., 1990, Ohya et al., 1984). Penetrometer-based methods include seismic cone penetrometer (Campanella et al., 1986, Robertson et al., 1986) and seismic flat plate dilatometer (Hepton, 1988).

2.3.1.2 Non-Invasive Methods

Non-invasive methods for measuring shear wave velocity are typically surface-based and do not require the use of a borehole or penetrometer. Non-invasive methods can include refraction or reflection-based methods, along with surface wave-based methods. Discussion of non-invasive methods is provided in the following sections of this report.

2.3.1.3 Seismic Refraction

Typical seismic refraction surveys for geotechnical engineering applications are conducted at the surface using a spread of geophones, a source capable of producing sufficient energy to survey the desired depth, and a computer to record data (Reynolds, 2011). Energy sources comprise of a number of devices, including blanks fired from a shotgun, a sledgehammer striking a metal plate, or a wave generator (Miller et al., 1986, 1992, 1994). Compressional or P waves generated by the energy source travel in three modes: along the ground surface in the direct wave, by reflection along the top of the refractor, and, most importantly, the critically refracted wave. Seismic refraction surveys rely on the assumption that velocity increases with depth, with deeper layers of soil or rock having a higher velocity than the layer above (Green, 1974). Geophones will

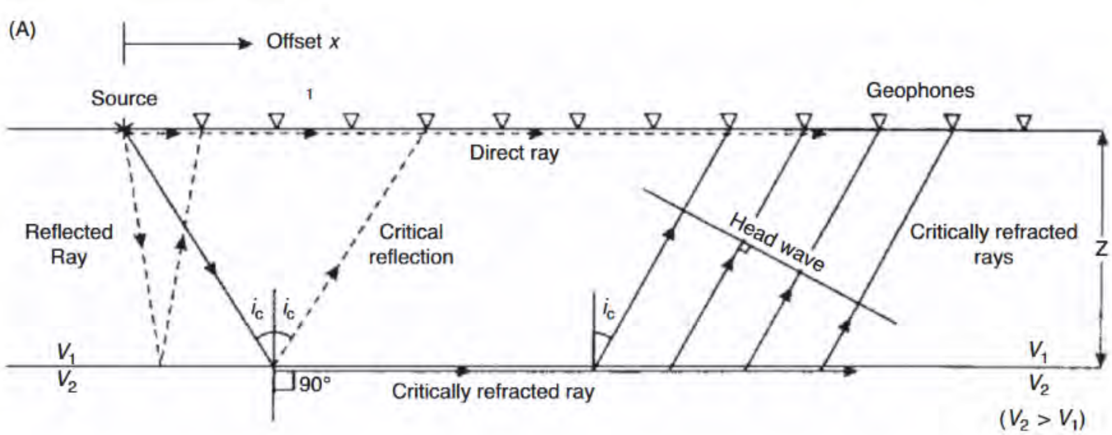

Figure 5: Diagram of typical seismic refraction survey (Reynolds, 2011)

record the first arrivals of waves, and at some distance known as the crossover distance, the critically refracted wave will arrive before the direct wave. First arrivals can be picked from geophone records, and a change in slope of the travel-time-distance curve will be observed at the crossover distance.

For typical surveys, either 24 or 48 geophones are used and are spaced evenly along the spread (Reynolds, 2011). Geophone spacing and spread length control the depth that is able to be surveyed, along with lateral resolution (Musset and Khan, 2000). Shots can be taken off either end of the spread in what is called an off-end shot, along the spread in a split-spread shot, or at the start or end of the spread in an on-end shot. Shots will typically be taken from both ends of the spread. Multiple shots are taken at each location to stack the files in post-processing to increase the signal-to-noise ratio.

2.3.1.4 Seismic Reflection

Seismic reflection surveys rely on the reflection of an incident wave at some impedance contrast at depth (Reynolds, 2011). Waves are reflected and the travel times, known as two-way travel time (TWTT), are recorded by sensors at the ground surface. At each point of incidence on the reflector in the area corresponding to the first Fresnel zone, incident waves are reflected. The point of reflection is always halfway between the source and receiver, and the spacing between reflection points is half of the geophone spacing, causing subsurface coverage to be half of the geophone spread.

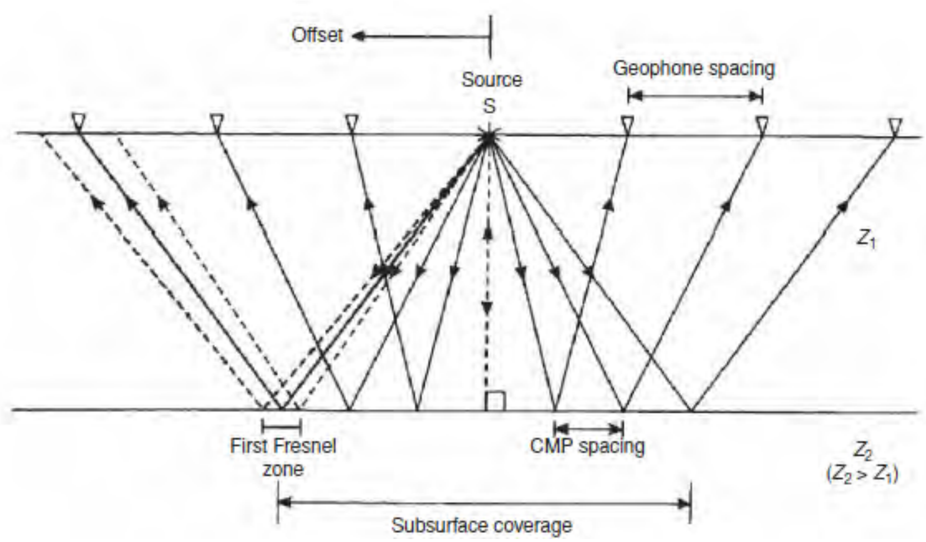

Figure 6: Diagram of typical seismic reflection survey (Reynolds 2011)

Typical reflection surveys for engineering applications use either 12, 24, or sometimes 48 geophones at the ground surface, a seismograph, and an energy source (Reynolds, 2011). Different shot locations will be selected to allow for the same point on the reflector to be measured multiple times, referred to as the fold of coverage. Traces from the same point of reflection can be gathered into a common midpoint gather (CMG) for use in interpretation of the subsurface.

2.3.1.5 Multichannel Analysis of Surface Waves

Multichannel Analysis of Surface Waves (MASW) is another common surface-based technique for measuring the V_S profile of a given site at a relatively shallow depth (Park et al., 1999). The method relies primarily on surface waves that have lower frequencies (approximately 1 to 30 Hz) and has a shallower survey depth that is dependent on site conditions and survey geometry. Either active or passive sources of waves can be used with passive wave sources having a lower frequency than active wave sources.

MASW surveys assume seismic velocities increase with depth, meaning longer wavelengths will propagate faster than shorter wavelengths as they can travel through higher velocity layers. Due to this dispersion of travel times, there is a dispersion of frequency. Dispersion curves are created by plotting frequency versus the propagation velocity. The dispersion curve with the lowest velocity is known as the fundamental mode and is used to calculate V_S profiles.

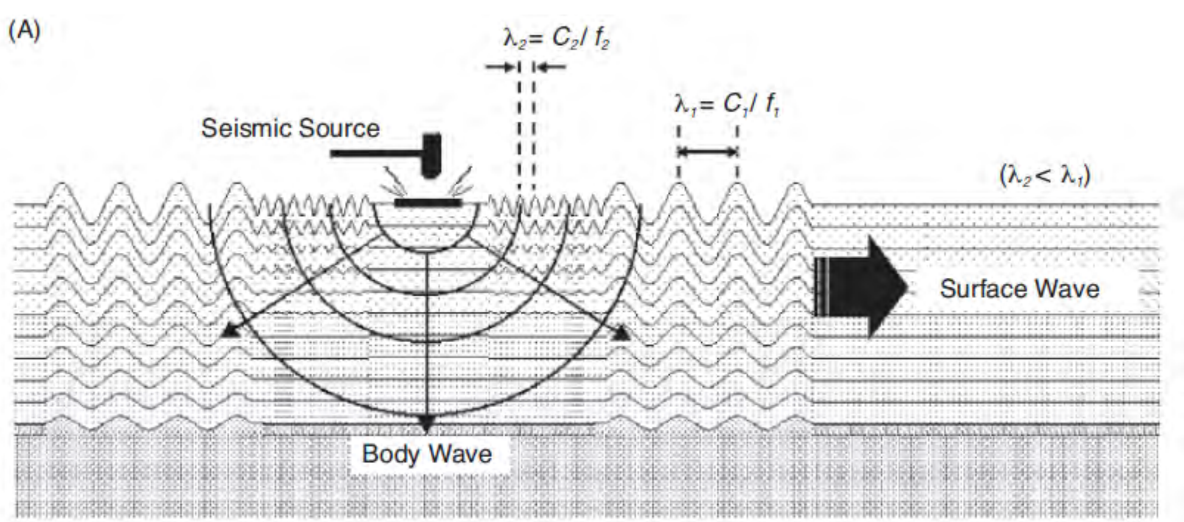

Figure 7: Diagram of typical MASW survey (Reynolds, 2011)

2.3.2 Indirect Methods

In cases where direct methods are not available, researchers have developed different approaches to estimate V_{S30} through indirect methods. Indirect methods are based on correlations between soil and/or site properties (e.g., in situ test results, amplification, fundamental frequency, geology, or topographic slope) and V_S or V_{S30} measurements available in the study area. Most of these methods were developed in active seismic regions where more V_S measurements are accessible and then expanded to other regions.

2.3.3 Correlations with SPT Data

One of the most commonly used in-situ tests for a typical geotechnical site exploration is the standard penetration test (SPT). The test method comprises of driving a split spoon sampler a total of 18 inches (0.46 m) in three increments of 6 inches (0.15 m) in a pre-drilled borehole. The number of blows required to drive the split spoon, called a blowcount, are recorded for each interval. The blowcount for the first interval is not considered as it is assumed that the soil at the bottom of the drilled borehole is very highly disturbed and not representative of the in-situ conditions of the soil. The second and third blowcounts are summed to give the "N" value for the SPT boring. Much previous work has been done to attempt to better standardize the SPT by correcting to a common percentage of energy transferred by the hammer to the drill rod (ASTM D6066). Commonly corrections are applied to 60% energy transfer from the hammer. Corrections for other factors such as rod length, borehole diameter, and effective stress can also be applied to the raw N value. Corrections are necessary for SPT blowcounts to reduce variability due to differences in equipment, site conditions, and other factors. When using a correlation to SPT blowcounts it is important to consider the correction factors applied to the blowcounts used to create the correlation. Wair et al. (2012) presented guidelines for estimating shear wave velocity profiles from the results of common in-situ tests. The authors provide multiple references to correlations between V_S and SPT blowcounts dating back to 1978 and provide guidance for which correlations to use. The references presented in this report are discussed in the following section as well as the recommendations presented in the report. Additional correlations are presented in the following sections with discussion on their possible validity for use in Alabama.

2.3.3.1 Ohta and Goto (1978)

Ohta and Goto (1978) developed empirical equations for estimation of V_S based on combinations of four index properties. Index properties considered were SPT blowcount, depth, geologic age, and soil type. Geologic ages considered by the authors were Holocene and Pleistocene. Soil type is divided into clay, fine sand, medium sand, coarse sand, sand and gravel, and gravel. Silts were placed into the clay category. SPT hammer efficiency was not reported in the original study but can be assumed to be 67% based on contemporary studies in Japan of the same era presented in Wair et al. (2012).

Using these indices, a total of 15 equations were developed using regression analysis considering every possible combination of the four selected indices. Results for the 15 proposed equations can be found in Table 3. The results indicated that the equation developed using all four indices (Figure 8) performs the best for the authors' dataset.

Table 3: Correlation coefficients and probable error for developed equations (Ohta and Goto, 1978)

Equation No.	Concerned Index	Probable Error	Correlation Coefficient
1	Soil type	36.3%	0.463
2	Geological epoch	31.5%	0.621
3	Depth	29.6%	0.670
4	Geological epoch, Soil type	28.5%	0.696
5	N-Value	27.4%	0.719
6	N-Value, Soil type	27.2%	0.726
7	Depth, Soil type	25.2%	0.765
8	Depth, Geological epoch	25.1%	0.767
9	N-Value, Geological epoch	24.2%	0.784
10	N-Value, Geological epoch, Soil type	24.0%	0.787
11	N-Value, Depth	22.1%	0.820
12	Depth, Geological epoch, Soil type	22.0%	0.822
13	N-Value, Depth, Soil type	21.5%	0.830
14	N-Value, Depth, Geological epoch	20.3%	0.848
15	N-Value, Depth, Geological Epoch, Soil type	19.7%	0.856

$V_S = 68.79N^{0.171}D^{0.199}$	1 (Alluvium)	1 (Clay/Silt)
	1.303 (Diluvium)	1.086 (Fine Sand)
		1.066 (Medium Sand)
		1.135 (Coarse Sand)
		1.153 (Sand and Gravel)
		1.448 (Gravel)

V_S in m/s, D in meters

Figure 8: Ohta and Goto (1978) proposed set of equations for V_S estimation

2.3.3.2 *Imai and Tonouchi (1982)*

Imai and Tonouchi (1982) used a large dataset of 1654 SPT blowcounts and V_S measurements in Japan to develop empirical equations for V_S. Data was collected from 386 boreholes at 250 individual sites. Correlation equations were developed that consider SPT blowcount, geologic age, and depositional environment. Similarly to Ohta and Goto (1978), hammer efficiency is not presented but can also be assumed to be 67% (Wair et al., 2012). Depositional environments considered were alluvial and man-made fill. The complete dataset along with the regression line is presented in Figure 9.

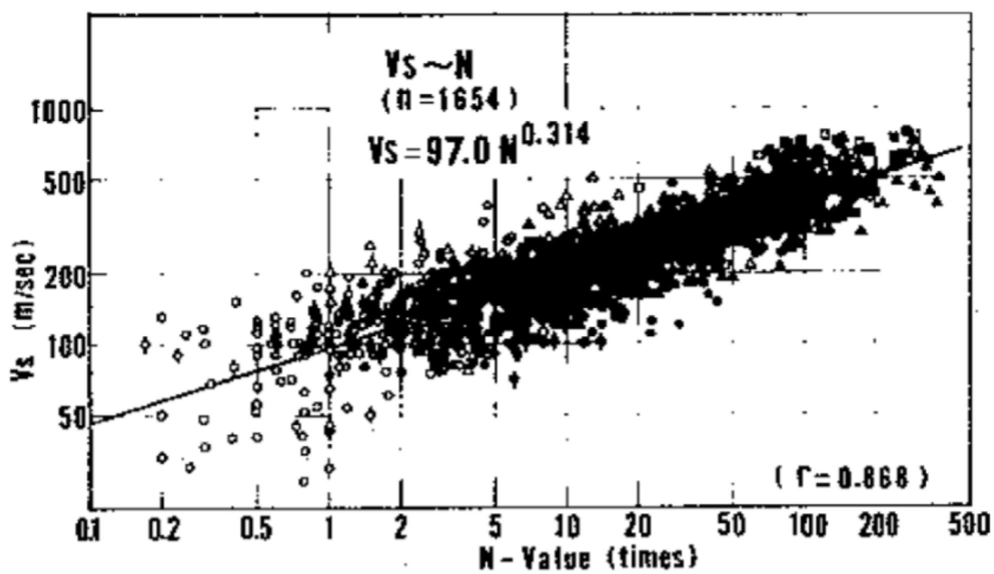

Figure 9: Complete dataset along with regression (Imai and Tonouchi, 1982)

2.3.3.3 *Seed et al. (1983)*

Seed et al. (1983) developed a relationship between maximum shear modulus and SPT blowcount based on a review of previous studies. Using an assumed unit weight of 120 pcf, Equation 1 was developed to estimate V_S in units of meters per second. It should be noted that the proposed equation is only applicable to sands at depths of less than 15 meters (50 feet).

$$V_s = 56\sqrt{N_{60}} \qquad \text{Equation 1}$$

2.3.3.4 Jinan (1987)

The original Jinan (1987) study was not available but is summarized in Wair et al. (2012). The study was conducted at a site in Shanghai China. Soils encountered were a 25 meter (82 ft) thick layer of relatively soft Holocene clays and silts overlying a layer of firmer Pleistocene clays, silts, and sands to the maximum depth tested of 60 meters (197 ft). SPT blowcounts for the top 20 meters (66 ft) were generally less than 5 and blowcounts below that layer ranged from 10 to 40. Hammer efficiency was not reported but can be assumed to be 60% based on contemporary Chinese studies (Seed et al., 1985). The equation derived is presented in Equation 2 with a coefficient of determination of 0.49.

$$V_s = 116.1(N_{60} + 0.31)^{0.20} \qquad \text{Equation 2}$$

2.3.3.5 Lee (1992)

A total of 491 pairs of V_S and SPT data were taken from the Taipei basin in Taiwan. Index properties considered in analysis include SPT blowcount, depth, and soil type. Geologic age was not considered since there is little variation within the area of interest. Soil types were divided into four groups: sands (SM), clays (CL), silts (MH), and a combined clay/silt group.

Correlation equations developed follow the simple linear model, the intrinsically linear model, and the multiple regression model. Multicollinearity between depth and SPT blowcount was of concern as SPT blowcount will increase with depth (Fletcher, 1965). Equations with a coefficient of determination greater than 0.7 were not considered to mitigate the multicollinearity problem. Stepwise selection as well as the ratio of standard error estimate to mean response of each coefficient were also used to detect multicollinearity. Equations developed for sands were not able to meet these criteria while equations developed for clays and silts were able to. Proposed equations were presented in Table 4.

Table 4: Recommended regression equations (Lee 1992)

Soil Type	Regression Equation	R^2
SM	$V_s = 71.9*(D+1)^{0.890}$	0.763
CL	$V_s = 86.1*N^{0.116}*(D+1)^{0.244}$	0.216
ML	$V_s = 82.8*N^{0.134}*(D+1)^{0.233}$	0.423
CL/ML	$V_s = 84.5*N^{0.118}*(D+1)^{0.246}$	0.287

2.3.3.6 Hasancebi and Ulusay (2007)

Hasancebi and Ulusay (2007) selected an alluvial basin site in Yenisehir, Turkey for analysis. Typical subsurface conditions consist of a stiff layer of silty clay underlain by a layer of silty sand that is medium dense to loose. In some localities silty clay was observed underlying the layer of sand as well as interbedded gravel at shallow depths. V_S measurements were taken using seismic refraction. The SPT energy ratio was not reported but the authors do present equations for both N and N_{60}.

Equations were developed for use on all soils, clays and silts, and sands. Clays and silts were combined due to a relative lack of data on silts in the author's dataset. Developed equations for uncorrected blowcounts are presented in Figure 10 while equations for energy corrected blowcounts are presented in Figure 11.

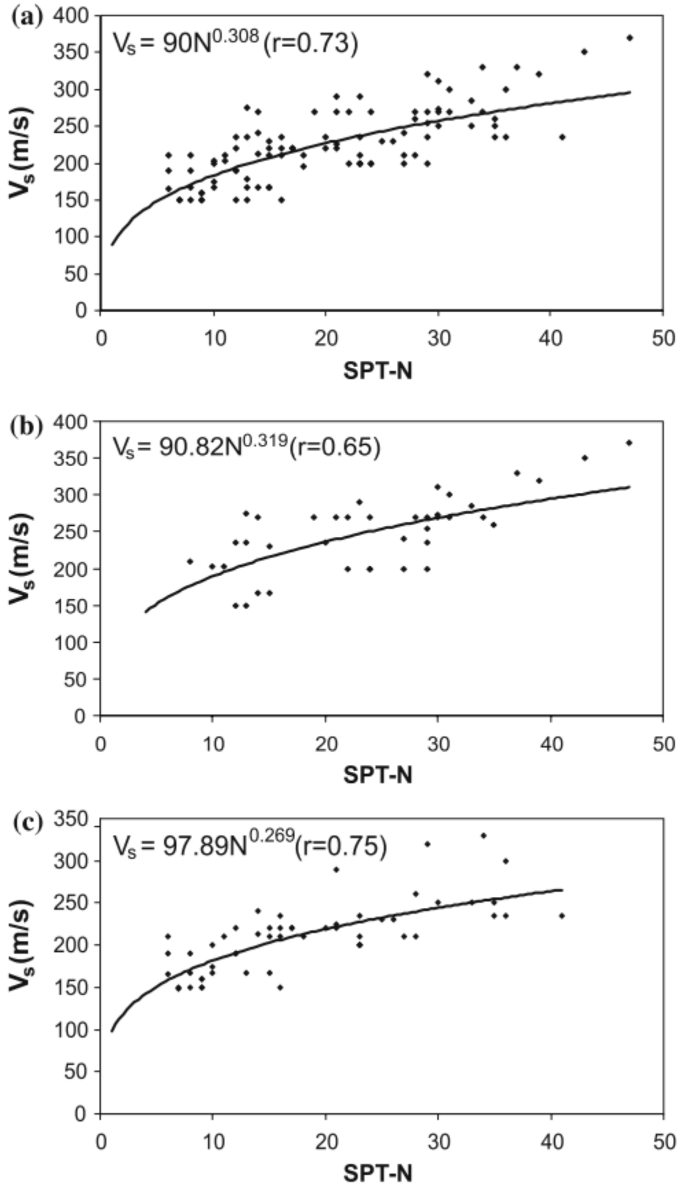

Figure 10: SPT N value and V_S relationships for (a) all soils, (b) sandy soils, and (c) clayey soils (Hasancebi and Ulusay, 2007)

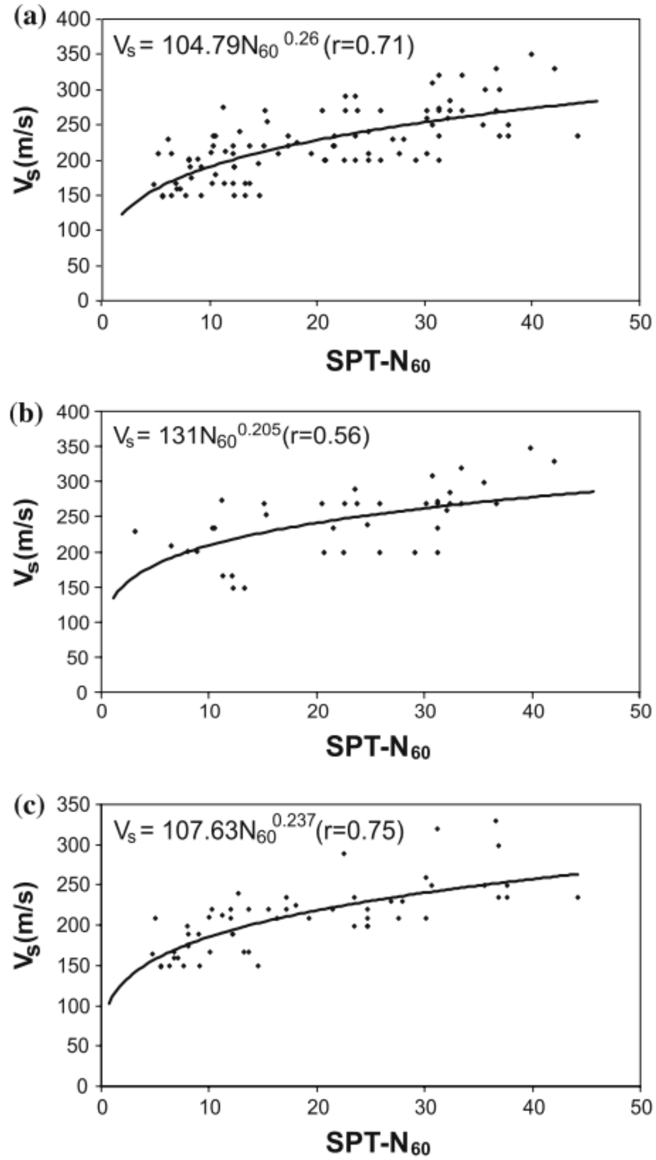

Figure 11: SPT N_{60} value and V_S relationships for (a) all soils, (b) sandy soils, and (c) clayey soils (Hasancebi and Ulusay, 2007)

2.3.3.7 Wair et al. 2012

Guidelines for estimation of V_S in California were provided in a 2012 report to the Pacific Earthquake Engineering Research Center (PEER). The report presents the previously discussed references along with additional sources not discussed in this study. The authors develop their own set of equations based on some of the stronger equations presented in the report.

Equations were developed for sandy soils, clay and silty soils, gravels, and for all soils. Energy corrected blowcounts (N_{60}) should be used for correlation along with corrections for a non-standard practice (i.e., borehole diameter, sampler liner, and rod length). Blowcounts were capped at a value of 100 to remain consistent with previous building codes. Equations were developed for Quaternary soils, but age scaling factors were provided for Holocene and Pleistocene soils. Developed equations are presented in Table 5.

Table 5: Recommended correlation equations (Wair et al., 2012)

Soil Type	Shear Wave Velocity for Quaternary Soils (m/s)	Age Scaling Factors	
		Holocene	Pleistocene
All Soils	$30N_{60}^{0.215}\sigma'_v{}^{0.275}$	0.87	1.13
Clays and Silts	$26N_{60}^{0.17}\sigma'_v{}^{0.32}$	0.88	1.12
Sands	$30N_{60}^{0.23}\sigma'_v{}^{0.23}$	0.9	1.17
Gravels-Holocene	$53N_{60}^{0.19}\sigma'_v{}^{0.18}$	---	---
Gravels-Pleistocene	$115N_{60}^{0.17}\sigma'_v{}^{0.12}$	---	---

2.3.3.8 Fatehnia et al. (2015)

Fatehnia et al. (2015) developed a correlation equation for V_S estimation based on data collected at multiple sites in Florida. The total number of sites was not disclosed, but the authors do note that 28 boreholes were drilled. For the 28 borings, SPTs were conducted continuously from the ground surface to a depth of 15 feet (4.57 meters) and then at an interval of 2.5 feet (0.76 meters) until borings reached termination. Criteria for termination of borings is not disclosed. A total of 300 SPT blowcounts were obtained for analysis. V_S was measured using MASW.

The authors used a model tree algorithm to develop their correlation equation. 70% of the data were used for correlation prediction while the remainder 30% were used to measure error. The authors present Equation 3 to estimate V_S in units of meters per second from uncorrected blowcounts. The proposed equation has a correlation coefficient of 0.893 ($R^2 = 0.797$) with their dataset and can be seen in Figure 12.

$$V_s = 77.1N^{0.355} \qquad \text{Equation 3}$$

Tab ... azhagan et

City	Num o Borel	...	SPT N value of rebound layer	
			on t (a)	Correlation coefficient (R^2)
Bangalore	1	...	39	0.829
Chennai	5	...	.3	0.822
Coimbatore	9	...	17	0.826
Vizag	2	...	56	0.870
Combined	5	...	45	0.823

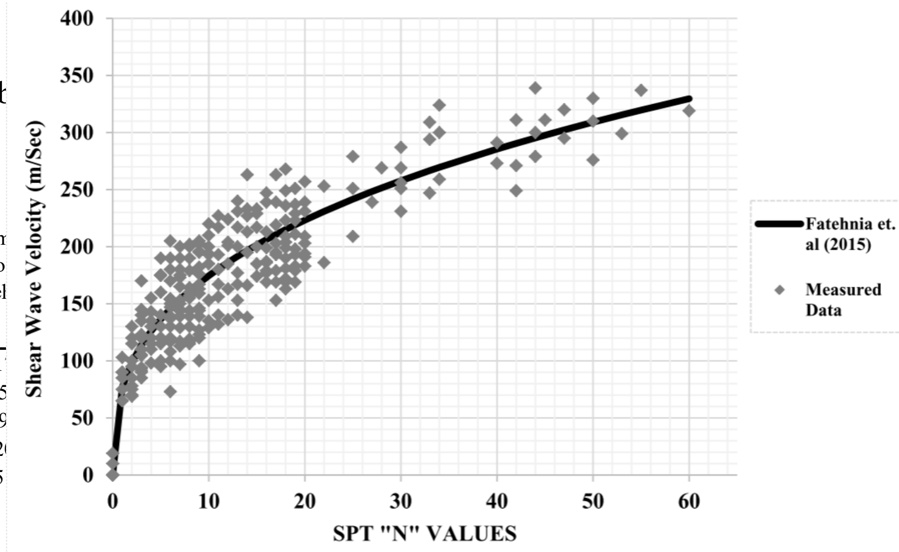

Figure 12: Proposed correlation for all soil types (Fatehnia et al., 2015)

2.3.3.9 Anbazhagan et al. (2016)

Anbazhagan et al. (2016) selected multiple sites within the intraplate seismic region in South India to develop equations for estimation of V_S. A total of 51 boreholes were drilled in sites across south India near major cities (Bangalore, Chennai, Coimbatore, and Vizag) with MASW surveys having been used to measure V_S. Soils primarily consisted of clays with blowcounts increasing with depth overlying a fractured layer of quartzite rock to a depth of 40 m (131 ft). SPT blowcounts for the layer of quartzite were taken as 100.

Equations were developed based on uncorrected blowcounts for each of the nearby cities and for a combined case. Equations considering blowcounts of 100 along with equations that do not consider blowcounts of 100 were developed. Equations follow a power fit in the form of Equation 4. Developed equations are provided in Table 6.

$$V_s = aN^b \qquad \text{Equation 4}$$

2.3.4 Correlation to Cone Penetration Testing (CPT)

Another commonly used in-situ test for typical geotechnical site explorations is the cone Penetration Test (CPT). CPT is performed by pushing an instrumented cone into the ground at a static rate of 0.2 cm/s (0.08 in/s) and measuring cone tip resistance (q_c) and sleeve friction (f_s) (ASTM D5778). The most common types of CPT testing are the conventional CPT, the piezo-CPT

(CPTu), and the seismic CPT (SCPT or SCPTu). The CPTu incorporates a piezometer behind the cone to measure pore water pressure and allows for correction of the tip resistance value due to pore pressures acting on the tip of the cone. The seismic CPT includes a geophone or accelerometer located in the cone tip to allow for downhole measurements of seismic velocities.

Wair et al. (2012) compiled a list of CPT based correlations to V_S. Table 7 contains the compiled list of correlation equations presented by the authors. Correlation equations were grouped based on soil type with equations for sands, clays, silts, and for all soils presented. Equations for gravels were not presented as CPT is not suitable for gravely soils (Schmertmann, 1978). For the sites in California that were considered, the authors recommend the use of the average value obtained from the use of Equations 5.7 (Mayne, 2006), 5.9 (Andrus et al., 2005), and 5.10 (Robertson, 2009). Since the equations presented were primarily developed for Quaternary and Holocene soils, they can tend to underpredict V_s for Pleistocene soils but are generally acceptable for all Quaternary soils (Robertson, 2009). If the thickness of Holocene and Pleistocene soils is known, age scaling factors can be applied to results. Age scaling factors for Holocene and Pleistocene soils are 0.92 and 1.12 respectively.

Table 7: CPT based correlation equations presented in Wair et al. (2012). Equations recommended for use are bolded.

Soil Type	Study	Geologic Age	Number of Data Pairs	R^2	V_s (m/s)
All Soils	Hegazy & Mayne (1995)	Quaternary	323	0.70	$(10.1\log(q_c)-11.47)^{1.67}(100f_s/q_c)^{0.3}$
	Mayne (2006)	Quaternary	161	0.82	$\mathbf{118.8\log(f_s)+18.5}$
	Piratheepan (2002)	Holocene	60	0.73	$32.3q_c^{0.089}f_s^{0.121}D^{0.215}$
	Andrus et al. (2007)	Holocene & Pleistocene	185	(H) 0.71 (P) 0.43	$\mathbf{2.62q_t^{0.395}I_C^{0.912}D^{0.124}SF}$
	Robertson (2009)	Quaternary	1035	---	$\mathbf{[(10^{(0.55Ic+1.68)})(q_t-\sigma_v)/p_a]^{0.5}}$
Sand	Sykora & Stokoe (1983)	---	256	0.61	$134.1+0.0052q_c$
	Balidi et al. (1989)	Holocene	---	---	$17.48q_c^{0.131}\sigma'_v{}^{0.27}$
	Hegazy & Mayne (1995)	Quaternary	133	0.68	$13.18q_c^{0.192}\sigma'_v{}^{0.179}$
	Hegazy & Mayne (1995)	Quaternary	92	0.57	$12.02q_c^{0.319}f_s^{-0.0466}$
	Piratheepan (2002)	Holocene	25	0.74	$25.3q_c^{0.163}f_s^{0.029}D^{0.155}$
Clay	Hegazy & Mayne (1995)	Quaternary	406	0.89	$14.13q_c^{0.359}e_0^{-0.532}$
	Hegazy & Mayne (1995)	Quaternary	229	0.78	$12.02q_c^{0.319}f_s^{-0.0466}$
	Mayne & Rix (1995)	Quaternary	339	0.83	$9.44q_c^{0.435}e_0^{-0.532}$
	Mayne & Rix (1995)	Quaternary	481	0.74	$1.75q_c^{0.627}$
	Piratheepan (2002)	Holocene	20	0.91	$11.9q_c^{0.269}f_s^{0.108}D^{0.127}$

2.3.5 Correlations for Rock

Seismic velocity of rock is not directly tied to rock quality designation (RQD) however both seismic velocities and RQD tend to decrease as rock becomes less weathered and fractured (Kahraman 2001, Biringen and Davie 2013). There are a limited number of existing correlations to either V_P or V_S from RQD. The following sections will provide discussion on available RQD based correlations.

2.3.5.1 El-Naqa (1996)

El-Naqa (1996) considers a site of a proposed dam in Wadi Mujib, Jordan to develop a relationship between RQD and compressional wave velocity of rock. Bedrock at the site consists of mostly yellow limestones interbedded by marls and thin shales. 10 boreholes were drilled at the site and seismic refraction was used to measure V_P.

The complete dataset and regression line are presented in Figure 13 where the dashed lines represent confidence limits of 90 and 95% respectively. The equation for the regression line is presented in Equation 5 and can be rearranged to determine V_P in the form of Equation 6. V_P can be converted to V_S using known ratios for different soil and rock types. Typical V_P/V_S ratios for sandstone, limestone, and dolomite, range from 1.6 to 1.9 (Pickett, 1963). Using an average value of 1.75, V_S can be calculated using Equation 7.

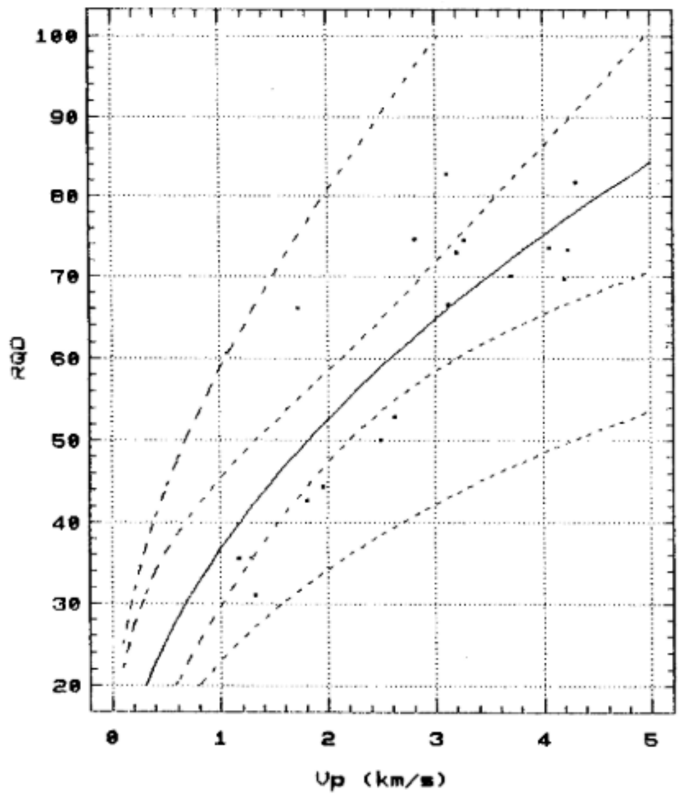

Figure 13: Complete dataset and regression including 90 and 95% confidence intervals (El-Naqa, 1996)

$$RQD = 36.7 * {V_P}^{0.52} \qquad \text{Equation 5}$$

$$V_P = \sqrt[0.52]{\frac{RQD}{36.7}} \quad (km/s) \qquad \text{Equation 6}$$

$$V_s = \frac{\sqrt[0.52]{\frac{RQD}{36.7}}}{1.75} \quad (km/s) \qquad \text{Equation 7}$$

2.3.5.2 Biringen and Davie (2013)

Biringen and Davie (2013) consider three sites in the Eastern United States for development of relationships between RQD and V_S for igneous, sedimentary, and metamorphic rock. Multiple boreholes were drilled at each site to varying depths (ranging from 150 to 300 feet) with suspension logging used to take measurements of V_S. Both RQD and V_S were averaged over 5-ft intervals.

The first site considered is located in South Carolina. Geology of the site consists primarily of hard igneous rock with some inclusions of metamorphic rock with rock consisting of granodiorite, quartz diorite, gneiss or migmatite. The upper layer of bedrock is moderately weathered with decomposed layers comprising 50% of the volume. Figure 14 presents the dataset from the South Carolina site along with the proposed equation for igneous rock.

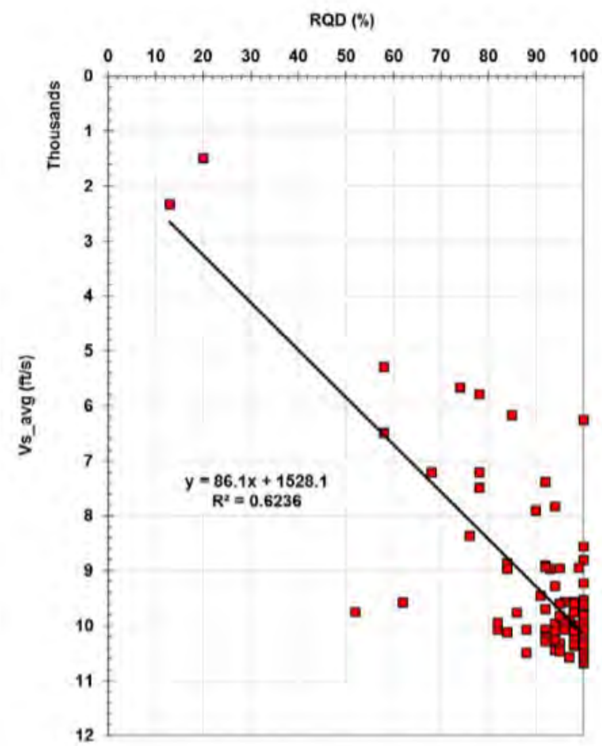

Figure 14: Correlation to V_S from RQD as developed from South Carolina igneous rock database (Biringen and Davie, 2013)

The second site is located in Virginia. Bedrock of the site is comprised primarily of metamorphic rock, consisting of mainly gneiss, ranging from quartz gneiss with biotite to biotite granite gneiss, and some biotite hornblende gneiss or quartz gneiss with feldspar or muscovite.

Figure 15 presents the dataset from the Virginia site along with the proposed equation for metamorphic rock.

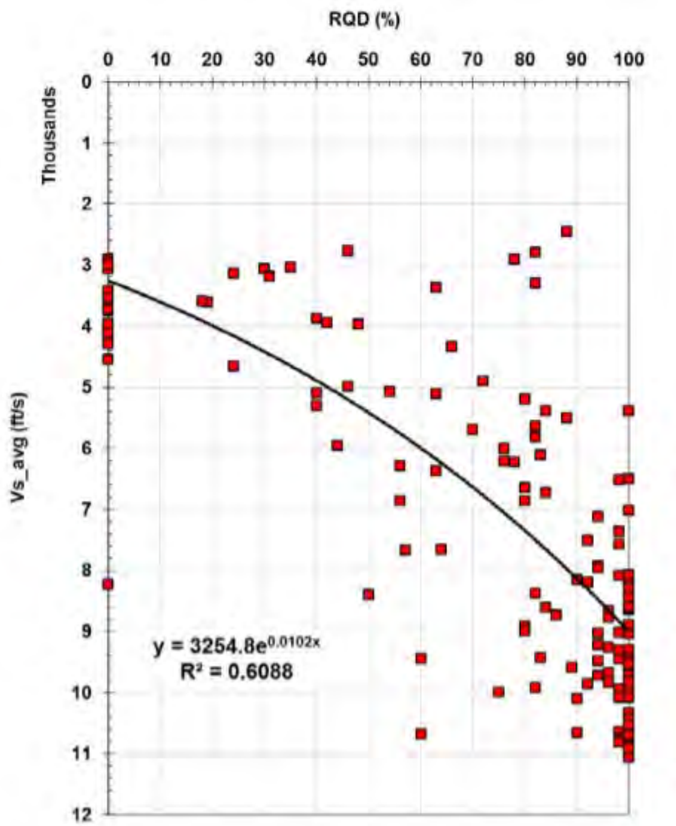

Figure 15: Correlation to V_S from RQD as developed by Virginia metamorphic rock database (Biringen and Davie, 2013)

The final site considered in the study is located in Florida. The site is located partially in the Key Largo formation which consists of white coralline limestone, frequently having a very open structure. The Key Largo formation is underlain by the Fort Thompson formation at the site. The Fort Thompson formation consists of white limestone with varying amounts of shells and some sand. The complete dataset for the Florida site and the proposed equation for sedimentary rock is presented in Figure 16.

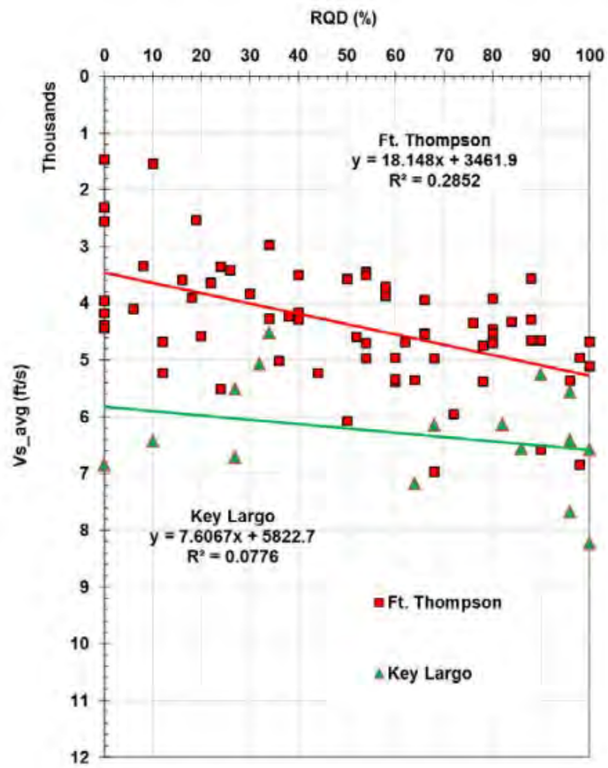

Figure 16: Correlation to V_S from RQD as developed by Florida Fort Thompson and Key Largo databases (Biringen and Davie, 2013)

2.3.5.3 Salaamah et al. (2019)

Salaamah et al. (2019) selects the site of the Bener dam in Indonesia to develop a relationship between RQD and V_P. The Bener Dam plan is located on the Bogowonto River in Indonesia and rock consists of andesite, tuff, lapilli tuff, agglomerates, and andesite lava. The database used by the authors was taken from a report on stabilization of the dam. V_P measurements were taken using seismic refraction. RQD was measured in 15 boreholes drilled as a part of the dam stabilization project. Regression analysis was performed on the dataset to develop an equation for predicting V_P and results are presented in Figure 17.

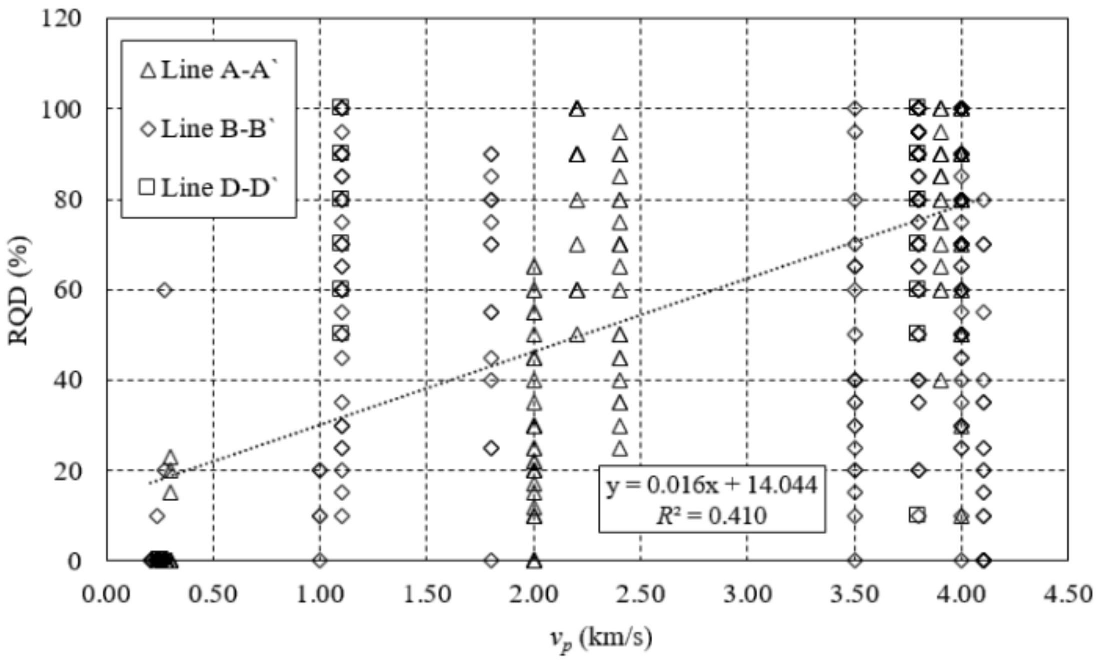

Figure 17: Combined correlation from all three survey lines for volcanic rock developed from Biringen Dam (Salaamah et al., 2018)

2.3.6 *Correlations with HVSR Measurements*

The HVSR technique is based on passive measurements of ambient seismic noise and was first introduced in 1989 (Nakamura, 1989, 2019). The HVSR method estimates the amplification and resonant frequency of ground motions that are affected by a surface layer (Nakamura, 2019). The HVSR method assumes that ground motions amplify the horizontal components near the fundamental frequency while the vertical component experiences little to no amplification (Nakamura, 1989). This was later observed to not always be true based on observations of the Mexico City basin (Lermo and Chávez-García, 1993). These findings were later reinforced by the Site Effects Assessment Using Ambient Excitations project (SESAME) funded by the European Union which aimed to standardize HVSR processing. The findings of the project revealed that under certain circumstances namely deep sedimentary basins and soft soils, vertical amplification can occur (SESAME 2004). The SESAME project helped to deepen the understanding of HVSR by issuing guidelines on HVSR data acquisition along with data processing as well as acknowledging some of the limitations of HVSR (Mucciarelli and Gallipoli, 2001, Bard, 2004).

The peak of the HVSR curve is associated with the fundamental frequency of the site (f_0) as well as the amplification of that frequency (A_0) (Nakamura, 2019). The fundamental frequency of the site for a single layered system is also related to the thickness of the layer (H) as well as shear wave velocity for that layer as described in Equation 8 (Kramer ,1996).

$$f_0 = \frac{V_s}{4H} \qquad \text{Equation 8}$$

Empirical correlations to obtain V_{S30} from f_0 have been developed by multiple authors. Discussion of available empirical correlations is found in the following sections.

2.3.6.1 Ghofrani and Atkinson (2014)

The authors use the Next Generation Attenuation-West2 (NGA-West2) database along with Japanese databases (K-NET and KiK-NET) to create a correlation equation between f_0 and V_{S30}. The database used by the authors contains recorded seismic events from 1996 to 2009. Using the HVSR parameters f_0 and A_0, correlation equations were developed separating the parameters along with an equation combining the two as seen in Equation 9.

$$\log_{10}(V_{S30}) = 2.56(\pm 0.01) + 0.20(\pm 0.02)\log_{10}(f_0) \qquad f_0 > 1Hz$$

$$\log_{10}(V_{S30}) = 2.86(\pm 0.01) - 0.46(\pm 0.02)\log_{10}(A_0) \qquad \text{Equation 9}$$

$$\log_{10}(V_{S30}) = 2.80(\pm 0.02) + 0.16(\pm 0.02)\log_{10}(f_0) - 0.50(\pm 0.03)\log_{10}(A_0)$$

2.3.6.2 McNamara et al. (2015)

McNamara et al. (2015) develops a relationship between HVSR fundamental frequency and V_{S30} for the Central Virginia Seismic Zone (CVSZ). A total of 218 permanent and 66 portable seismic stations were considered. Direct measurements of V_{S30} were performed at the locations of the portable seismic stations. Only recordings with clear peak frequencies were selected for use in development of this correlation, so the authors acknowledge that their correlation is not applicable to sites with complex or weak behavior. Measurements of HVSR and V_{S30} from 21 seismic stations were used to develop a correlation equation using least squares regression. A correlation coefficient of 0.89 (R^2 =0 .79) along with a standard deviation of 78.91 m/s were reported. Results are presented Figure 18 along with site class bins overlain on the plot.

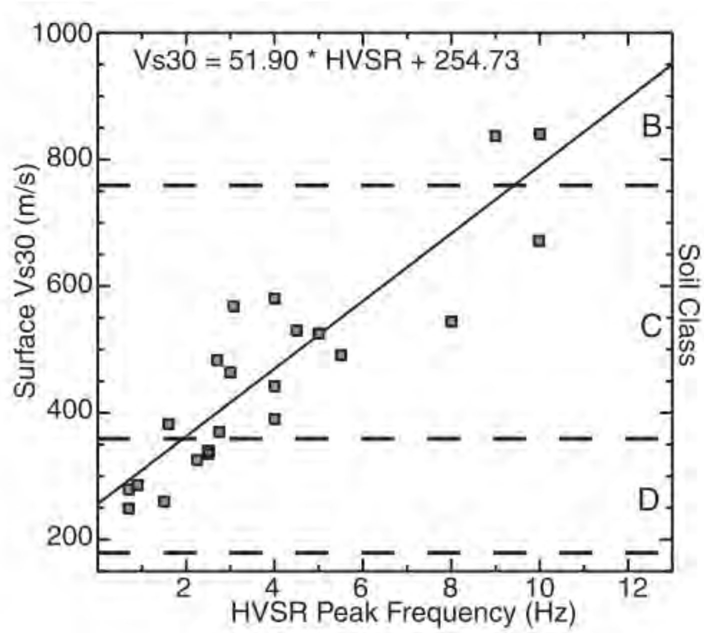

Figure 18: Comparison between HV$_S$R peak frequency and V_{S30} with site class bins overlain. (McNamara et al., 2015)

2.3.6.3 Hassani and Atkinson (2016)

Hassani and Atkinson (2016) utilized a database taken from the Next Generation Attenuation-East database (NGA East) to develop a relationship between HVSR and V_{S30}. Recording stations were scattered across CENA, with a large concentration of stations in the region of the Mississippi Embayment and a greater concentration of stations near Ontario from a supplemental database. Site classifications range from E to A with site class C being the most common.

Based on data from 41 sites from the database a relationship between HVSR peak frequency and V_{S30} presented in Equation 10. The authors acknowledge the limitations of the relatively low sample size as well as limitations in geologic conditions encountered as the equation is not applicable for sediments deeper than 30 meters.

$$\log_{10}(V_{S30}) = \begin{cases} 2.2(\pm 0.04) + 0.63(\pm 0.06)\log_{10}(f_{\text{peak}}) & f > 2\text{ Hz} \\ \log_{10}(250) & f \le 2\text{ Hz} \end{cases}. \quad \text{Equation 10}$$

2.3.6.4 Stanko and Markušić (2020)

A set of correlation equations for V_{S30} was developed based on 244 HVSR curves calculated from 3-component microtremor data in Croatia. V_{S30} was measured using surface based geophysical surveys (MASW and seismic refraction) at the same location or near where the microtremor data were taken. The study provided equations for different frequency ranges as seen in Equation 11. The authors emphasized that their developed equations can be applied to regions with similar characteristics and cannot be generalized for other areas.

$$\begin{aligned} \ln\left(V_{S30}\right) &= \ln(208 \pm 20) & f_0 &< 1Hz \\ \ln\left(V_{S30}\right) &= 5.34(\pm 0.9) + 0.46(\pm 0.15)\ln\left(f_0\right) & 1Hz \le f_0 &\le 10Hz \\ \ln\left(V_{s30}\right) &= \ln(600 \pm 80) & 10Hz < f_0 &< 30Hz \end{aligned} \qquad \text{Equation 11}$$

2.3.6.5 Sharma-Wagle et al. (2026)

The authors used a database of 2,861 three-component ambient noise recording from 536 unique sites located in New Zealand, Taiwan, Italy, Ecuador, Mexico, and the United States. Of these 2,861 recordings, 252 of these were taken from the Mississippi Embayment at 10 sites. Low dimensional models were developed using machine learning techniques that only considers the fundamental frequency and peak amplitude from the HVSR curve. Low dimensional models include the random forest and gradient boosted models. High dimensional models that consider the area under the entire HVSR curve were also developed. High dimensional models include the single and dual artificial neural network models. Both model classes integrate topographic information through the use of binned elevation as a proxy for geologic composition as well as topographic position index as a proxy for topographic features. Low dimensional models require a clear peak resonance frequency as defined by SESAME standards while the high dimensional models only consider frequencies within the range of 0.3 to 50 Hz.

Comparison of the models indicated that high-dimensional models more accurately predict V_{S30} as compared to the presented low dimensional models. For the high-dimensional models there was little to no difference between single and dual mode artificial neural networks. The authors recommend that for high-dimensional models, the single mode artificial neural network model (R^2=0.82) to be used while for low-dimensional models the random forest (R^2=0.69) and gradient boosted tree (R^2=0.68) models be used.

2.3.7 *Geospatial Correlations*

In addition to the other indirect methods presented in this section, correlations between V_{S30} and geospatial data (i.e., slope, geology, terrain classification, etc.) have been developed. Previous work in the application of geospatial methods for estimating V_{S30} in Alabama is presented in Carcamo (2022). Methods applied in Carcamo (2022) were based on terrain (Yong et al., 2012), hybrid slope-geology (Parker et al., 2017), and topographic slope (Wald and Allen, 2007). Those methods are applied in this study along with additional studies discussed in the following sections.

2.3.7.1 Wald and Allen (2007)

Wald and Allen (2007) developed a topographic slope-based model for estimation of V_{S30}. The model is supported by the hypothesis that as topographic slope increases, it is likely that surficial geology will be comprised of stiffer materials, thus V_{S30} will increase with topographic slope. Along with topography, sediment fineness is a proxy for lower shear wave velocity (Park and Elrick, 1998). Mountain front alluvial fan material typically grades finer as the distance from the mountain front increases and will deposit at decreasing slopes as energy is lost in the fluvial process.

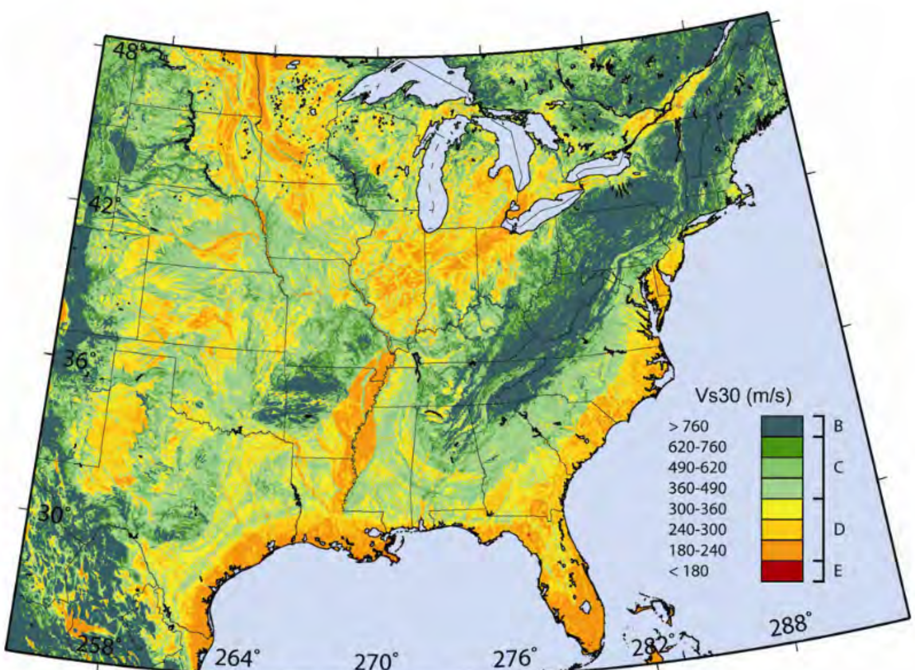

Figure 19: Wald and Allen, 2007 model for V_{S30} prediction based on topographic slope

For development of the model, the authors correlated 30 arc second topographic data with V_{S30} measurements taken from California, Utah, Tennessee, Missouri, Kentucky Washington, and Arkansas. The authors do present the limitation that the resolution selected can result in varying slope values for areas of high relief and additional correlations may be required for a more accurate estimate. Along with areas of high relief, in areas where the resolution of topography data is less than the ridge to valley wavelength, terrain will tend to be artificially flattened.

A model for the United States, taken from east of the Rocky Mountains is presented in Figure 19. On a coarse scale the authors indicate that the model is representative of V_{S30} but will tend to underpredict in flatter regions dominated by carbonaceous rock. The authors also noted the limitation of the model in this region due to a relative lack of V_{S30} measurements.

2.3.7.2 Yong et al. (2012)

A model for V_{S30} based on geomorphometry is presented in Yong et al. (2012). The authors used the terrain classification scheme developed in Iwahashi and Pike (2007) to create a consistent terrain classification map for global use shown in Figure 20. The algorithm developed divides terrain into 16 possible terrain classes using 3 taxonomic criteria: slope gradient, local convexity, and surface texture. V_{S30} values were taken from a number of sources, primarily from measured results and estimations in the state of California.

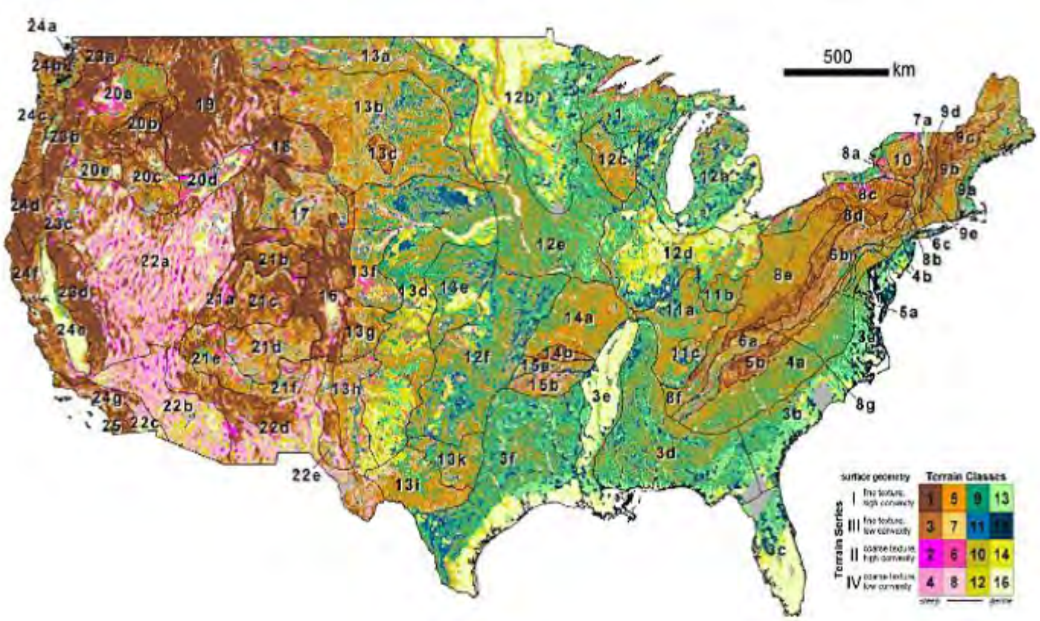

Figure 20: Terrain map of the United States (Iwahashi and Pike, 2007)

The model was initially developed and validated in California then expanded to the contiguous United States. Mean values of V_{S30} for all terrain types excluding type 13 are presented in Figure 21. The authors concluded that the model presented reduces standard deviation in stable continental regions as compared to the Wald and Allen (2007) model.

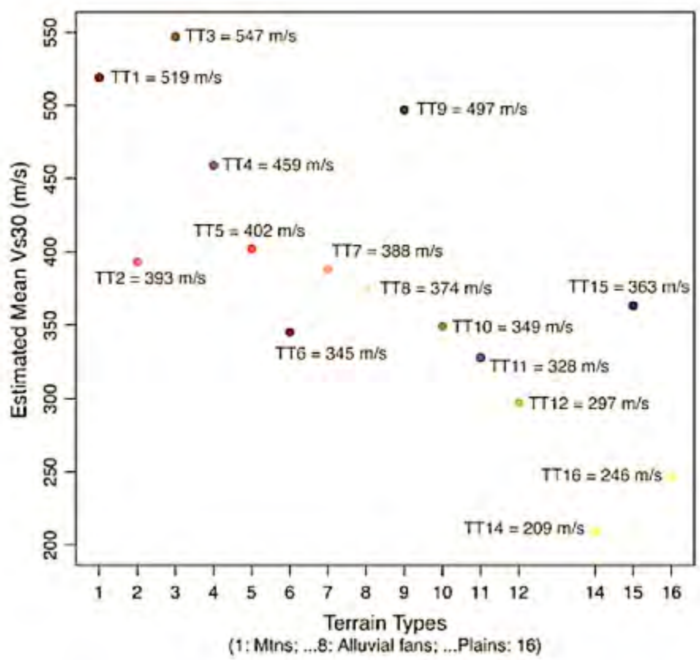

Figure 21: Mean values of V_{S30} for terrain types with no value provided for type 13 terrain (Yong et al., 2012)

2.3.7.3 Parker et al. (2017)

A hybrid slope-geology model for use in central and Eastern North America is presented in Parker et al. (2017). A database of 2775 V_{S30} values were used for development of the model. Despite effort to limit clustering, the authors still acknowledge the possibility of a regional bias in estimated values.

Groups were developed based on geologic age and were further subdivided based on geologic period and epoch. Developed groups were then correlated with the database of V_{S30} with log-log and semilog regressions. Developed geologic groups along with the mean V_{S30} for each group are presented in Table 8.

Table 8: Proposed V_{S30} estimation procedures based on large-scale geologic maps, Wisconsin glaciation, location of site in a basin, and topographic gradient (Parker et al., 2017)

Category*							Group Moments		Gradient Relationship				
									Semilog		Log–Log		
Group	Era	Period	Epoch	Wisconsin Glaciation?	Other Criteria	N	$\mu_{\ln V}$ (m/s)	$\sigma_{\ln V}$	c_0	c_1	c_2	c_3	$\sigma_{\ln V}$
1	C	Q	H	No	Alluvium, fluvial, and deltaic	308	210	0.23					
2	C	Q	H	No	All other lithology	183	221	0.29					
3	C	Q	H	Yes	In Ottawa, Canada	981	232	0.67	5.38	9.30			0.67
4	C	Q	H	Yes	Not in Ottawa, Canada	51	308	0.72			7.47	0.295	0.67
5	C	Q	Pli	No		284	271	0.36	5.47	31.4			0.31
6	C	Q	Pli	Yes	Till in Ottawa, Canada	104	777	0.57	6.51	22.4			056
7	C	Q	Pli	Yes	Other in Ottawa, Canada	60	377	0.65			7.20	0.22	0.63
8	C	Q	Pli	Yes	Not in Ottawa, Canada	63	448	0.65					
9	C	Q	U	No	Not in sedimentary basin	154	296	0.43			6.21	0.096	0.41
10	C	Q	U	No	In sedimentary basin	151	280	0.29					
11	C	Q	U	Yes	Not in sedimentary basin†	66	209	0.31	5.28	24.7			0.29
12	C	T				111	315	0.31			6.07	0.059	0.30
13	M					20	822	0.68					
14	P				In the Illinois basin‡	5	513	0.23					
15	P			No	Not in the Illinois basin	96	684	0.61					
16	P			Yes	Not in the Illinois basin	76	972	0.77					
17	p€					37	699	0.85					
18	p€				Site visit; hard-rock confirmation		2000						

*C, Cenozoic; Q, Quaternary; H, Holocene; Pli, Pleistocene; U, undivided; T, Tertiary; M, Mesozoic; P, Paleozoic, p€, Precambrian.
†Can be applied for within-basin sites with increased epistemic uncertainty (category unpopulated).

2.3.7.4 Geyin and Maurer (2023)

A model for V_{S30} in the United States based on multiple geospatial factors summarized in Table 9 is presented in Geyin and Maurer (2023). A total of 7081 measurements of V_{S30} from multiple regions within the contiguous United States were used for development of the model. Although the data represents a wide range of geographic and geologic settings, the data are primarily biased towards densely populated areas in regions of higher seismic activity. Machine learning techniques were used to develop the model as they are not limited on the number of variables considered. Of the dataset selected for analysis, 80% were used in training provisional models while the remaining 20% were used for validation.

Table 9: Input parameters, sources, and resolutions for Geyin and Maurer V_{S30} model (Geyin and Maurer, 2023)

Variable (units)	Source	Range in Data Set	Spatial Resolution
Depth to bedrock (cm)	Shangguan et al. (2017)	0-43,437	250m
Depth to groundwater (m)	Fan et al. (2020)	0-216	~1000m (30 arcsec)
Geologic unit	Horton et al. (2017)	Categorical	25-500m (varies)
Consolidation state	Horton et al. (2017)	0 or 1	25-500m (varies)
Distance to river (m)	Lehner and Grill (2013)	$0\text{-}8.4\text{x}10^4$	~90m (3 arcsec)
Compound topographhic index	Verdin (2017)	484-2858	~90m (3 arcsec)
Geomorphologic phonotype	Amatulli et al. (2018)	Categorical	~1000m (30 arcsec)
Topographic slope (%)	---	0-26.7	~1000m (30 arcsec)
Topographic position index	---	-37.38 to 22.94	~1000m (30 arcsec)
Profile curvature	---	-0.0012 to 0.0013	~1000m (30 arcsec)
Tangential curvature	---	$-9.0577\text{x}10^4$ to $9.35069\text{x}10^4$	~1000m (30 arcsec)
Roughness	---	0-284	~1000m (30 arcsec)
Terrain ruggedness index	---	0-90.88	~1000m (30 arcsec)
Vector ruggedness measure	---	0-0.0457	~1000m (30 arcsec)
Landform entropy	---	0-2.9572	~1000m (30 arcsec)
Landform uniformity	---	0.0536-1	~1000m (30 arcsec)
Landform Shannon index	---	0-2.0467	~1000m (30 arcsec)

Three provisional models were selected for further refinement. The three models were stacked, and regression kriging was applied to produce the model presented in Figure 22. The

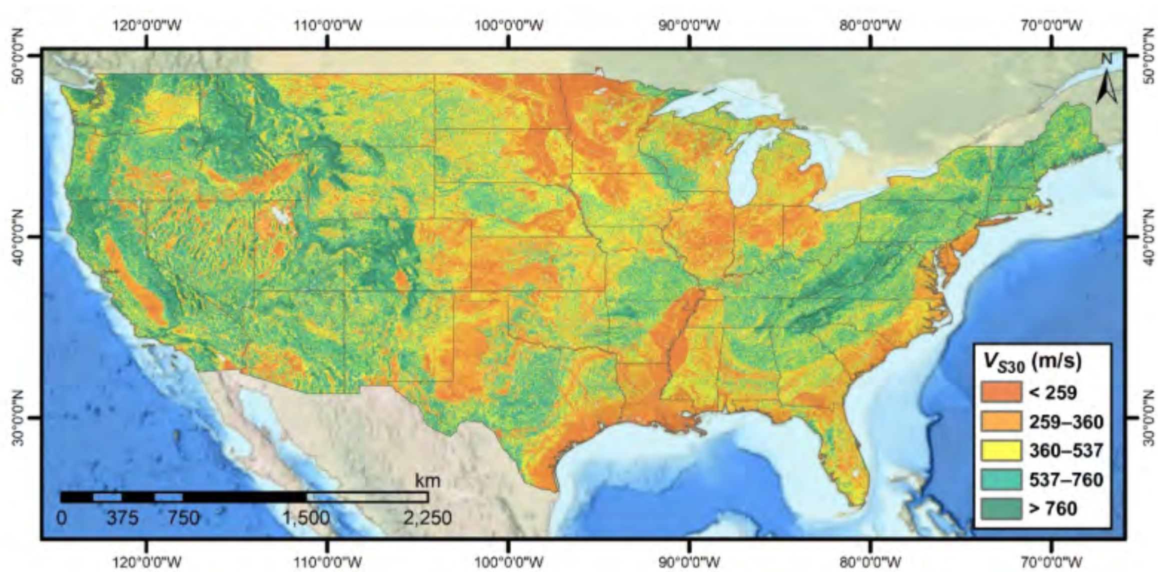

Figure 22: V_{S30} predictions from Model1alt with residual kriging for the continental US (Geyin and Maurer, 2023)

authors found a reduction in mean squared error (MSE) of 55% as compared to the model presented in Wald and Allen (2007).

2.3.7.5 Gann-Phillips et al. (2024)

A model for prediction of V_{S30} for the Atlantic and Gulf Coastal Plains is presented in Gann-Phillips et al. (2024). Coastal plains are characterized by nearly flat thick low-velocity sediments and sedimentary rock overlying high-velocity bedrock at depth. Previous models have failed to capture the behavior of these regions, so the authors sought to develop a more targeted model.

Generic V_S profiles for coastal plains were developed using the main components that control site amplification effects. The shallower portion of the profile (to a depth of approximately 200m) was developed based on physical measurements of V_S. Measured V_S profiles were collected from multiple data sources and were evaluated using a quality control process outlined by the authors.

Median profiles of V_S were developed for each of the geologic time periods to depths of 100m and 16km. Median V_{S30} values along with other median values for seismic design inputs are presented in Table 10. Other parameters presented alongside V_{S30} are depth to a V_S value of 1000m/s ($Z_{1.0}$), depth to a V_S value of 760 m/s ($Z_{0.76}$), and depth to a V_S value of 3000 m/s ($Z_{3.0}$).

Table 10: Values of V_{S30}, $Z_{1.0}$, $Z_{0.76}$, and $Z_{3.0}$ from the model database presented in Gann-Phillips et al. (2024) along with median values presented in Ahdi (2018) for comparison

Geologic Group	Median Model V_{s30}	$Z_{1.0}$ (m)	$Z_{0.76}$ (m)	$Z_{3.0}$ (km)	Median V_{s30} (m/s)	Median $V_{s30} \pm 1\sigma$ (m/s)
QH	237	874	582	15.31	202	155-263
QP	261	387	257	14.89	201	147-276
MEM	274	874	387	1.246	266	218-324
T	299	257	171	14.13	297	217-406
K	331	113	74.9	2.646	342	260-451

2.4 Summary

Alabama is generally considered a region with low to moderate seismic activity, but for critical infrastructure like bridges, even rare events must be considered in design. The latest edition of the AASHTO Guide Specifications (3rd Edition, 2023) uses SDC to determine the level of design requirements based on the expected seismic hazard. The SDC is determined based on the response spectrum for the site, which in turns depends on the location and site class. Site class is determined using a time-averaged shear wave velocity of the upper 100 ft (30 m) of the site (V_{S30}).

V_{S30} can be determined using direct measurements that can be either invasive or non-invasive. Direct measurements are the most reliable method for measuring V_{S30}, however in some cases direct measurements may not be economically feasible. In these cases, some estimate of V_{S30} may be made based on correlations between soil and/or site properties. For soil sites, SPT- and CPT-based correlations have been developed, but are often intended for Quaternary and Holocene soils and may underpredict values for older soils which are common in Alabama. For rock sites, fewer correlations are available, and some are made to compressional wave velocity (V_P) instead of V_S.

Correlations are also available to estimate V_{S30} directly based on either HVSR measurements or geospatial data. HVSR is a common geophysical survey that uses recordings of ambient noise. The technique measures the site's fundamental frequency (f_0) and fundamental amplitude (A_0). Both the fundamental frequency and amplitude can be used as a basis for correlation. Geospatial features of the site are commonly used as a basis for correlation to V_{S30}. Geospatial features are related to site geology or other material properties that have been shown to be correlated with V_{S30}. Geospatial features considered include topographic slope, surface geology, terrain classification, and others. All methods presented were primarily developed with data taken from areas of higher seismic activity, with little to no consideration for Alabama.

3 DATA COLLECTION

3.1 Introduction

In order to test the correlations discussed in the previous chapter, field surveys for direct measurement of V_s were conducted. Sites of field surveys were the locations of bridges or other infrastructure that also had corresponding SPT borings. For sites at the location of a bridge, SPT borings were typically drilled to a depth of approximately 100 ft (33 m), which provided enough data to correlate SPT blowcounts to a V_{s30} for the site. Borings conducted at the sites of other infrastructure projects do not typically extend to the same depths as bridge borings so extrapolation of deeper layers may be required for comparison of measured V_s to correlated V_s. All sites were in the western and northwestern corridors of the state, which have a higher degree of seismic activity than the rest of the state. V_s was measured using either MASW or seismic refraction. Sites with shallow rock are not good candidates for MASW surveys as higher modes will interfere with generating a quality dispersion curve so refraction-based surveys were used for these sites. A summary of the selected sites is shown in Table 11.

Table 11: Locations selected for field testing

Survey Location	Approximate Coordinates	Boring Number	Surveys Performed	V_{S30} (ft/s)
Cedar Bluff	34.27731, -85.67470	BR-0273 B-04	MASW, HVSR	3083
Beaver Creek	32.13762, -87.78266	4-BR1762L	MASW, HVSR	1145
	32.13794, -87.78266	4-BR1767L		1053
Big Prairie Creek	32.54165, -87.68057	8-BR3385R-2	MASW, HVSR	1178
Coldwell Creek	32.72850, -87.60641	10-BR4135	MASW, HVSR	1190
Moundville	32.84110, -87.61017	11-4588L	MASW, HVSR	1069
	32.841935, -87.61040	11-4590L		1027
Greensboro	32.76450, -87.58517	11-BR4292L	MASW, HVSR	804
Duck River	34.09289, -86.72132	BR-0091 B-06	Refraction, HVSR	3966[1]
Russellville High School	34.52492, -87.73752	B-03	MASW, HVSR	1594
	34.52517, -87.73774	BRF-0002(545) B-08		1400
Lauderdale County	34.95055, -87.69541	BR-3914 B2	MASW, Refraction, HVSR	2267[1]
	34.95057, -87.69579	BR-3914 B6		2906
Bluewater Creek	34.85717, -87.41544	B8	MASW, HVSR	2411
Blount County	33.93987, -86.39477	BR-0053(559)	Refraction, HVSR	3864[1]

Note: 1. V_{S30} was estimated based on refraction data where the deepest layer was assumed to extend to 100 feet.

3.2 Methodology

For MASW and refraction surveys, the survey equipment was nearly identical. The source of waves used for both survey techniques was an instrumented sledgehammer striking an aluminum plate on the ground surface. Care was taken that the aluminum plate was coupled with the ground so that the plate would not jump as it was struck by the hammer. Careful effort was taken so that the hammer would strike the plate at roughly the center and was lifted off of the plate after impact to not create any ringing effects. Either large (20 lb) or small (12 lb) sledgehammers were used as a wave source. The smaller hammer was primarily used in MASW surveys while refraction surveys utilized both sledgehammers. 4.5 Hz geophones were used for MASW surveys, and 14 Hz geophones were used for refraction surveys, and a select number of MASW surveys conducted at the same sites as some refraction surveys where the bedrock was not determined to be too shallow prior to testing. All geophones were recorded using a Geometrics Geode seismograph. The Geometrics Geode controller allows individual preamp gains to be set for each of the geophones. By default, geophones were set to a high gain preamp, but geophones within approximately 6 meters (23 ft) of the shot location were set to a low gain preamp. This was based off field observations of performance of geophones close to the source. Geophones within 2 m (6.6 ft) of the shot location would become overloaded regardless of preamp gain, so these were not considered for analysis for either MASW or refraction surveys.

3.2.1 Data Processing

MASW survey data were processed using Geopsy, an open-source software for geophysical applications (Wathelet et al., 2020a). The “Active F-K” tool was used to process the data. The tool utilizes a 2D transform to convert the data to the frequency domain and to obtain the phase velocity dispersion curve for the file (Wathelet, 2008). Each file was imported into the software and the transformation was performed. For files that a quality dispersion curve was generated, the generated curve was then saved. The saved curves were then averaged to create a representative dispersion curve for the site. The average curve was then resampled to improve the smoothness of the curve.

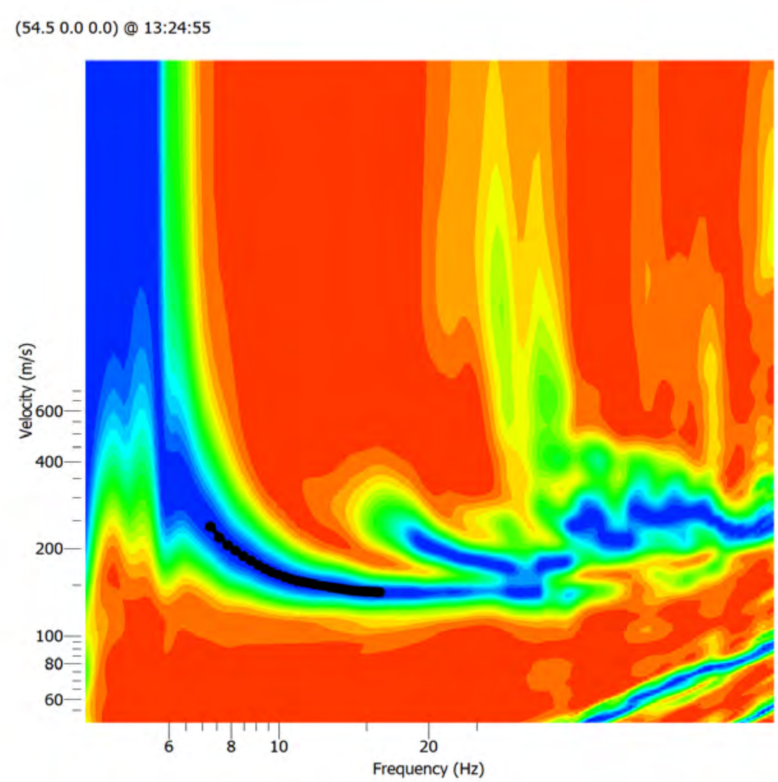

Figure 23: Example dispersion curve as displayed in Geopsy software

The DINVER package within Geopsy was then used to invert the average dispersion curve to provide a one-dimensional profile of V_S at the center of the geophone array. DINVER solves the inversion problem by randomly generating V_S profiles based on inputs provided by the user. Inputs provided were V_P, V_S, Poisson's ratio, density, and layering. Parameters can be set as a static value or a range of values for the provided layers and are able to be linked to one another or be considered independent. Following the solution of the inversion by the software, dispersion curves were generated by DINVER and compared to the provided dispersion curve and values of misfit were calculated. The solution generated is not unique, so the software provides output of the different profiles along with their misfit (Wathelet et al., 2020a).

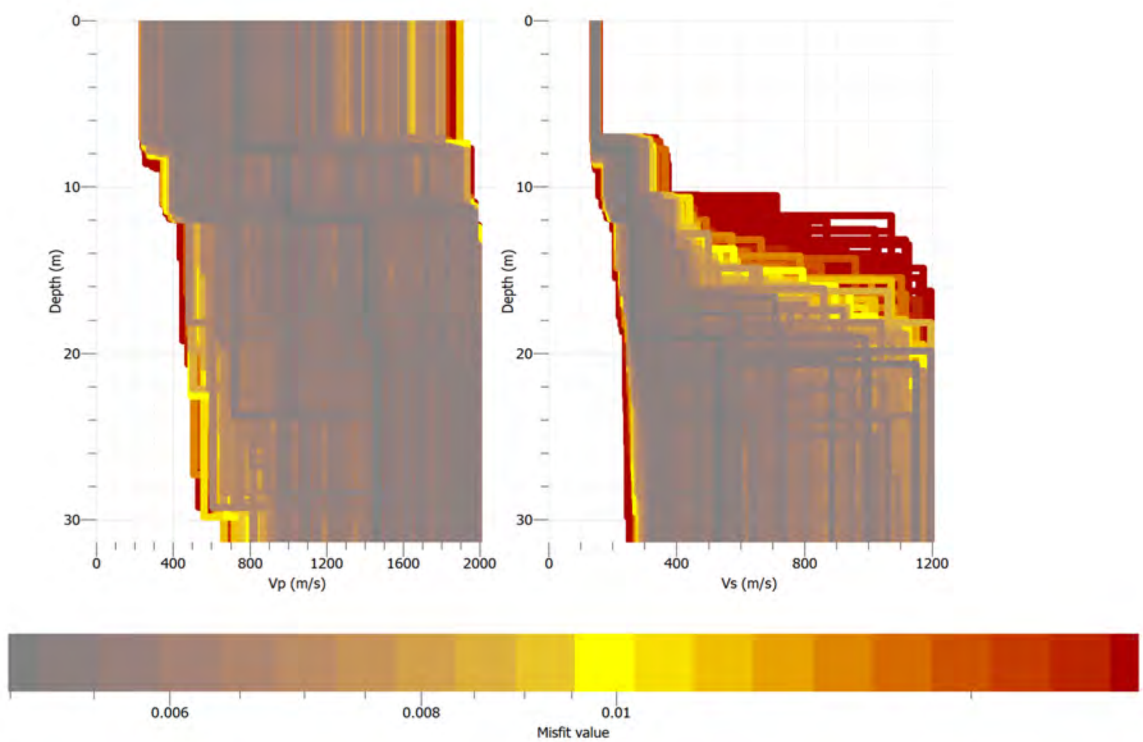

Figure 24: Example output ground profiles from inversion analysis in DINVER software

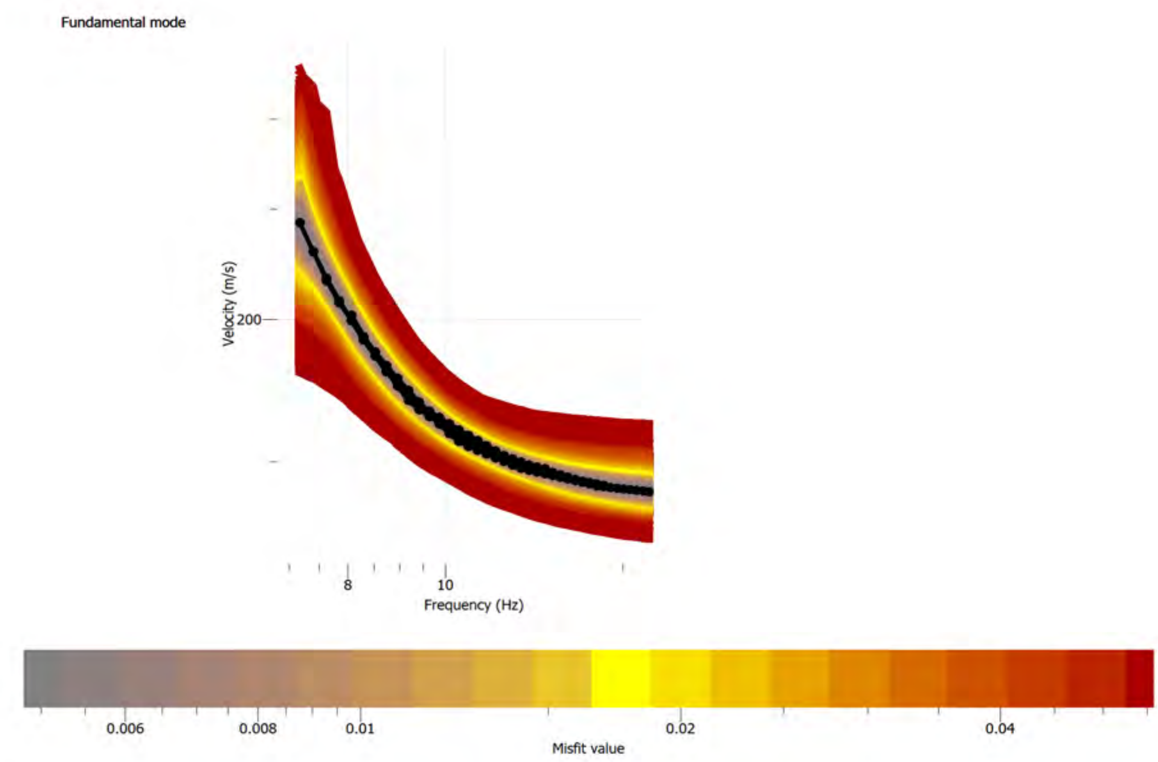

Figure 25: Comparison of dispersion curve generated by inversion analysis in DINVER to input dispersion curve

Refraction data were processed using the SeisImager software package provided by Geometrics (Geometrics, 2009). Typically, at least 5 shots will be taken at each location and stacked to provide enough data to minimize the effect of noise on interpretation of results. The software displays the file as a series of traces from each individual geophone. Each trace is by default normalized to their maximum amplitudes to prevent visual interference from one trace onto the next. First arrivals of the P-wave can then be selected from the software and can then be saved as a pick file, and an example can be seen in Figure 26 where the pink line represents the first arrival of the P-wave. Some files and shot locations contain too much noise to confidently determine first arrivals, so those were not considered in analysis.

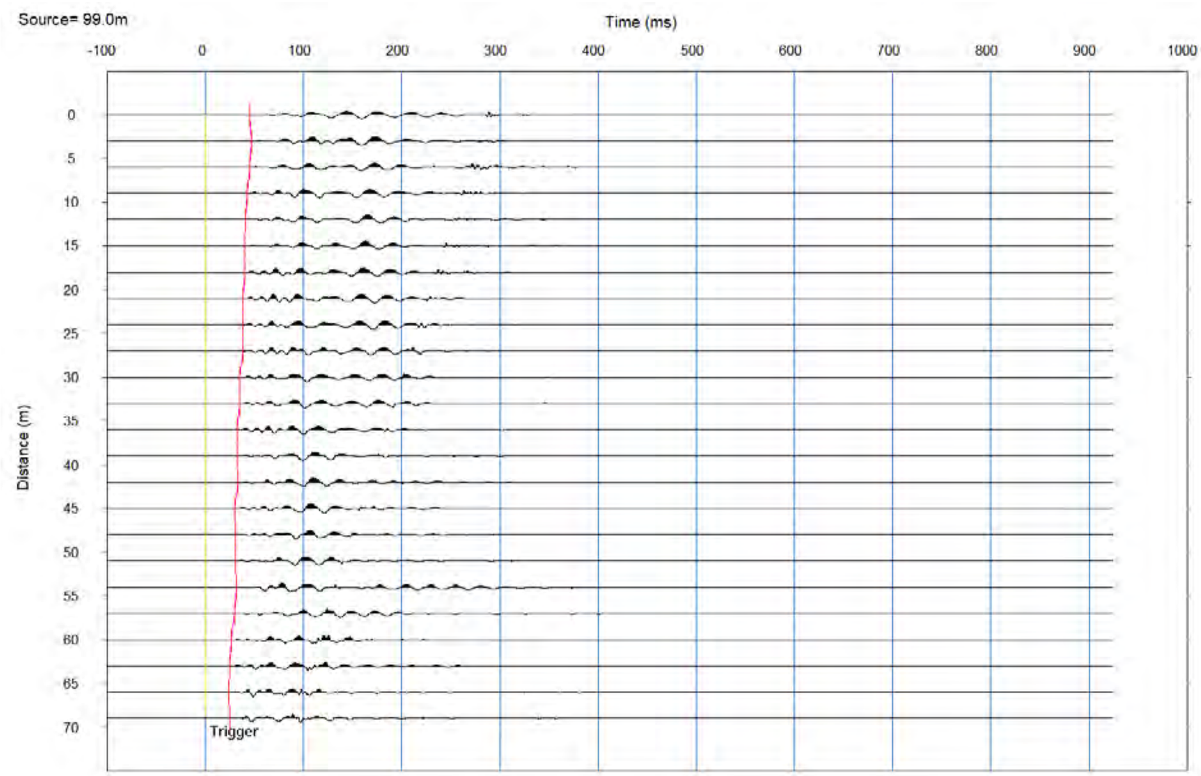

Figure 26: Refraction signal file as displayed in Pickwin with first arrivals of P-wave selected in pink

Following the selection of first arrivals, pick files were imported into the Plotrefra software package also provided by Geometrics (Geometrics, 2009). Inversions were performed using the time-term method. Layering can be assigned based on observation of the picked first arrivals where changes in slope are indicative of additional layers. An example of a two-layer travel time curve is presented in Figure 27. Once the layering is assigned then the inversion can be performed. Plotrefra provides a two-dimensional cross section of V_P below the geophone array. V_P can then be converted to V_s using Poisson's ratio (ν) of the material. Poisson's ratio can vary for different rock and soil types and ranges from 0.05 for very hard rocks to 0.45 for loose unconsolidated sediments but an average value of 0.25 was assumed. The ratio of V_P to V_s can be calculated using Poisson's ratio as shown in Equation 12.

$$\frac{V_P}{V_S} = \frac{(1-\nu)^{1/2}}{(1/2-\nu)} \qquad \text{Equation 12}$$

V_P can also be converted to V_s using known ratios for different soil and rock types. Typical V_P/V_s ratios for sandstone, limestone, and dolomite are discussed in Section 2.3.5. For

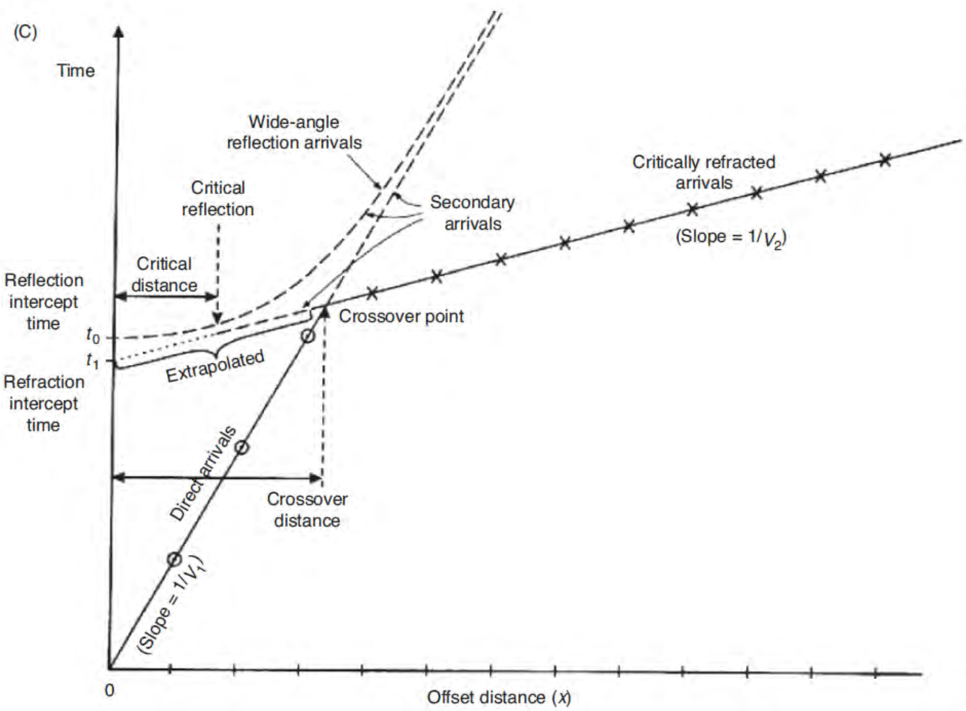

Figure 27: Travel time curve of a two layered model (Adapted from Reynolds 2011)

unconsolidated sediments, that ratio lies somewhere within the range of 2.0 to 4.0 (Herath et al., 2020). Careful consideration needs to be given to soil and rock that are beneath the groundwater table. Since the method of seismic refraction survey in this study is a measure of compressional wave velocities, saturated soils will have a V_P that is very close to water (1500 m/s). V_s is not affected as much as V_P under saturated conditions as shear waves cannot propagate through a fluid (Stümpel et al., 1984). Due to this, V_P/V_s ratios for saturated soils need to be increased to a range of 5.0 to 7.0 to account for saturated effects (Stümpel et al., 1984, Grelle and Guadagno, 2009).

HVSR data were collected alongside MASW and refraction data. HVSR data were collected and processed following a standardized procedure presented in Section 3.4.3.

3.2.2 SPT Boring Logs

At each of the sites selected for analysis in this study, at least one SPT boring was performed. Boring logs were provided by the Alabama Department of Transportation as well as other agencies. Boring logs were used to create representative ground profiles for the location of each geophysical survey. Ground profiles consist of representative layers of soil based on data provided by boring logs. Representative layers were determined empirically by soil type and SPT blowcounts and rely on experience of the researchers. SPT blowcounts of the layers determined by the researchers were averaged and assigned a depth of the center of the layer. An example ground profile is provided in Figure 28.

Ground profiles were primarily used in the inversion process for MASW data where layering parameters were assigned to constrain the model. Layering parameters included compressional wave velocity (V_P), Poisson's ratio (ν), density (ρ), and shear wave velocity (V_S). Along with these parameters, depth to each input layer can be assigned as a static value or within a range of values. Depths of layers were informed by the generated ground profiles.

3.3 Results from Field Testing

Direct measurements were taken at each of the sites presented in Table 11 to provide a V_S profile that can be used for comparison against the indirect methods presented in this report. Geophysical surveys were performed following the methodology presented in Section 3.2 of this report. The following sections provide discussion of results of direct measurements.

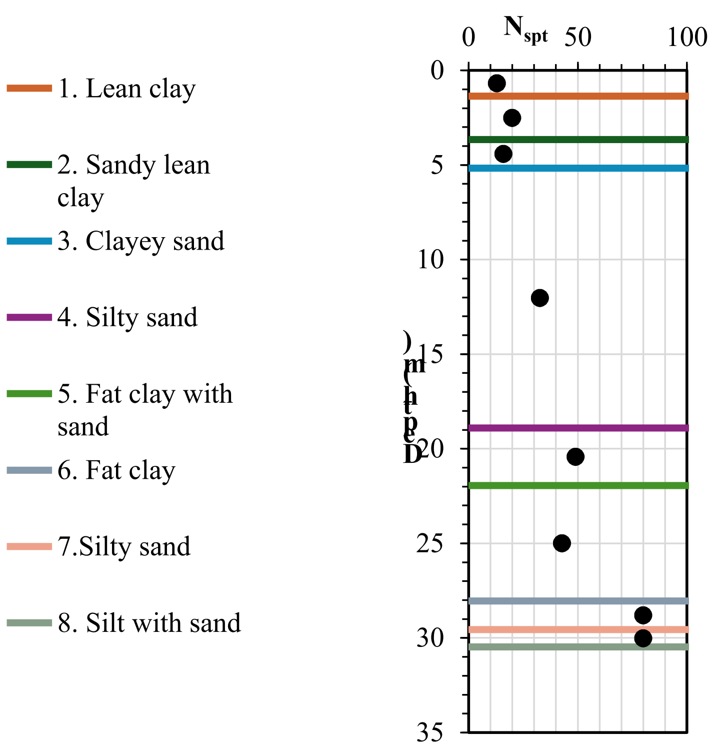

Figure 28: Example ground profile derived from SPT boring logs

3.3.1 Cedar Bluff, AL Site

Location and Geology

The site is located along Alabama state highway 273 outside of Cedar Bluff, AL (34.27731, -85.67470). The geophysical survey was conducted on January 25, 2025 using an active MASW survey. Terrain was relatively flat and free of vegetation along the survey line. The MASW survey line can be seen in Figure 29.

The site is underlain by the Red Mountain formation which is characterized by interbedded yellowish-gray to moderate-red sandstone, siltstone and shale; greenish gray to moderate red fossiliferous partly silty and sandy limestone with few thin hematitic beds (Osborne et al. 1989). From boring logs, soils expected to be encountered at the site were silts and clays underlying a layer of fill material at the ground surface. Rock was expected to be encountered at a depth of approximately 15 m (49 ft).

Figure 29: Cedar Bluff MASW survey line

Data Collection

An active MASW survey was conducted at the site. The survey used 24 4.5 Hz natural frequency geophones spaced at 3 meters for a total spread length of 69 meters. Active data were recorded at a sampling frequency of 2000 Hz with a recording length of 1.5 seconds, an offset of 0 seconds, and a delay of -0.1 seconds. No acquisition filters were used. Energy sources for the active survey were placed at multiple locations along the spread, with off-end, end on, and split-spread shots being used.

MASW Results

An example dispersion curve as measured from the site along with the 10 best inverted ground profiles are shown in Figure 30. The inverted profile with the minimum value of misfit indicated that a softer layer extends to a depth of 7.2 meters with a V_S of approximately 277 m/s (908 ft/s) underlain by a stiffer layer that extends to a depth of approximately 7.6m (49 ft) with a V_S of 923 m/s (1650 ft/s). This layer is underlain by the rock layer extending to a depth of 30m with a V_S of 4054 m/s (13296 ft/s). In the provided SPT boring located nearest to the survey location, gravels and sands were encountered to depths of approximately 14 meters. The measured V_S at depths of greater than 7.6m indicates that rock was present so these SPT datapoints will not be considered in analysis. This V_S profile gives a V_{S30} of 940 m/s (3083 ft/s) which places the site into the lower end of site class B.

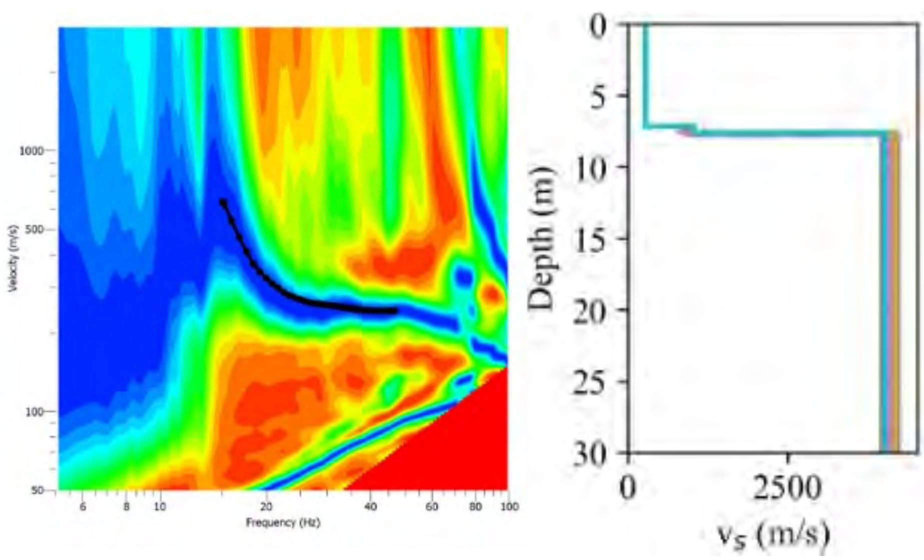

Figure 30: Results of Cedar Bluff MASW survey showing (A) dispersion curve and (B) inverted ground profiles

3.3.2 West Alabama Surveys

The first aggregated group of sites is referred to as the West Alabama group. All sites were in the western corridor of the state and tied to projects within the greater west Alabama highway improvement project. Each site in the West Alabama group was the site of a bridge or overpass where recent SPT borings had been performed as a part of bridge replacement project. Each SPT boring was drilled to a minimum depth of 98 ft (30 m). All surveys performed in this group of sites were MASW surveys. Along with active MASW surveys, each survey line also had at least one corresponding passive HVSR survey.

Beaver Creek Site

Location and Geology

The Beaver Creek site is located along Highway 43 in Marengo County Alabama (32.13762, -87.78266). Geophysical surveys were performed on February 20, 2025. Terrain was mostly flat at the site with minimal vegetation at the locations of seismic surveys. Two geophysical surveys were conducted at this site as documented in Figure 31.

The site was primarily underlain by alluvium and lower terrace deposits of the Holocene series (Osborne et al., 1989). From boring logs, soils encountered were primarily clays with varying degrees of stiffness and some interbedded loose sands.

Data Collection

Two active MASW surveys were performed at the site. For the first active survey, 24 4.5 Hz natural frequency geophones were used at a spacing of 1.5 meters for a total spread length of 34.5 meters. For the second active survey, 24 4.5 Hz natural frequency geophones were used at a

Figure 31: MASW survey locations for (A) Line 1 and (B) Line 2 for Beaver Creek surveys

spacing of 3 meters for a spread length of 69 meters. Data for both surveys were recorded with the same settings with a sampling frequency of 2000 Hz, a recording length of 1.5 seconds, an offset of 0 seconds, and a delay of -0.1 seconds. No acquisition filters were used. Energy sources for both active surveys were placed at multiple locations along the spread, with off-end, end on, and split-spread shots being used.

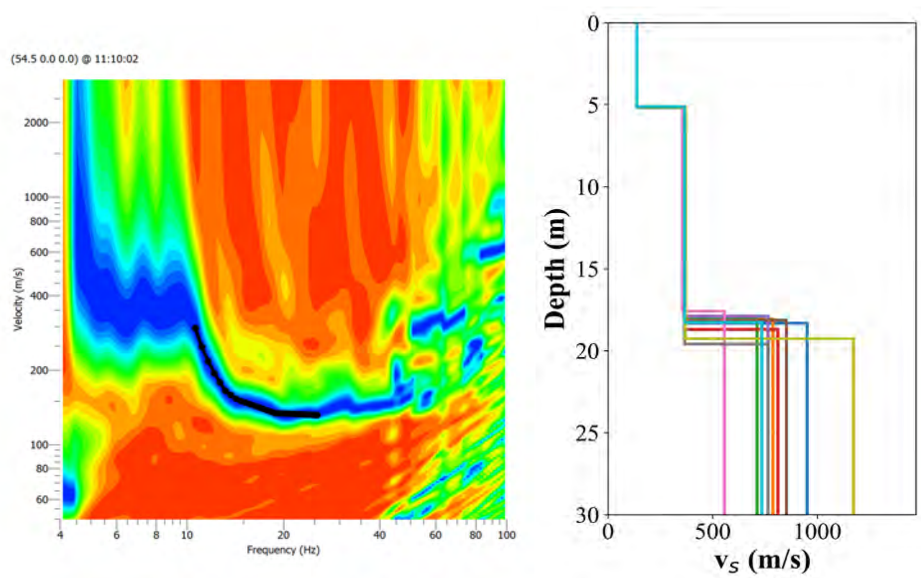

Figure 32: Results of first MASW survey conducted at Beaver Creek site showing (A) dispersion and (B) the 10 best fit inverted ground profiles

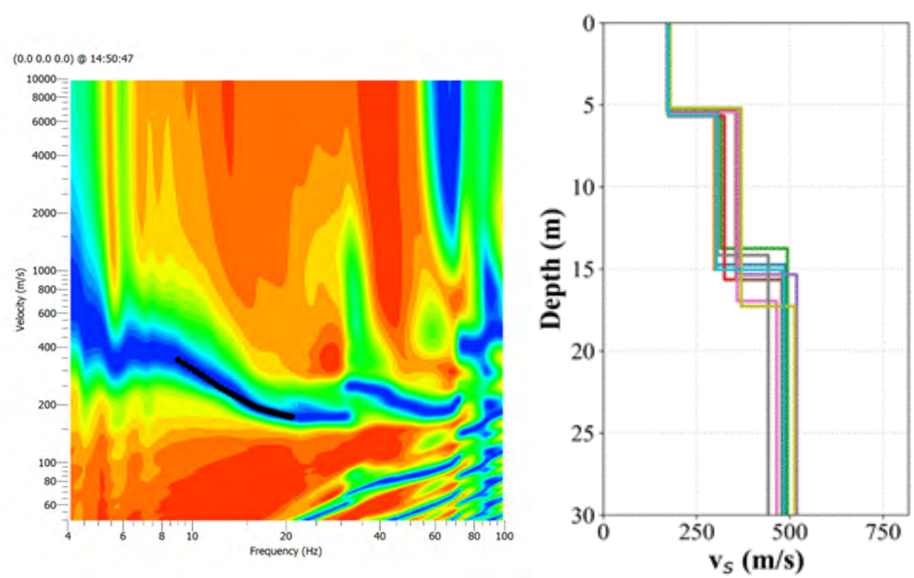

Figure 33: Results of second MASW survey conducted at Beaver Creek site showing (A) dispersion and (B) the 10 best fit inverted ground profiles

MASW Results

An example dispersion curve alongside the 10 best fit inverted ground profiles for the first MASW survey line are shown in Figure 32. The inverted profile with the minimum value of misfit shows a soft layer to a depth of 5 meters (16 feet) with a V_S of 134 m/s (440 ft/s) underlain by a stiffer layer with a V_S of 356 m/s (1168 ft/s) that extends to a depth of 18 meters (59 feet). Below this layer, a very stiff layer of clay was encountered with a V_S of 950 m/s (3116 ft/s) to a depth of 30 meters (98 feet) where the extent of the survey was reached. This V_S profile gives a V_{S30} of 349 m/s (1145 ft/s) which places the site into the upper bound of class C/D.

An example dispersion curve alongside the 10 best fit inverted ground profiles for the second MASW survey line are shown in Figure 33. The inverted profile with the minimum value of misfit indicates the shallowest layer underlying the second survey line is stiffer in comparison to the first survey line, having a V_S of 174 m/s (571 ft/s) also extending to a depth of approximately 5 meters (16 feet). The underlying layers below were, however, softer than those underlying the first survey line. A layer of soft soil extending to a depth of 14.7 meters (48 feet) with a V_S of 306 m/s (1004 ft/s) was encountered. This layer was underlain by a stiffer layer of clay with a V_S of 486 m/s (1594 ft/s). This V_S profile gives the site a V_{S30} of 321 m/s (1053 ft/s) which places the site into the lower bound of class C/D.

Big Prairie Creek Site

Location and Geology

The Big Prairie Creek site is located adjacent to a bridge on Highway 69 in Prairieville Alabama (32.54165, -87.68057). Geophysical surveys were conducted on February 20, 2025. Topography of the site was relatively flat with minimal vegetation at the location of the seismic survey as shown in Figure 34.

The site is primarily underlain by alluvium and lower terrace deposits of the Holocene series (Osborne et al., 1989). From boring logs, soils encountered were primarily interbedded silty and clayey sands with some sandy clay overlying a layer of elastic silt.

Figure 34: Big Prairie Creek seismic survey line

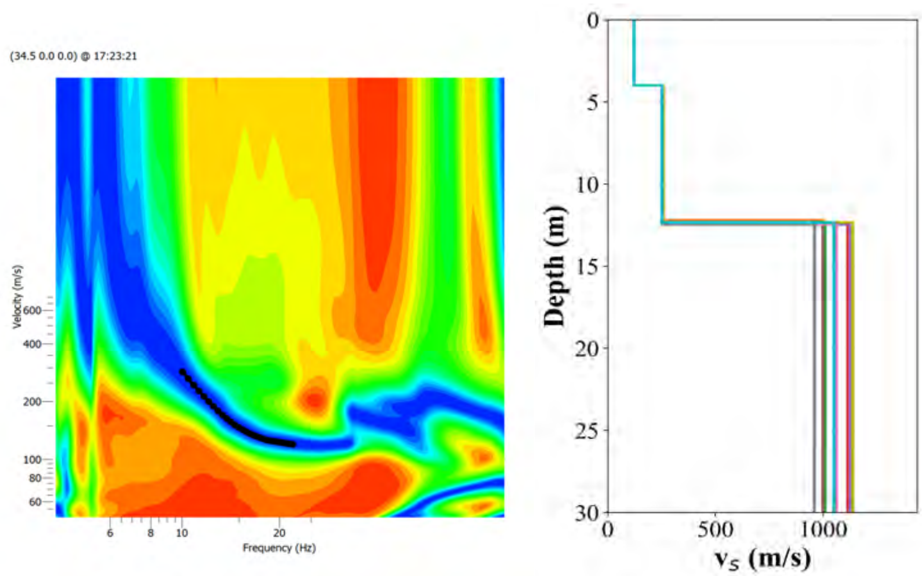

Figure 35: Results of MASW survey conducted at Big Prairie Creek site showing (A) dispersion and (B) the 10 best fit inverted ground profiles

Data Collection

A single active MASW survey was conducted at the site. The survey used 24 4.5 Hz natural frequency geophones spaced at 1.5 meters for a total spread length of 34.5 meters. Data were recorded with a sampling frequency of 2000 Hz, a recording length of 1.5 seconds, an offset of 0 seconds, and a delay of -0.1 seconds. No acquisition filters were used. Energy sources were placed at multiple locations along the spread, with off-end, end on, and split-spread shots being used.

MASW Results

An example dispersion curve alongside the 10 best fit inverted ground profiles for the MASW survey are shown in Figure 35. Considering the inverted profile with the minimum value of misfit indicates the V_S profile is divided into three layers. The first layer extends to a depth of 4m (13ft) and has a V_S of 124 m/s (407 ft/s). This layer corresponds with the softer sands and clays near the surface. The next layer extends to a depth of 12m (39ft) and has a V_S of 261 m/s (856 ft/s). This layer corresponds with the denser silty and clayey sands encountered at the site. The last layer observed has a V_S of 1000 m/s (3280 ft/s). This layer corresponds with the hard clay and elastic silt encountered in the SPT boring. This V_S profile gives a V_{S30} of 359 m/s (1178 ft/s) which places the site into class C/D.

Coldwell Creek Site

Location and Geology

The Coldwell Creek site is located south of Raven Road outside of Greensboro, AL (32.72850, -87.60641). Geophysical surveys were conducted on February 21, 2025. Topography of the site was flat and vegetation at the ground level was minimal at the time of the survey. The seismic survey line is shown in Figure 36.

Figure 36: Coldwell Creek seismic survey line

The site is underlain by the Eutaw formation which is characterized by gray to greenish-gray fine to medium grained glauconitic sand cross bedded with dark clay (Osborne et al., 1989). Soils encountered in a SPT boring at the site were primarily clayey sands with a layer of fat clay with varying amounts of sand.

Data Collection

A single active MASW survey was conducted at the site. The survey used 24 4.5 Hz natural frequency geophones spaced at 1.5 meters for a total spread length of 34.5 meters. Data were recorded with a sampling frequency of 2000 Hz, a recording length of 1.5 seconds, an offset of 0 seconds, and a delay of -0.1 seconds. No acquisition filters were used. Energy sources were placed at multiple locations along the spread, with off-end, end on, and split-spread shots being used.

MASW Results

An example dispersion curve alongside the 10 best fit inverted ground profiles for the MASW survey are shown in Figure 37. The inverted profile with the minimum value of misfit indicates the first layer encountered extends to a depth of approximately 4m (13ft) and has a V_S of 142 m/s (466 ft/s). This layer corresponds with the loose sands near the ground surface and the underlying fat clay. The next layer that can be observed below extends to a depth of 14m (46ft) and has a V_S of 333 m/s (1092 ft/s). This layer corresponds with the silty sand encountered in the boring log. Underlying this layer there is more uncertainty in the inverted models and there is

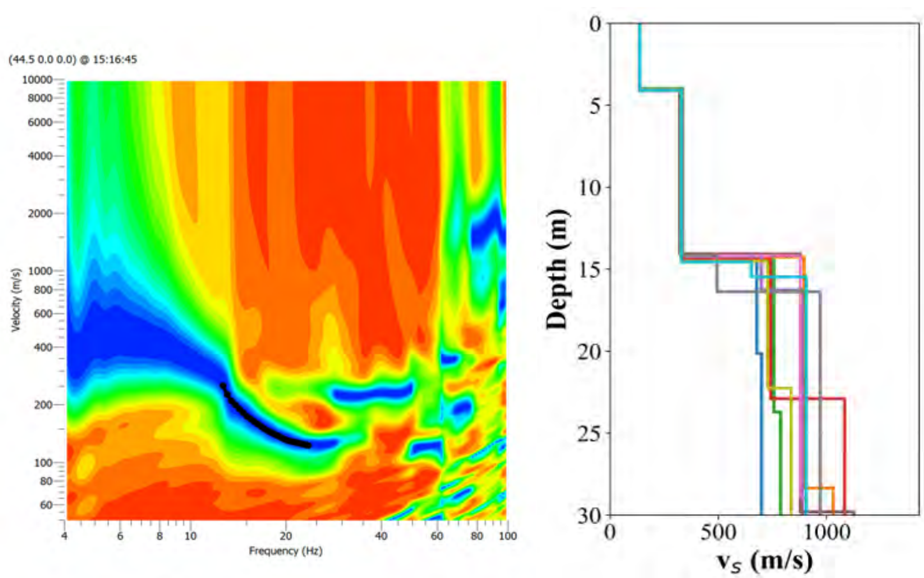

Figure 37: Results of MASW survey conducted at Coldwell Creek site showing (A) dispersion and (B) the 10 best fit inverted ground profiles

variation in the number of layers and magnitude of V_S. This layer has extends to a depth of 30m and has a V_S of 671 m/s (2200 ft/s). This layer corresponds with the dense silty sands encountered at these depths in the boring. The V_S profile gives a V_{S30} of 363 m/s (1190 ft/s) which places the site into class C/D.

Moundville, AL Site

Location and Geology

The Moundville site is located along Alabama Highway 69 in Moundville, AL (32.84110, -87.61017). Geophysical surveys were conducted on February 20, 2025. Terrain was flat in topography. The site was primarily wooded with access roads that were used to lay out survey lines. Seismic survey lines are presented in Figure 38.

The site is underlain by the Eutaw formation which is characterized by light greenish gray to yellowish-gray cross-bedded, well-sorted micaceous, fine to medium quartz sand that contains beds of greenish gray silty clay and medium dark gray carbonaceous clay (Osborne et al., 1989). SPT borings were drilled to a depth of 100 feet and primarily encountered sandy soils overlying clays and a layer of elastic silt with fat clays being encountered prior to termination of the borings.

Figure 38: Moundville seismic survey line (A) 1 and (B) 2

Data Collection

Two active MASW surveys were conducted at the site. The surveys used 24 4.5 Hz natural frequency geophones spaced at 1.5 meters for a total spread length of 34.5 meters. Data were recorded with a sampling frequency of 2000 Hz, a recording length of 1.5 seconds, an offset of 0 seconds, and a delay of -0.1 seconds. No acquisition filters were used. Energy sources were placed at multiple locations along the spread, with off-end, end on, and split-spread shots being used.

MASW Results

An example dispersion curve alongside the 10 best fit inverted ground profiles for the first MASW survey are shown in Figure 39. Considering the inverted profile with the minimum value of misfit indicates the first layer extends to a depth of 1m (3.3ft) with a V_S of 196 m/s (643 ft/s). This layer corresponds with the sandy lean clay encountered near the ground surface. The next layer encountered extends to a depth of approximately 2.4m (8ft) and has a V_S of 253 m/s (830 ft/s). This corresponds with the upper portion of the layer of silty sand encountered in the SPT boring. The next layer extends to a depth of approximately 20.5m (67ft) and has a V_S of 411 m/s (1348 ft/s). This spans multiple soil layering boundaries and encompasses sands, silts, and clays.

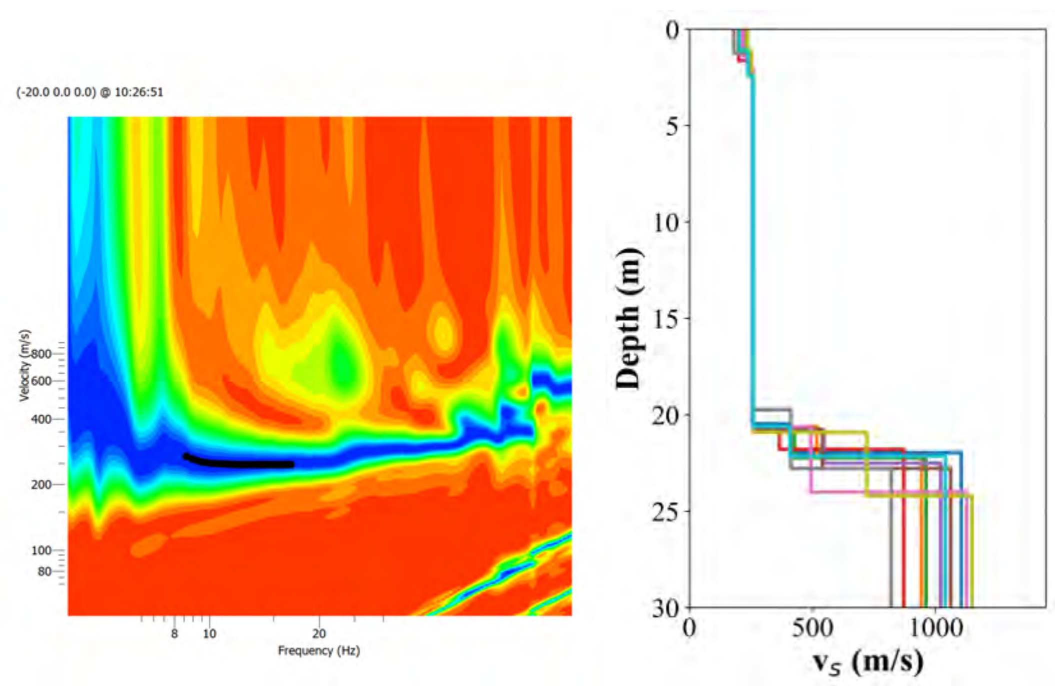

Figure 39: Results of first MASW survey conducted at Moundville site showing (A) dispersion and (B) the 10 best fit inverted ground profiles

The final layer observed has a V_S of 1120 m/s (3674 ft/s) and is subject to more uncertainty than the layers lying above. This V_S profile gives the site a V_{S30} of 326 m/s (1069 ft/s) which places it into the lower bound of class C/D.

An example dispersion curve alongside the 10 best fit inverted ground profiles for the second MASW survey are shown in Figure 40. Considering the inverted profile with the minimum value of misfit indicates near the ground surface, there are three layers with shear wave velocities that are all very close in magnitude. Those layers can be considered as a singular layer in analysis with a V_S of approximately 270 m/s (886 ft/s) that extends to a depth of approximately 23.7m (78ft). This singular layer would span multiple soil types, encompassing sands and clays with varying degrees of sand content. The next layers that can be observed from inverted ground profiles are subject to more uncertainty, but it can be observed that there are 2 layers that extend to depths of approximately 26.7 and 30m respectively (88 and 100ft). These layers have shear wave velocities of 994 and 1130 m/s (3260 and 3706 ft/s). This V_S profile gives a V_{S30} of 313 m/s (1027 ft/s) which places the site into the lower bound of class C/D.

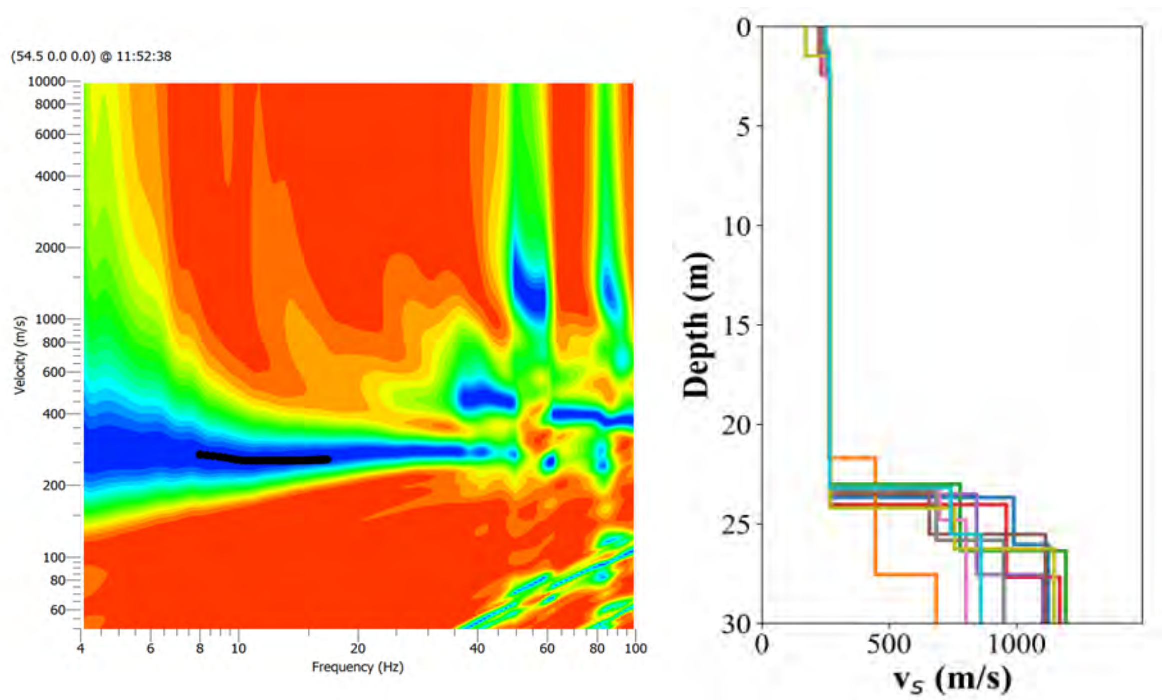

Figure 40: Results of second MASW survey conducted at Moundville site showing (A) dispersion and (B) the 10 best fit inverted ground profiles

Greensboro, AL Site

Location and Geology

The Greensboro site is located alongside AL-69 in Greensboro, AL (32.76450, -87.58517). Geophysical surveys were conducted on February 21, 2025. Topography of the site was mildly sloped with minimal vegetation. The seismic survey line is presented in Figure 41.

The site is underlain by alluvial, coastal, and low terrace deposits of the Holocene series which were characterized by fine to coarse quartz sand containing clay lenses and gravel in places (Osborne et al., 1989). Soils encountered during a SPT boring local to the survey line were primarily sands with varying contents of fines and sandy lean clays.

Figure 41: Greensboro seismic survey line

Data Collection

A single active MASW survey was conducted at the site. The survey used 24 4.5 Hz natural frequency geophones spaced at 1.5 meters for a total spread length of 34.5 meters. Data were recorded with a sampling frequency of 2000 Hz, a recording length of 1.5 seconds, and an offset of 0 seconds, and a delay of -0.1 seconds. No acquisition filters were used. Energy sources were placed at multiple locations along the spread, with off-end, end on, and split-spread shots being used.

MASW Results

An example dispersion curve alongside the 10 best fit inverted ground profiles for the MASW survey are shown in Figure 42. Considering the inverted profile with the minimum value of misfit indicates the first layer has a V_S of approximately 146 m/s (479 ft/s) and extends to a depth of 7.4m (24ft). This layer corresponds with the layers of sand with varying fines contents. The next layer that can be observed from inverted ground profiles extends to a depth of 11m (36ft) and has a V_S of 215 m/s (705 ft/s). This layer corresponds with the layer of lean clay observed in the boring. The next layer encountered extends to a depth of 23m (75ft) and has a V_S of 306 m/s (1004 ft/s) This layer corresponds with silty sand observed in the SPT boring. The final layer that extends down to a depth of 30m (100ft) has a V_S of 466 m/s (1528 ft/s). This layer is also in the same layer of silty sand. This V_S profile gives a V_{S30} of 245 m/s (804 ft/s) which places the site into class D.

3.3.3 Northwest Alabama Surveys

The second aggregated group of sites is the Northwest Alabama Group. Sites selected for the Northwest Alabama surveys were selected due to availability of SPT borings. The MASW technique was used for sites with a greater depth to rock while refraction was used for sites when rock was encountered shallower to the ground surface. SPT borings for the sites in the Northwest

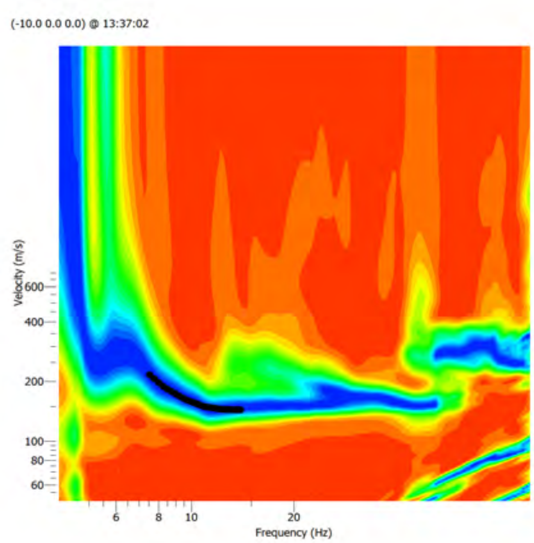

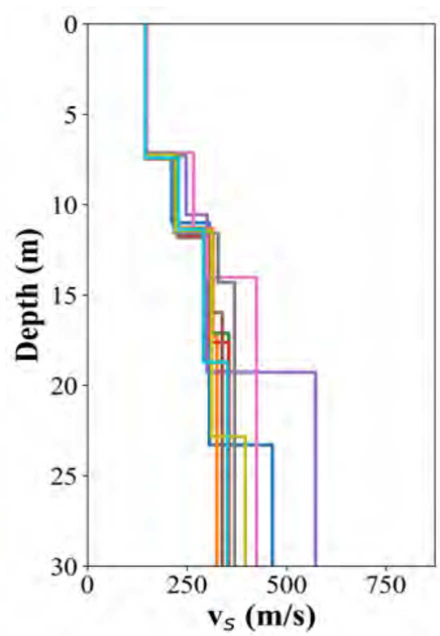

Figure 42: Results of MASW survey conducted at Greensboro site showing (A) dispersion and (B) the 10 best fit inverted ground profiles

Alabama group have a varying degree of depths, ranging from 23.5 ft to 102.1 ft (7.2 m to 31.1 m) so extrapolation of some deeper layers may be required in interpretation of results. HVSR surveys were performed alongside active surveys at these sites.

Duck River Site

Location and Geology

The first site in the Northwest Alabama group is located along Duck River in Hanceville, AL (34.09289, -86.72132). Geophysical surveys were conducted on May 6, 2025. Terrain at the site was flat with minimal vegetation at the time of the survey. The seismic survey line is shown in Figure 43

The site is underlain by the lower part of the Pottsville formation, which is characterized by light gray, thick bedded to massive pebbly quartzose sandstone with varying amounts of interbedded shale, siltstone, and coal (Osborne et al., 1989). Boring logs of the site indicate that depth to rock was approximately 18.5 feet (5.6 meters) however visual inspection of the site indicates that rock was to be encountered shallower to the ground surface at the locality of the seismic survey line.

Figure 43: Seismic survey line at Duck River site

Data Collection

Due to the presence of shallower rock at the site the seismic refraction technique was used. A single active refraction survey was conducted at the site. The survey used 24 14 Hz natural frequency geophones spaced at 3 meters for a total spread length of 69 meters. Data were recorded with a sampling frequency of 16000 Hz, a recording length of 1.5 seconds, an offset of 0 seconds, and a delay of -0.1 seconds. No acquisition filters were used. Energy sources were placed at multiple locations along the spread, with off-end and end on shots being used. A minimum of 5 shots were taken at each location for stacking to increase signal to noise ratio.

Refraction Results

Travel time curves presented in Figure 44 indicate a two layered system. Inversion analysis was performed and the compressional wave velocity model was calculated as presented in Figure 45. V_P/V_S ratios of 0.4 and 0.6 were used to calculate the probable range of V_S for the site and are presented in Table 12. Extending the lower layer to a depth of 30m and using a median value of V_S from the probable range give a V_{S30} of 1209 m/s (3,966 ft/s) which places the site into class B.

Table 12: Calculated range of V_S profile for Duck River site

Parameter	Layer 1	Layer 2
Compressional Wave Velocity (m/s)	1020	3506
Shear Wave Velocity (lower bound m/s)	408	1402.4
Shear Wave Velocity (upper bound m/s)	612	2103.6

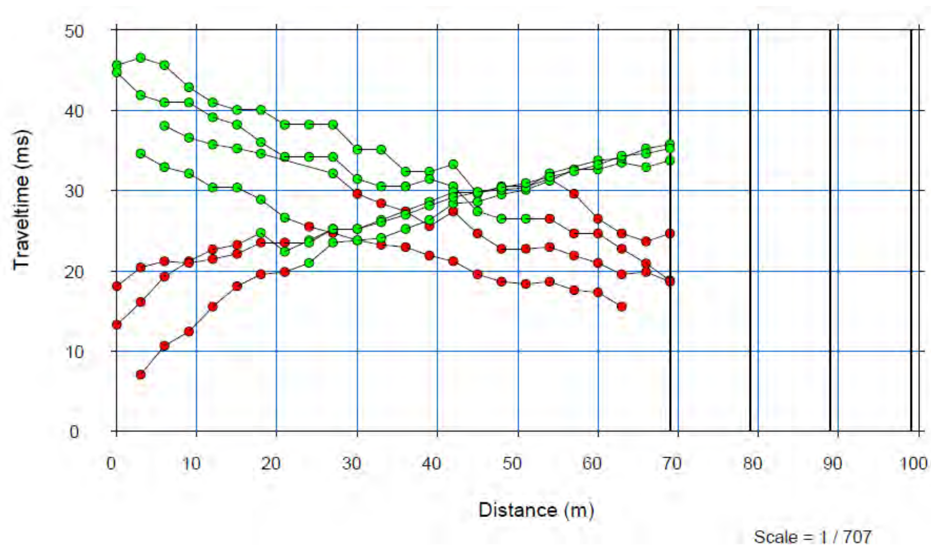

Figure 44: Appended travel time curves for Duck River site

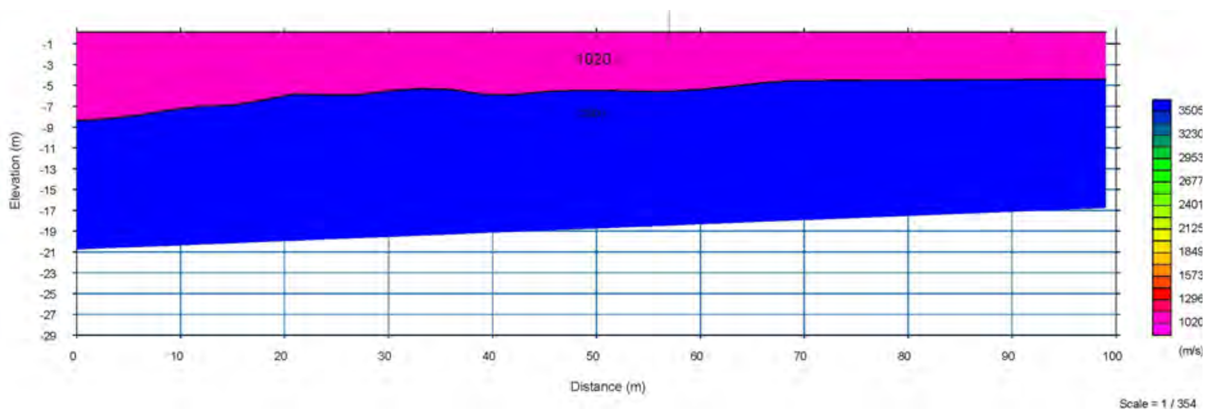

Figure 45: V_P model for Duck River site

Russellville High School Site

Location and Geology

The Russellville High School site is located at Russellville High School in Russellville AL (34.52492, -87.73752). Geophysical surveys were conducted on March 27, 2025. Topography of the site was flat with minimal vegetation at the time of the survey.

The site is underlain by the Gordo formation which is characterized by massive beds of cross-bedded sand, gravelly sand, and lenticular beds of locally carbonaceous partly mottled moderate red and pale red purple clay (Osborne et al., 1989). SPT borings were performed prior to additions on the school in 2020.

Data Collection

Two active MASW surveys were conducted at the site. The surveys used 24 4.5 Hz natural frequency geophones spaced at 1.5 meters for a total spread length of 34.5 meters. Data were recorded with a sampling frequency of 2000 Hz, a recording length of 1.5 seconds, an offset of 0 seconds, and a delay of -0.1 seconds. No acquisition filters were used. Energy sources were placed at multiple locations along the spread, with off-end, end on, and split-spread shots being used.

MASW Results

An example dispersion curve alongside the 10 best fit inverted ground profiles for the first MASW survey are shown in Figure 46. Considering the inverted profile with the minimum value of misfit indicates that there are 5 layers present. The first layer extends to a depth of approximately 0.9m (3ft) and has a V_S of 110 m/s (361 ft/s). This corresponds with the layer of soft sandy lean clay present directly below the ground surface. The second layer extends to a depth of 2.4m (8ft) and has a V_S of 146 m/s (479 ft/s). This layer corresponds with the layer of sandy silty clay directly underlying the previous layer of sandy lean clay. The next layer extends to a depth of 3.9m (13ft) and has a V_S of 285 m/s (935 ft/s). This layer corresponds with the layer of clayey gravel encountered in the SPT boring. The next layer extends to a depth of 5.4m (18ft) and has a V_S of 500 m/s (1640 ft/s). This corresponds with the layer of sandy fat clay encountered in the SPT boring. The final layer extends to a depth of 30m from the inverted ground profiles but can only be directly compared to the SPT boring to a depth of 7.6m (25ft) where the boring was terminated. This layer is subject to more uncertainty than shallower layers, but all profiles agree that it is stiffer than the shallower layers. The V_S of this layer is 677 m/s (2221 ft/s) and corresponds with a layer of clayey gravel encountered in the SPT boring. This V_S profile gives a V_{S30} of 486 m/s (1594 ft/s) and places the site into class C.

An example dispersion curve alongside the 10 best fit inverted ground profiles for the second MASW survey are shown in Figure 47. Considering the inverted profile with the minimum value of misfit indicates that there are two layers present as opposed to the 5 for the first survey line. SPT boring logs agree with the results of these inverted ground models only showing a layer of sandy lean clay overlying a layer of fat clay. The layer of sandy lean clay extends to a depth of 4.75m (16ft) and has a V_S of 236 m/s (774 ft/s). The underlying fat clay extends to a depth of 7.6m (25ft) in the SPT boring while the inverted ground profile extends to a depth of 30m (100ft). This layer has a V_S of 492 m/s (1614 ft/s). This ground profile is subject to more uncertainty as the value of misfit of the inverted model is greater than those of survey line 1. This V_S profile gives a V_{S30} of 427 m/s (1400 ft/s) which places the site into the upper bound of class C/D.

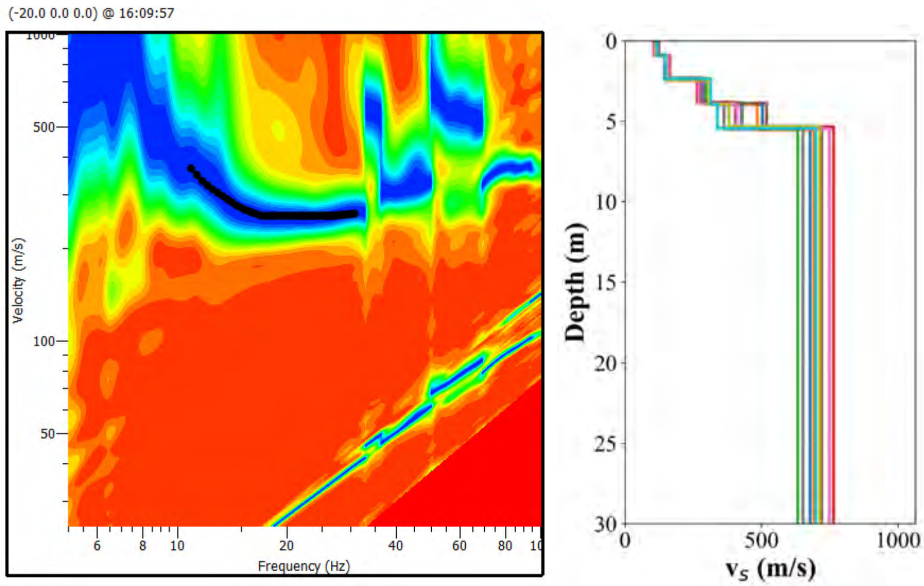

Figure 46: Results of first MASW survey conducted at Russellville High School site showing (A) dispersion and (B) the 10 best fit inverted ground profiles

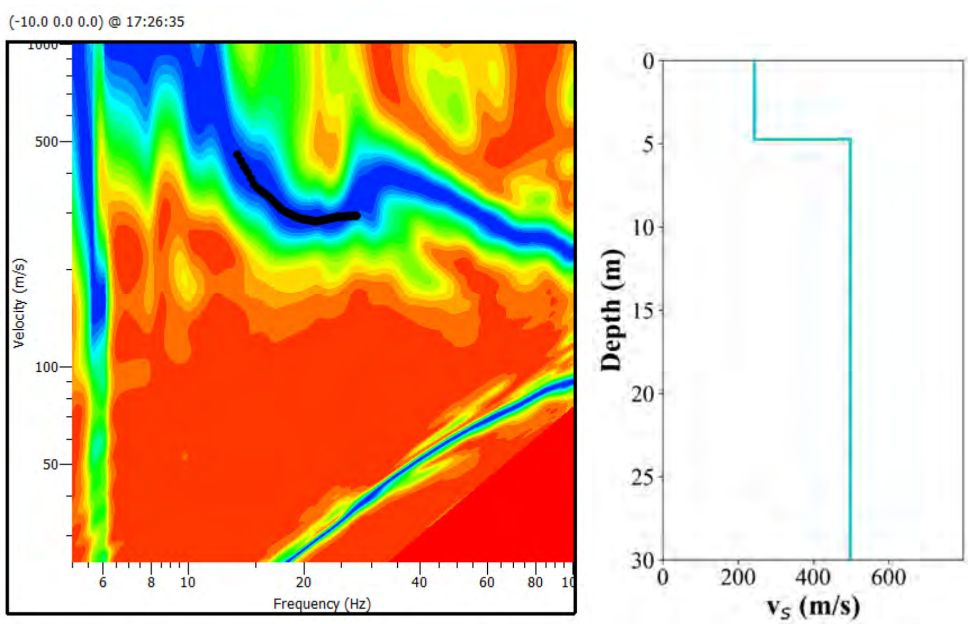

Figure 47: Results of second MASW survey conducted at Russellville High School site showing (A) dispersion and (B) the 10 best fit inverted ground profiles

Bluewater Creek Site

Location and Geology

The Bluewater creek site located near a bridge over the Bluewater creek along State Route 2 in Lauderdale County Alabama (34.85717, -87.41544). Geophysical surveys were conducted on March 27, 2025. Topography of the site was relatively flat with little vegetation at the time of the survey.

The site is located within the Fort Payne Chert formation which is characterized by light gray medium to finely crystalized limestone (Osborne et al., 1989). Rock was encountered at a shallow depth around 10 ft (3 m), and in some areas in the site a thin layer of limestone is encountered that is overlying clay. Rock coring was performed on the underlying limestone and RQD ranges from as low as 36% up to 97%.

Data Collection

MASW was selected as the survey technique for this site due to proximity to State Route 2. A single active MASW survey was conducted at the site. The survey used 24 14 Hz natural frequency geophones spaced at 1.5 meters for a total spread length of 34.5 meters. Data were recorded with a sampling frequency of 2000 Hz, a recording length of 1.5 seconds, an offset of 0 seconds, and a delay of -0.1 seconds. No acquisition filters were used. Energy sources were placed at multiple locations along the spread, with off-end, end on, and split-spread shots being used.

MASW Results

An example dispersion curve alongside the 10 best fit inverted ground profiles for the MASW survey are shown in Figure 48. Considering the inverted profile with the minimum value of misfit indicates there are 4 layers present. The first layer extends to a depth of 0.9m (3ft) and has a V_S of 250 m/s (820 ft/s). This layer corresponds with the layer of lean clay observed near the ground surface. The next layer observed extends to a depth of 3.1m (10ft) and has a V_S of 259 m/s (850 ft/s). This corresponds with the layer of clayey sand with gravel observed in the boring. These two layers are very close in magnitude of V_S and also have SPT blowcounts that are close in magnitude (11 and 12 respectively). The next layer extends to a depth of 7.3m (24ft) and has a V_S of 417 m/s (1368 ft/s). This layer corresponds with the layer of clayey sand with gravel observed in the SPT boring. The final layer has a V_S of 1220 m/s (4002 ft/s). This layer likely corresponds with limestone encountered at the site though inversion analysis indicates that it is encountered at

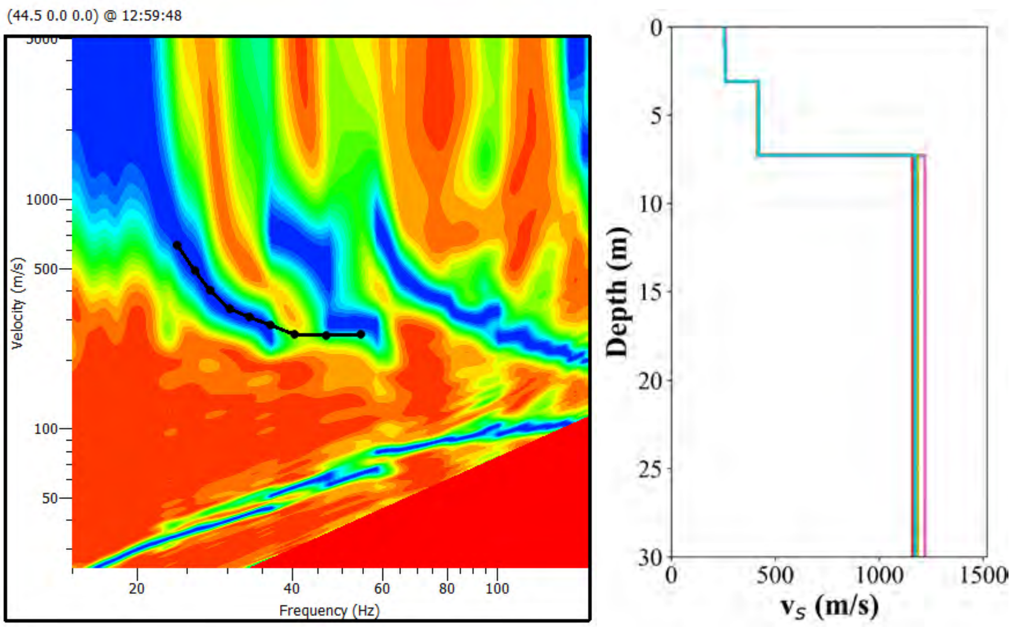

Figure 48: Results of MASW survey conducted at Bluewater Creek site showing (A) dispersion and (B) the 10 best fit inverted ground profiles

a shallower depth as compared to the locations where borings were performed. This V_S profile gives the site a V_{S30} of 735 m/s (2411 ft/s) which places the site into class B/C.

Lauderdale County Site

Location and Geology

The Lauderdale County site is located alongside County Road 8 in Florence Alabama near a bridge overpass (34.95055, -87.69541). Geophysical surveys were conducted on March 28, 2025. Topography at the site was flat with minimal vegetation. The site was open and access to locations of borings on both sides of the bridge was possible. Due to the ease of access, two survey lines were laid out at the site. The first survey line was located approximately 100 meters (328 feet) from Lauderdale County Road 8 into a large clearing in the wooded area local to the site. The second survey line was located approximately 10 meters (33 feet) off of the road. Survey line 1 is shown in Figure 49.

The Lauderdale County site is underlain by the Fort Payne Chert formation which is characterized by light gray medium to finely crystalized limestone. Boring logs from the immediate area indicate that depth to rock was relatively shallow, 9 feet (2.65 meters) in depth at the shallowest.

Figure 49: First seismic survey line at Lauderdale County site

Data Collection.

MASW and refraction surveys were used at this site. The MASW surveys used 24 14 Hz natural frequency geophones spaced at 1.5 meters for a total spread length of 34.5 meters. Data were recorded with a sampling frequency of 2000 Hz, a recording length of 1.5 seconds, an offset of 0 seconds, and a delay of -0.1 seconds. The refraction surveys used 24 14 Hz natural frequency geophones spaced at 1.5 meters for a total spread length of 34.5 meters. Data were recorded with a sampling frequency of 16000 Hz, a recording length of 1.5 seconds, an offset of 0 seconds, and a delay of -0.1 seconds No acquisition filters were used. Energy sources were placed at multiple locations along the spread, with off-end, end on, and split-spread shots being used.

Refraction Results

Results of refraction surveys were only reliable from the first survey location. Travel time curves presented in Figure 51 indicate a two layered system. Inversion analysis was performed to calculate the compressional wave velocity model presented in Figure 50. V_P/V_S ratios of 0.4 and 0.6 were used to calculate the probable range of V_S for the site and are presented in Table 13. Extending the lower layer to a depth of 30m and using a median value of V_S from the probable range gives a V_{S30} of 691 m/s (2,267 ft/s) which places the site into class B/C.

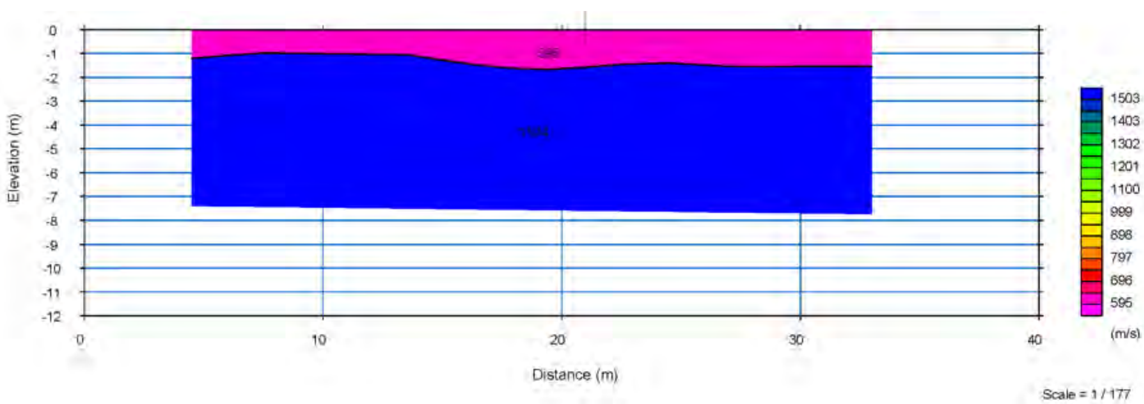

Figure 50: V_P model for Lauderdale County site

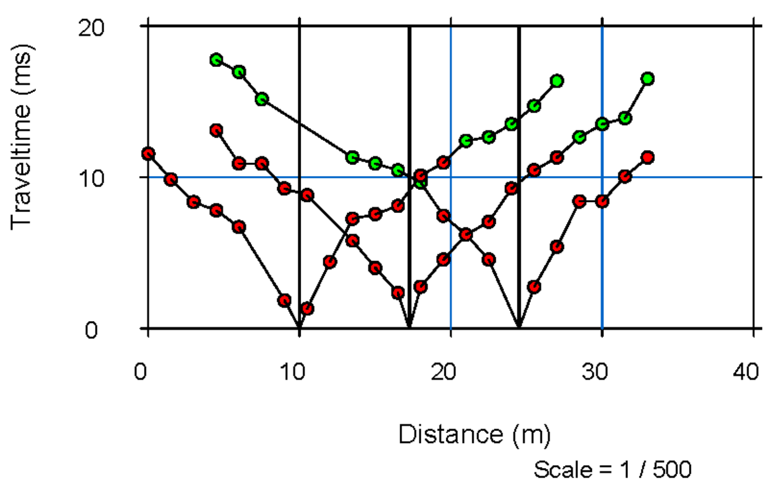

Figure 51: Appended travel time curves for Lauderdale County site

Table 13: Calculated range of V_S profile for Lauderdale County site

Parameter	Layer 1	Layer 2
Compressional Wave Velocity (m/s)	595	1504
Shear Wave Velocity (lower bound m/s)	238	601.6
Shear Wave Velocity (upper bound m/s)	357	902.4

MASW Results

MASW results were only reliable for the second survey line. An example dispersion curve alongside the 10 best fit inverted ground profiles for the second MASW survey are shown in Figure 52. Considering the inverted profile with the minimum value of misfit indicates there are two layers present. The first layer extends to a depth of 4m (13ft) and has a V_S of 412 m/s (1351 ft/s). This layer corresponds with the layer of clay encountered in the SPT boring. The second layer has a V_S of 1086 m/s (3562 ft/s). At this layer in the SPT boring, fragments of chert begin appearing in the clay before limestone was encountered but a clear transition to rock was not observed in the inverted ground profiles. This V_S profile gives a V_{S30} of 886 m/s (2906 ft/s) which places the site into the upper end of class B/C.

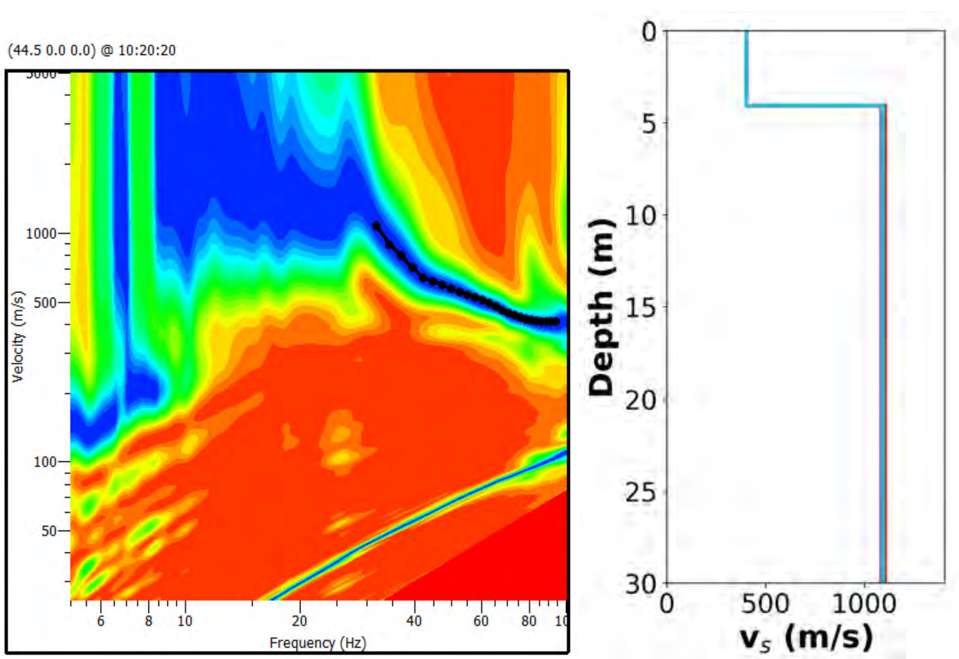

Figure 52: Results of second MASW survey conducted at Lauderdale County site showing (A) dispersion and (B) the 10 best fit inverted ground profiles

Blount County Site

Location and Geology

The Blount County site is located alongside US Highway 231 in Oneonta Alabama (33.93987, -86.39477). Geophysical surveys were performed on May 6, 2025. Topography of the site was flat with minimal vegetation at the time of the survey.

The site is underlain by the lower portion of the Pottsville formation which is characterized by light gray thin to thick bedded quartzose sandstone and conglomerate containing interbedded dark gray shale, siltstone, and coal. Boring logs from the site indicate that soils to be encountered were clayey and the water table was relatively shallow. Sandstone was encountered at a shallow depth in all of the borings performed at the site.

Data Collection

Due to the presence of shallower rock at the site the seismic refraction technique was used. A single active refraction survey was conducted at the site. The survey used 24 14 Hz natural frequency geophones spaced at 3 meters for a total spread length of 69 meters. Data were recorded with a sampling frequency of 16000 Hz, a recording length of 1.5 seconds, an offset of 0 seconds, and a delay of -0.1 seconds. No acquisition filters were used. Energy sources were placed at multiple locations along the spread, with off-end and end on shots being used. A minimum of 5 shots were taken at each location for stacking to increase signal to noise ratio.

Refraction Results

Travel time curves presented in Figure 53 indicate a two layered system. Inversion analysis was performed to calculate the compressional wave velocity model presented in Figure 54. V_P/V_S ratios of 0.4 and 0.6 were used to calculate the probable range of V_S for the site and are presented in Table 14. Extending the lower layer to a depth of 30m and using a median value of V_S from the probable range gives a V_{S30} of 1178 m/s (3,864 ft/s) which places the site into class B.

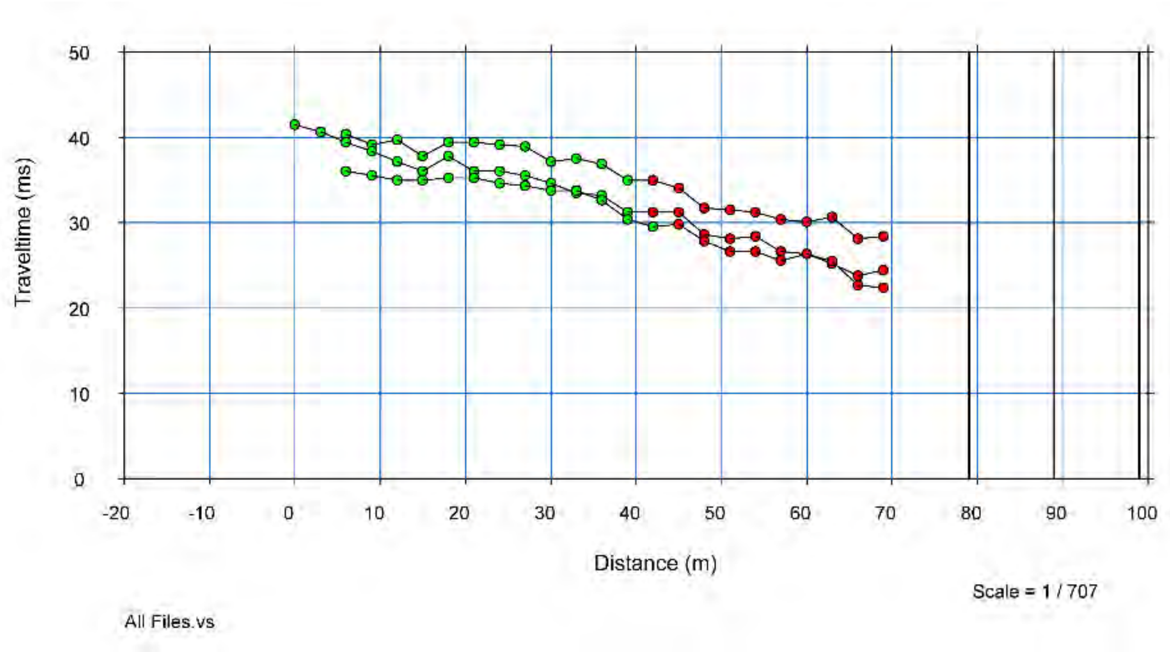

Figure 53: Appended travel time curves for Blount County Site

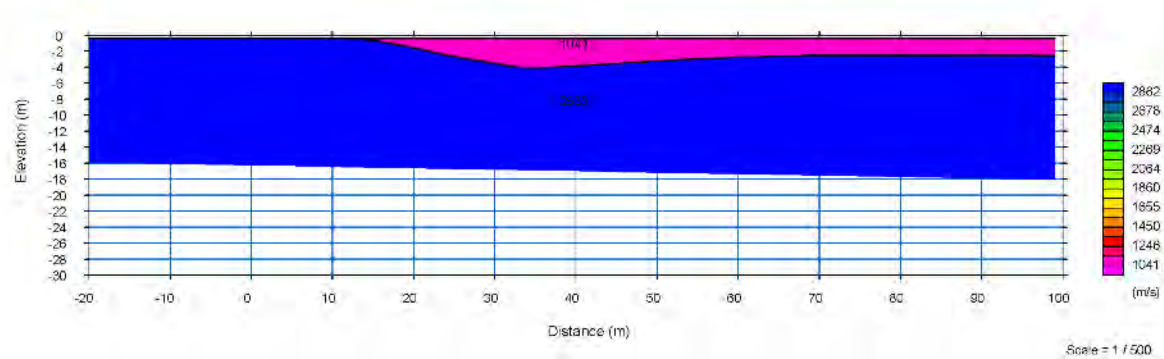

Figure 54: V_P model for Blount County site

Table 14: Calculated range of V_S profile for Blount County site

Parameter	Layer 1	Layer 2
Compressional Wave Velocity (m/s)	1041	2883
Shear Wave Velocity (lower bound m/s)	416.4	1153.2
Shear Wave Velocity (upper bound m/s)	624.6	1729.8

3.4 Summary of Tested Sites

The fifteen sites tested in this study are shown along with the sites tested by Carcamo (2022) in Figure 55. This represents the full database, which will be used to evaluate the correlations in the next chapter. As shown in this figure, the majority of the sites in the northern and northeastern portions of the state would be classified as B or BC indicating rock at relatively shallow depths. This is expected based on the geology in these regions. In the western and southern part of the state where the coastal plain is located, the sites tend to be softer as expected. There are of course exceptions where local conditions differ from these regional patterns, but the overall pattern of site class results is consistent with expectations based on the geology.

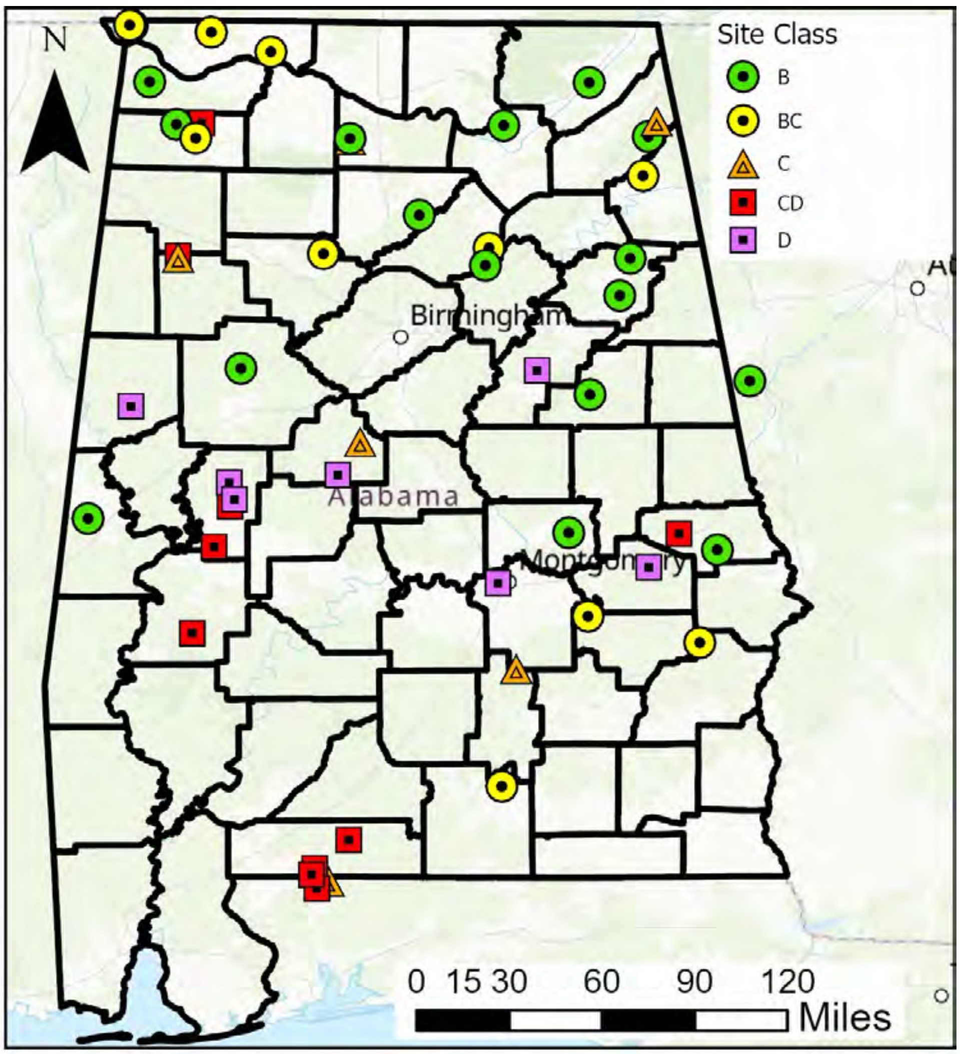

Figure 55: Map of Alabama showing the locations of the sites tested in this study and Carcamo (2022). Each symbol indicates the site class as determined by the measured V_S profile.

3.5 HVSR Testing

3.5.1 Recording Devices

Single station triaxial geophones were used to record the horizontal (North and East) and vertical (Z) components of the passive signals. Three recorders were acquired for this project from two brands as described hereafter.

GEObit - GEOtinyMK3 Digital Seismometer

Two GEObit GEOtinyMK3 compact digital seismometers (Figure 56) were procured to record ambient vibration data during field measurements. The instrument integrates a three-component seismic sensor, digitizer, and recorder within a single enclosure and utilizes a high-resolution 24-bit analog-to-digital converter with configurable sampling rates ranging from 1 to 1000 samples per second. The system includes an internal GPS receiver that synchronizes measurements to Coordinated Universal Time (UTC), ensuring accurate timing and consistency across sites. The Geobit instrument provides a broadband operational bandwidth of approximately 10 s to 98 Hz, enabling reliable recording of low-frequency ambient vibrations relevant to site response characterization. The instrument is 130 mm (5.1 in) in diameter and 115 mm (4.5 in) in height with a weight of 2.6 kg (5.7 lb). The unit operates on a 9-18 VDC power supply with low power consumption and is designed for continuous operation in harsh field environments (GEObit Instruments 2023). The measurement is configured through the instrument's network interface over an ethernet connection. During measurement, the recorded data were stored locally on a removable SD card within the device but typically retrieved over the ethernet interface. The interface was connected over a manually configured network settings using a static IPv4 address (192.168.1.2) with subnet mask (255.255.255.0) and gateway (192.168.1.1).

Figure 56. GEOtinyMK3 low power compact digital seismometer (GEObit Instruments 2023)

PASI - GEMINI-2 HVSR Data Acquisition System

One PASI GEMINI-2 HVSR data acquisition unit was also acquired. The instrument is a portable triaxial geophone system specifically designed for HVSR testing. The instrument consists of three orthogonally oriented geophones housed within a waterproof container and coupled to a dedicated 24-bit digital acquisition system connected to a field computer via USB interface. The triaxial sensor has a natural frequency of approximately 2 Hz (±10%), which is well suited for detecting the low-frequency ground motions associated with soil resonance and site fundamental frequency estimation. The system allows user-defined acquisition parameters such as sampling interval, recording duration, trigger conditions, and signal stacking, enabling flexible data collection under varying field conditions. The instrument has compact dimensions of approximately 128 mm (5 in) in diameter and 80 mm (3.1 in) in height and a weight of about 2.10 kg (4.6 lb), facilitating rapid deployment and stable placement during field measurements (PASI 2013).

Figure 57. PASI Gemini-2 HVSR data acquisition unit (PASI 2013)

3.5.2 Data Collection

The reliability of the HVSR depends on consistent measurement procedures, appropriate data processing, and careful interpretation of the results. Established guidelines emphasize the importance of standardized acquisition and quality control procedures to ensure that HVSR measurements produce statistically meaningful estimates of site frequency (SESAME 2004). The duration of the signal recordings is typically controlled by the minimum expected frequency peak of the site, and the recommended values are presented in Table 15.

Table 15. Recommended minimum recording duration according to expected frequency peak (SESAME 2004)

Minimum Expected f_0 Hz	**Recommended minimum recording duration Minutes**
0.2	30
0.5	20
1	10
2	5
5	3
10	2

Generally, artifacts with high stiffness were avoided, hence the recordings were located as far from buildings, trees, and utilities as possible. At all the sites in this study, a consistent setup was used to ensure that the devices were isolated and well coupled into the testing site. This was achieved by burying the sensor over half the sensor height with granular material (usually sand) and covering the buried device with a plastic bucket (Figure 58) as specified by Foti et al. (2018). Figure 59 shows images of field deployment of each instrument used in this study as well as the connection type.

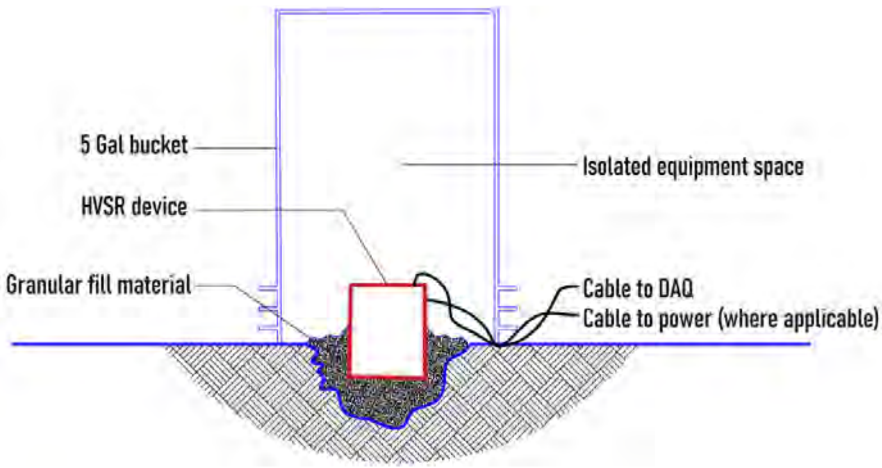

Figure 58. Equipment setup used at various sites for HVSR signal collection

(a) **(b)** **(c)**

Figure 59. Field deployment of (a) PASI Gemini (USB connection to PC), (b) Geotiny_21 (https://192.168.1.21:9091), and (c) Geotiny_30 (https://192.168.1.30:9091)

3.5.3 Data Analysis

HVSR analysis was performed on ambient vibration records collected using three-component seismic sensors to estimate the fundamental site frequency and support site characterization. The recorded time histories were first screened to remove transient noise and align the three components. The signals were then divided into stationary time windows of equal duration for frequency-domain processing. For each window, Fourier amplitude spectra of the horizontal and vertical components were computed, smoothed using the linear-rectangular function, and combined to generate individual HVSR curves, from which a representative median curve and associated statistical parameters were determined. The reliability and clarity of the HVSR peak were evaluated in accordance with the SESAME guidelines (SESAME 2004). Reliability checks assess the stability and repeatability of the HVSR curve while clarity checks evaluate the definition of the spectral peak and consider factors such as peak amplitude, frequency stability, and the absence of competing peaks within adjacent frequency bands to ensure that the identified resonance frequency represents a distinct and physically meaningful site response. The criteria for the checks are presented in SESAME (2004).

3.5.4 Results

The open-source tool ***HVSRpy*** by Vantassel (2025) was used to analyze the collected data. Forty-six (46) distinct HVSR recordings were collected in total using a combination of the triaxial geophones already described. Figure 60 shows a typical plot of the signals recorded by the three components of the triaxial geophones (the North-South, the East-West, and the vertical components). The signal plot was from survey line 1 of the Blount County site located in Northwest Alabama.

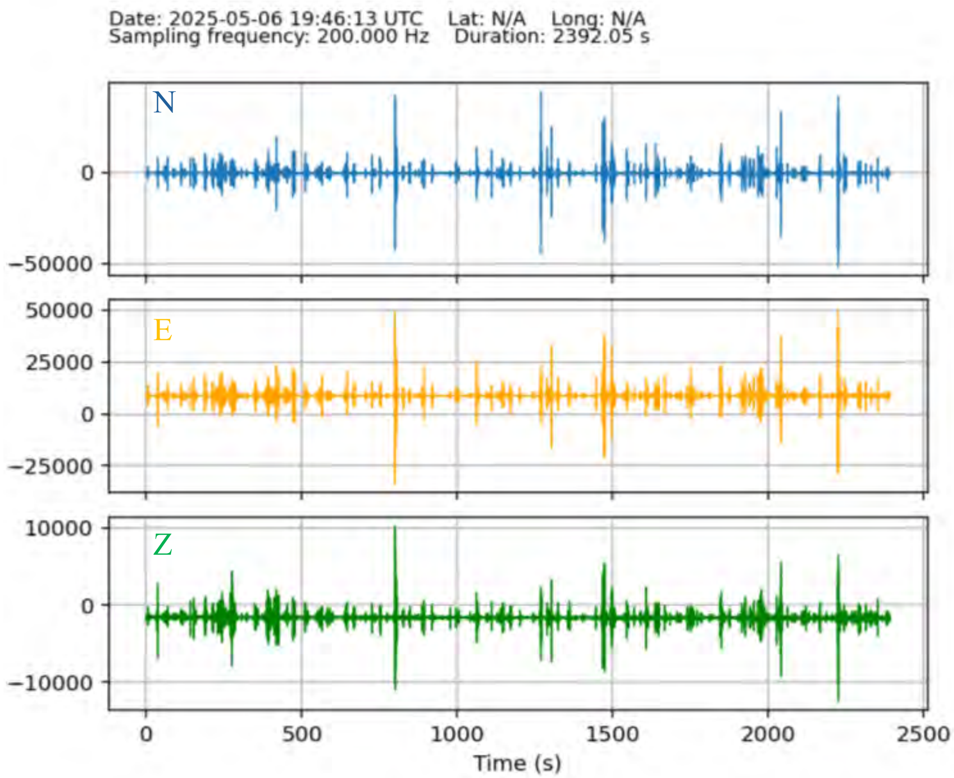

Figure 60. Signals (N, E, and Z) from passive survey at Blount County-Northwest Alabama

The HVSR analysis of this recording produced a well-defined peak at a frequency of 15 Hz with a corresponding peak amplitude of 8.6. The analysis was conducted over a frequency range of 0.1 to 50 Hz using an 80-second window length, with 29 accepted windows contributing to the final mean HVSR curve. The variability in the peak frequency, represented by a standard deviation (σf_n) of 2.926 Hz, falls within acceptable limits for stable peak identification and satisfies both the clarity and reliability criteria defined by the SESAME (2004) guidelines.

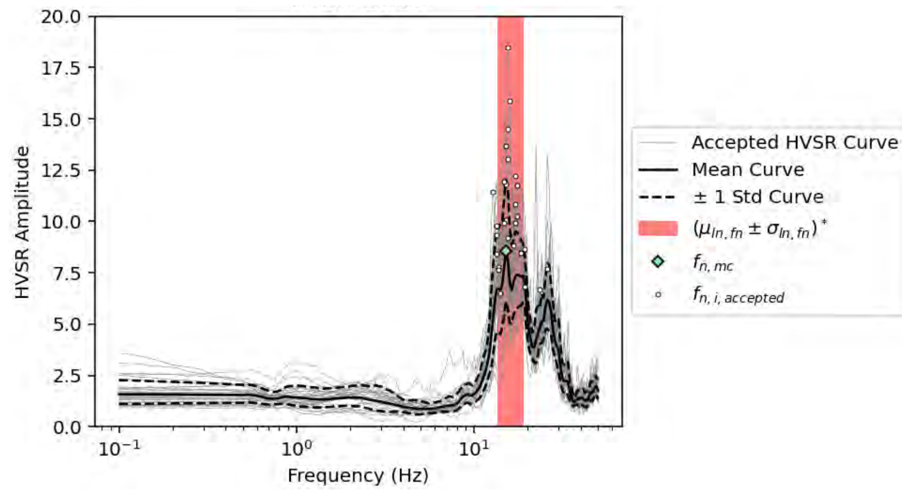

Figure 61: HVSR curves for the Blount County site - Northwest Alabama

For brevity, the results from all the sites are presented in Table 16. The presented results include the fundamental frequencies, the amplitudes, reliability checks and clarity checks.

Table 16. Summary of HVSR results from all sites sorted by region within the state

Region	Site name	Line number	Instrument	f_0 (Hz)	$f_0 - \sigma_{log}$ (Hz)	$f_0+\sigma_{log}$ (Hz)	A_0	σ_A	Sampling Frequency (Hz)	Reliable	Clear
Northwest Alabama Sites	Blount County	Line 1	GTN21	15.1	12.8	17.9	8.4	3.5	200	✓	x
		Line 1	GTN30	15.1	12.6	18.3	9.2	3.4	200	✓	✓
		Line 1	PASI	18.0	14.7	21.9	6.2	3.4	200	✓	x
	Blue water creek	Line 1	GTN21	24.1	15.3	37.8	4.6	2.4	200	✓	✓
		Line 1	GTN30	50.3	39.9	63.4	2.6	0.4	200	✓	✓
		Line 1	PASI	19.8	16.5	23.8	1.8	0.5	200	✓	x
	Duck River	Line 1	GTN21	18.0	17.0	19.0	4.8	2.1	200	✓	✓
		Line 1	GTN30	18.0	12.1	26.7	4.6	1.6	200	✓	✓
		Line 1	PASI	18.0	14.1	22.9	3.9	2.1	200	✓	x
	Lauderdale County	Line 1	GTN21	24.6	13.3	45.3	1.9	0.8	200	✓	x
		Line 1	GTN30	24.3	20.1	29.5	2.0	0.8	200	✓	x
		Line 1	PASI	26.2	21.2	32.4	1.4	0.4	200	✓	x
	Lauderdale County	Line 2	GTN21	24.4	12.8	46.3	4.8	2.2	200	✓	✓
		Line 2	GTN30	26.4	14.6	47.7	7.0	4.5	200	x	x
		Line 2	PASI	26.4	18.9	36.9	3.3	1.7	200	✓	✓
	Russelville HS	Line 1	GTN21	5.7	3.8	8.6	2.6	0.5	200	✓	x
		Line 1	GTN30	6.4	1.6	25.0	2.6	0.8	200	✓	x
		Line 1	PASI	6.6	2.2	19.5	1.8	1.4	200	✓	x
	Russelville HS	Line 2	GTN21	7.0	5.2	9.5	2.4	0.9	200	✓	x
		Line 2	GTN30	7.0	5.3	9.3	3.0	0.7	200	✓	x
		Line 2	PASI	7.9	5.1	12.3	0.8	0.2	200	✓	x
West Alabama Sites	Beaver Creek	Line 1	GTN21	3.9	2.6	6.0	3.7	1.7	200	x	x
		Line 1	PASI	6.9	5.4	8.7	3.3	1.6	100	✓	x
	Beaver Creek	Line 2	GTN21	7.3	5.1	10.6	1.9	0.9	200	✓	x
		Line 2	GTN30	7.3	5.3	9.9	1.8	0.8	200	✓	x
		Line 2	PASI	6.6	5.9	7.4	2.1	0.6	100	✓	✓
	Big Prairie Creek	Line 1	GTN21	6.2	3.1	12.5	2.8	1.4	200	✓	x
		Line 1	GTN21_B	6.6	4.0	10.9	3.6	1.9	200	✓	x
		Line 1	GTN30	6.6	6.3	7.0	5.0	1.8	200	✓	✓
		Line 1	GTN30_B	6.5	5.0	8.5	4.5	1.6	200	✓	x
		Line 1	PASI	6.2	3.6	10.8	2.5	1.2	100	✓	x
	Big Prairie Creek	Line 2	GTN21	7.2	6.6	8.0	7.9	1.4	200	✓	✓
		Line 2	GTN30	6.9	6.4	7.5	8.8	1.2	200	✓	x
		Line 2	GTN30_B	6.5	4.6	9.3	4.1	1.6	200	✓	x
	Coldwell Creek	Line 1	GTN21	0.9	0.2	4.8	2.0	0.2	200	✓	x
		Line 1	PASI	5.6	2.7	11.7	1.7	0.4	200	✓	x
	Coldwell Creek	Line 2	GTN30	0.8	0.2	3.2	2.0	0.4	200	✓	x
	Greensboro	Line 1	GTN21	3.6	0.8	16.7	2.8	1.5	200	✓	x
		Line 1	PASI	3.5	1.1	10.9	2.1	0.6	100	✓	x
	Moundville	Line 1	GTN21	0.6	0.5	0.7	4.7	1.6	200	✓	✓
		Line 1	PASI	1.0	0.1	9.5	1.6	0.7	100	✓	x
	Moundville	Line 2	GTN21	0.6	0.5	0.7	4.1	1.2	200	✓	✓
		Line 2	GTN30	0.6	0.5	0.7	4.8	1.3	200	✓	✓
		Line 2	PASI	0.4	0.0	5.9	1.4	0.4	200	✓	x
	Cedar Bluff	Line 1	GTN21	10.1	4.1	25.3	4.2	1.8	200	x	x
		Line 1	GTN30	9.2	3.0	28.7	3.1	1.7	200	✓	x
		Line 1	PASI	10.0	4.4	22.9	3.8	3.0	200	x	x

3.6 Summary

To properly evaluate the correlations presented in Chapter 2 of this report, direct measurements at multiple sites across the state were needed. Sites considered were at the location of bridges or other infrastructure where in-situ data is available for these correlations to be applied. Sites were located within the Western and Northwestern corridors of the state which have a higher degree of seismic activity as compared to the rest of the state. Direct measurements at these sites consist of either MASW or refraction surveys. A summary of sites selected for seismic surveys is provided in Table 11.

Equipment for MASW and refraction surveys were nearly identical with the only common difference being the fundamental frequency of geophones used. Refraction surveys used 14 Hz fundamental frequency geophones while most MASW surveys used 4.5 HZ fundamental frequency geophones with the exception of MASW surveys conducted alongside refraction surveys. Energy sources and the seismograph were identical for both survey types. Recording parameters were nearly identical with the only difference being in sampling frequency.

MASW surveys were conducted at sites with a deeper depth to bedrock as shallower rock will tend to cause interference due to higher modes which interfere with the fundamental mode required to perform inversion analysis. MASW data were processed using the open source Geopsy software package provided by Wathelet et al. (2020a). Dispersion curves were picked from individual signal files and averaged for inversion. Inversion was performed in DINVER, also included in the Geopsy software package. DINVER requires input parameters such as $V_{P,}$ V_S, Poisson's ratio, density, and layering. Inversion is performed by the software and misfit values are assigned to generated ground profiles along with the dispersion curves required to generate ground profiles. The ground profile with the lowest value of misfit is generally considered to be the most reliable profile for the site.

Refraction surveys were conducted at sites with shallower bedrock where higher modes would interfere with the researchers' ability to select a dispersion curve from the fundamental mode. Refraction data were processed using the SeisImager software package provided by Geometrics. Multiple shots were taken at each location to stack in postprocessing to increase the signal to noise ratio. First arrivals of P-waves were selected from the signal files. Changes in slope of the first arrivals reflect arrivals of critically refracted waves from a deeper layer of higher velocity. The number of slope changes indicates the number of layers present. Plotrefra, also provided by Geometrics, was used for inversion of ground models of V_P. V_P was then converted to V_S using known ratios.

Field surveys were conducted at all of the sites documented in Table 11. Active surveys along with passive HVSR surveys were conducted at all sites. The first site visited was located near Cedar Bluff, AL and a V_{S30} of 686 m/s was measured using a MASW survey (class B/C). The aggregated group of sites within the West Alabama corridor were all surveyed using the MASW technique as rock was not encountered in any of the boring logs. All sites with the exception of the Greensboro site are placed into class C/D with the Greensboro site being classified into class D. The sites within the Northwest corridor are more varied than those in the Western corridor. MASW was used at sites with deeper rock while refraction was used at shallower rock sites. Measured values of V_{S30} were generally higher than those measured at West AL sites with the Duck River and Blount County sites being classified into class B, the Bluewater Creek and Lauderdale County sites being classified as class B/C, and the Russellville High School site being classified as C and C/D.

HVSR surveys were conducted using three separate sensors. Two of the sensors were GEOtinyMK3 low power compact digital seismometers while the third was a PASI GEMINI-2. At all sites sensors were partially buried using granular material and covered with a 5-gallon bucket to ensure sensors were isolated and well coupled with the ground, in accordance with guidelines presented in Foti et al. (2018). Transient noise was screened and the three recording components were aligned before the signal was divided into equal length components for use in analysis. Fourier amplitude spectra were then computed, smoothed, and then combined to get HVSR curves for each of the sites. The reliability and clarity of the HVSR peak were then checked using SESAME guidelines. Of the 46 distinct HVSR curves, only 6 did not pass the reliability check.

4 EVALUATION OF SHEAR WAVE VELOCITY CORRELATIONS FOR USE IN ALABAMA

4.1 Introduction

One of the key tasks in the current project was to evaluate existing V_S and V_{S30} correlations to understand which ones were most applicable to sites in Alabama. The sites described in Chapter 3 were used to compare the SPT-based and HVSR-based correlations. These were supplemented by the database of sites from Carcamo (2022) to evaluate geospatial correlations. Only a subset of the comparisons are presented here, reflecting the most promising correlations. The full set of comparisons are shown in McLeod (2026).

4.2 Comparisons of SPT Estimation Methods

To evaluate the SPT-based correlations, blowcounts from borings performed near the seismic surveys were compared with the measured V_S profiles. Pairs of measured and estimated V_S values were then compared. Before performing these comparisons, the boring logs were screened to eliminate artificially high or low blowcounts, such as those were the sampler met refusal (i.e., a blowcount of 50/0.5" or similar) or when hollow stem augers were used to sample sandy soils below the water table. This is a characteristic sign of soil disturbance or heave, which is commonly observed when hollow stem augers are used to collect SPT blow counts in sandy soils below the water table. The National Academies report (2021) on state of the practice in liquefaction evaluation states that "SPT blow counts recorded in hollow stem auger borings below the water table are particularly susceptible to error due to soil disturbance and may result in abnormally low blow count values."

Comparisons were made in terms of both 1:1 plots to understand overall agreement and residuals. Residuals were calculated in natural log units in order to give more equal weight to estimation error at lower and higher velocities. Residuals were then analyzed to determine any biases within the data. To determine agreement between measured and estimated data, mean squared error was calculated. A lower mean squared error reflects a better fit with the measured data. The relative error in the comparisons was also compared with the uncertainty bounds of $\pm$30% required in the AASHTO Guide Specifications when using correlations.

4.2.1 *Imai and Tonouchi (1982)*

The SPT-based estimation method with the lowest mean squared error when applied to all soils from this study was Imai and Tonouchi (1982) with a MSE of 0.377 (

(B)

Figure 62). The correlation tends to predict V_S within the $\pm$30% bounds but does tend to overpredict at lower velocities. At higher velocities (greater than 1450 ft/s), the equation tends to underpredict $V_{S.}$ Performance for clays, silts, and sands was comparable. From the 1:1 plot presented in **(B)**

Figure 62 (B), the correlation performs best for V_S less than 1450 ft/s).

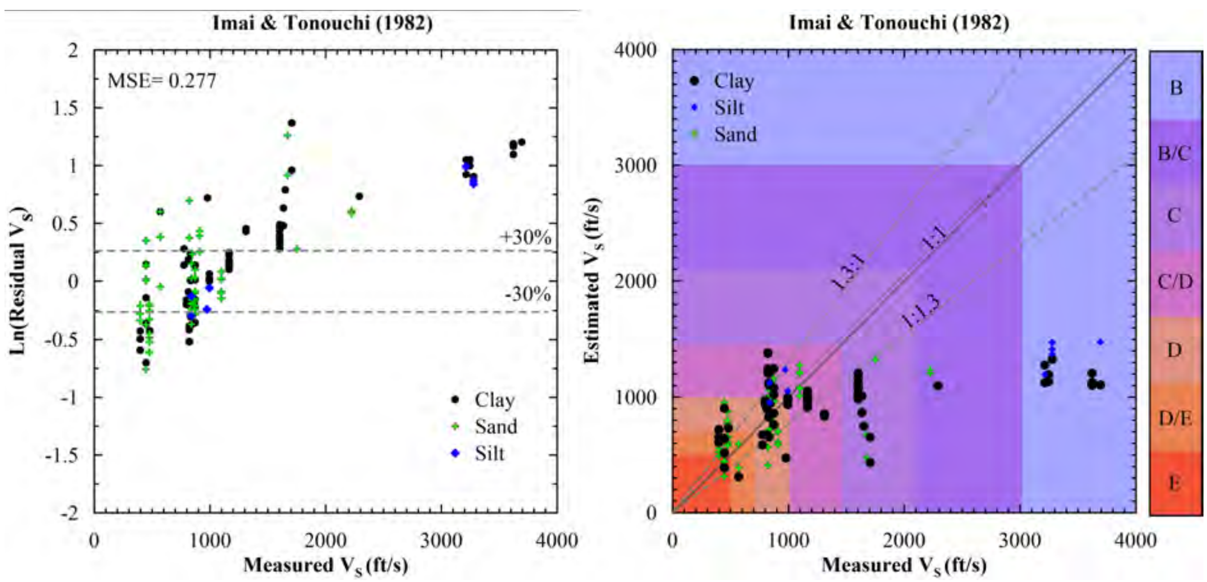

(A) **(B)**

Figure 62: Comparisons of estimated to measured V_S showing (A) residuals plotted against measured V_S and (B) 1:1 comparison of measured to estimated V_S for Imai and Tonouchi (1982) correlation equation

4.2.2 *Wair et al. (2012) - All Soils Correlation*

The second best performing SPT-based estimation method was the "All Soils" correlation presented by Wair et al. (2012) (

(B)

Figure 63). This correlation was more conservative than Imai and Tonouchi (1982), as reflected in the higher MSE of 0.574. This is because the correlation tends to underpredict V_S across the entire range of velocities encountered. Residuals of predicted V_S values tend to lie above the -30% bound recommended by AASHTO, indicating that the correlation can provide conservative estimates of V_S, which may be desirable to ensure that site class is not underpredicted, but may also lead to overly conservative designs if a higher SDC is estimated than actually applies at the site.

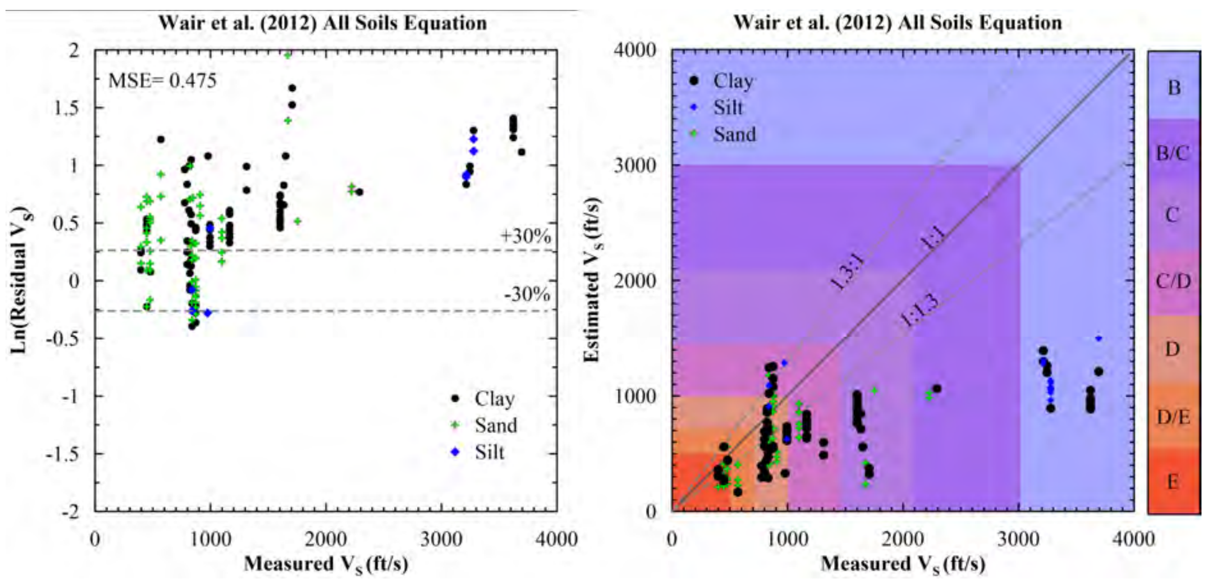

(A) **(B)**

Figure 63: Comparisons of estimated to measured V_S showing (A) residuals plotted against measured V_S and (B) 1:1 comparison of measured to estimated V_S for Wair et al (2012) all soils correlation equation

4.2.3 Performance of SPT-based Estimation Methods on Individual Soil Types

SPT-based estimation methods can also be evaluated for their performance on individual soil types. For this study soils were grouped into clays/silts and sands. Clays and silts were combined in a similar manner as some of the previously discussed studies within the literature review of this study. Additionally, silts have a low sample size within this study when eliminating blowcounts that indicate sampler refusal, only containing 8 viable blowcounts for analysis. Sands were considered as their own group. Gravels were not considered as a part of this study as gravels are not suitable for testing using conventional SPT methods.

Clays and Silts

The SPT-based estimation method with the lowest mean squared error when applied to clays and silts in this study was Imai and Tonouchi (1982) with a MSE of 0.361 (Figure 64). The

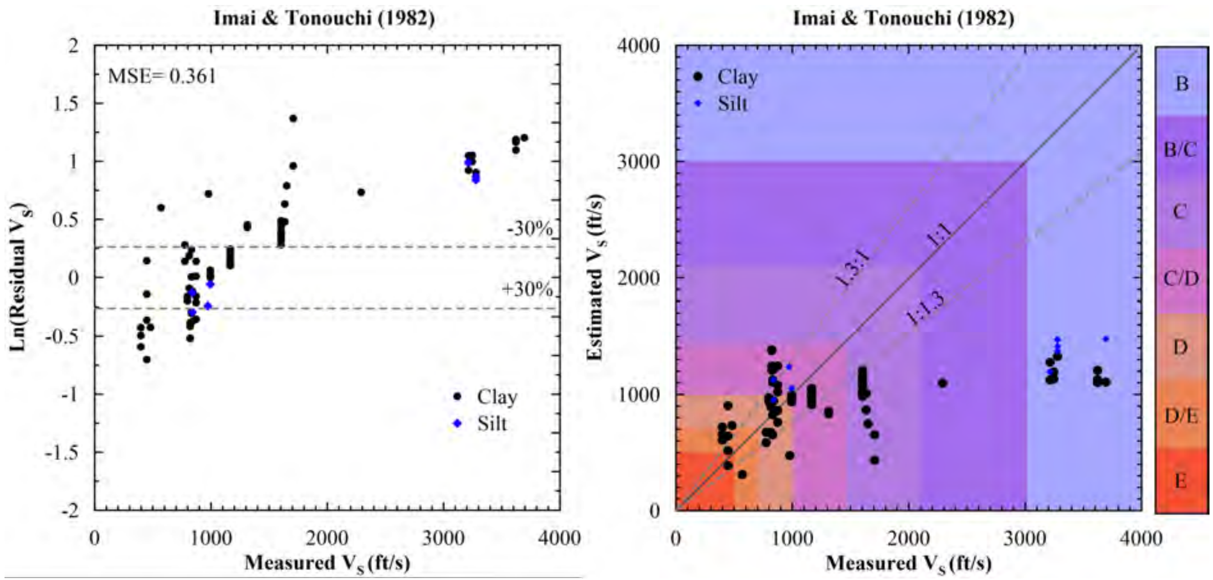

(A) **(B)**

Figure 64: Comparisons of estimated to measured V_S showing (A) residuals plotted against measured V_S and (B) 1:1 comparison of measured to estimated V_S for Imai and Tonouchi (1982) correlation equation for clays and silts

correlation tends to perform in a similar manner as when applied for all soils. From the 1:1 plot presented in Figure 64 (B), the correlation performs best for velocities that would fall into site classes C and lower (V_S of less than 1450 ft/s).

Sands

The SPT-based estimation method with the lowest mean squared error when applied to sands in this study was the energy corrected blowcount equation for sands presented in Hasancebi and Ulusay (2007) with a MSE of 0.387 (Figure 65). Residuals typically fall within the ±30% range recommended by the AASHTO Guide Specifications, with some tendency to overpredict at velocities around 500 ft/s. From the 1:1 plot presented in Figure 65 (B), the correlation performs best for velocities that would fall into site classes C and lower (V_S of less than 1450 ft/s).

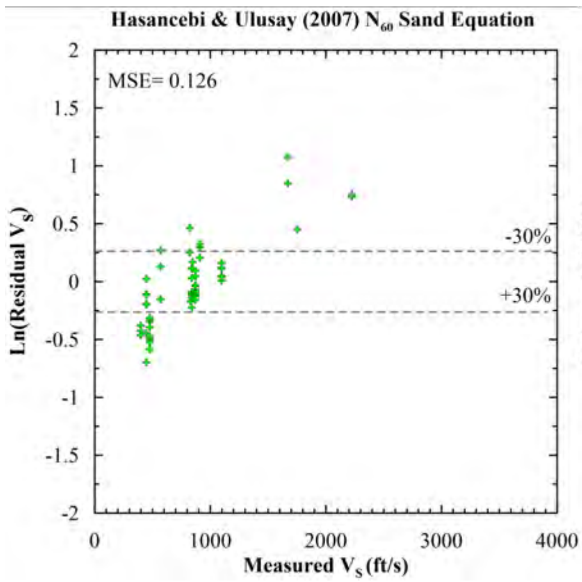

(B)

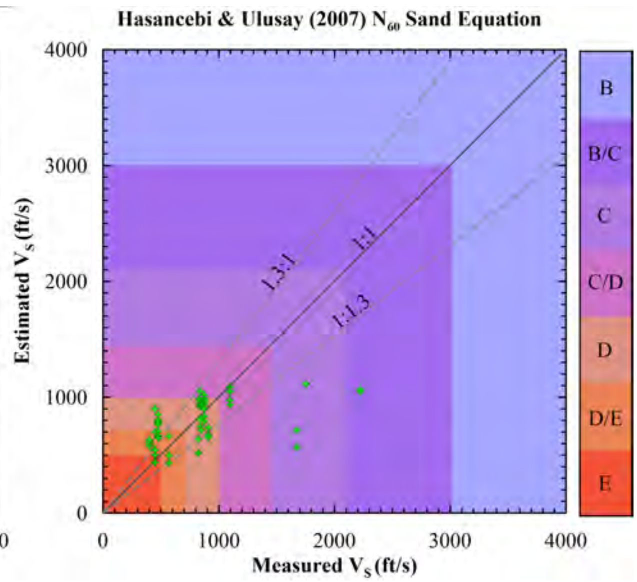

(B)

Figure 65: Comparisons of estimated to measured V_S showing (A) residuals plotted against measured V_S and (B) 1:1 comparison of measured to estimated V_S for Imai and Tonouchi (1982) correlation equation for clays and silts

4.2.4 Summary of Findings from SPT-based Correlations

SPT-based correlations can provide a reasonable estimate of V_S at lower velocities but tend to underestimate higher velocities. With these limitations, SPT-based correlations would be best used as a preliminary check to estimate V_{S30} and site class to determine the SDC. If this check indicates SDC B, a direct measurement should be taken as these correlations tend to underpredict velocities for stiffer sites and can artificially increase risk.

4.3 Comparisons of RQD Based Estimation Methods

RQD based estimation methods were applied to the appropriate sites in the same manner as SPT-based estimation methods. All rock encountered at the sites visited as a part of this study was classified as sedimentary rock so only the El-Naqa (1996), and Biringen and Davie (2013) sedimentary rock equations were able to be applied. Residuals were calculated in natural log units and mean squared error was calculated for the three correlation equations.

4.3.1 *El-Naqa (1996)*

The correlation equation presented in El-Naqa (1996) has significant scatter as seen in Figure 66. Only 2 data points fell within the ±30% range suggested by AASHTO (2023) for estimating V_S. This indicates that the correlation equation is a poor fit for the sites analyzed in this study. This is also reflected in the higher MSE of 2.305.

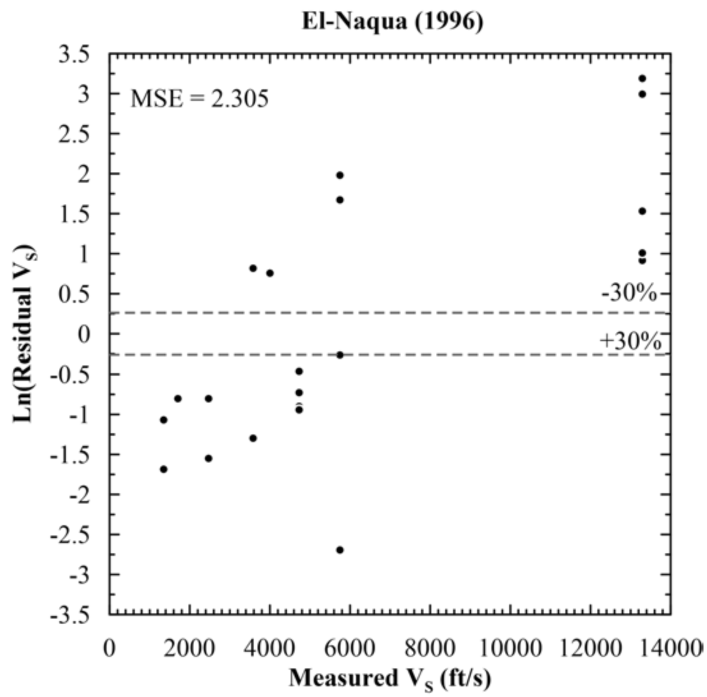

Figure 66: Residual plot of El-Naqa (1996) correlation equation for rock

4.3.2 *Biringen and Davie (2013)*

Both the Key Largo and Fort Thompson correlation equations were able to be applied to rock encountered in this study. The Key Largo correlation equation, shown in Figure 68, has a lower MSE as compared to the correlation equation presented in El-Naqa (1996) but most residuals are negative indicating that the equation was unconservative by overpredicting V_S. The Fort Thompson equation, shown in Figure 67, performs better than the Key Largo equation for sites in this study as reflected by a lower MSE of 0.779. More data points fall within the +-30% range required by AASHTO but for lower values of V_S (less than 4000 ft/s) the equation will tend to overpredict V_S making it potentially unconservative.

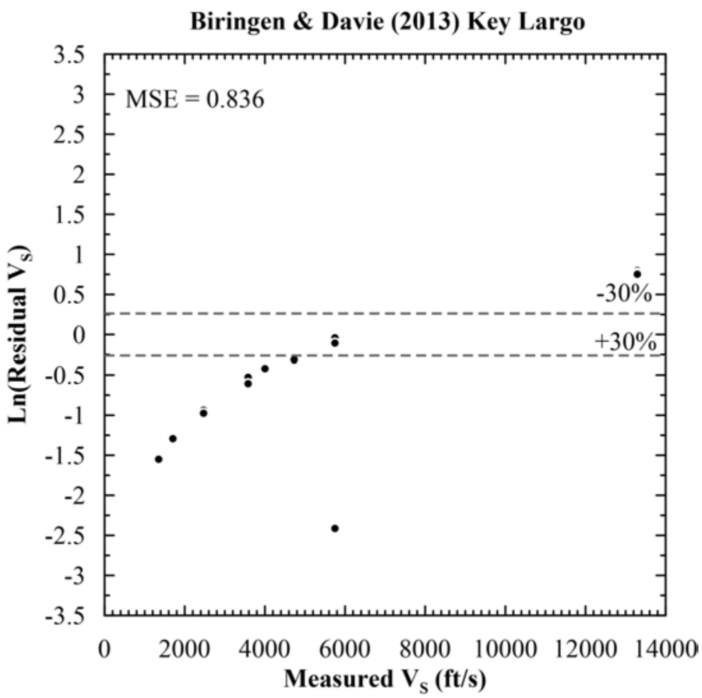

Figure 68: Residual plot of Biringen and Davie (2013) Key Largo correlation equation

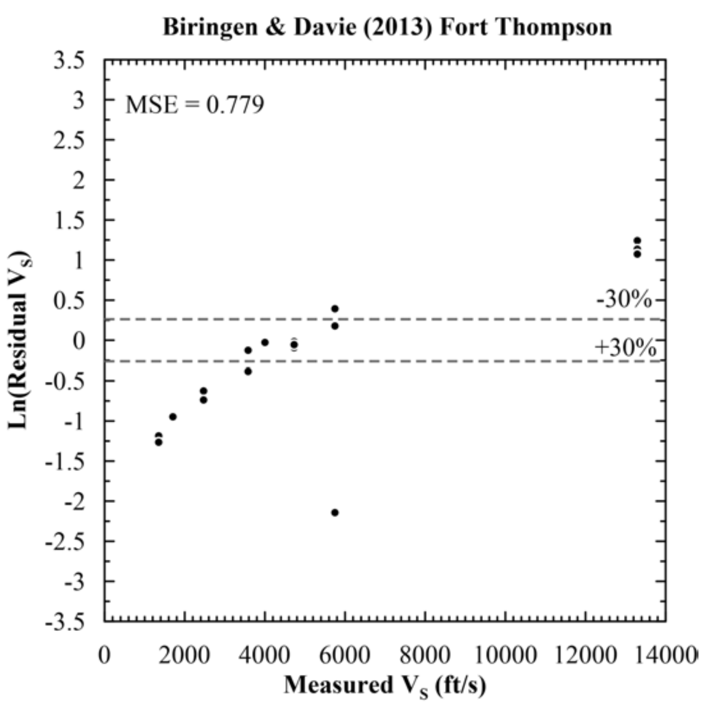

Figure 67: Residual plot of Biringen and Davie (2013) Fort Thompson correlation equation

4.3.3 Summary of Findings from RQD Correlations

RQD-based correlations exhibit greater scatter than SPT-based correlations, particularly in the El-Naqa (1996) equation. For lower measured velocities, the Biringen and Davie (2013) equations tend to overpredict velocities due to the linear fit of their regression models. At higher velocities (greater than 3500 ft/s) the Ft. Thompson equation provided more reasonable estimates of V_S while the Key Largo equation still tends to overpredict. Given the limited database and large uncertainty, the existing RQD-based correlations are not likely to be reliable in Alabama. As previously discussed, rock sites are unlikely to fall into SDC B and so the use for rock correlations in this study is limited.

4.4 HVSR-Based Correlations

The SESAME reliability and clarity checks for the HVSR curves are presented in Table 16. The HVSR results used for the correlation to V_{S30} presented hereafter are only from HVSR curves that passed the reliability check. The four correlation methods described in Chapter 2 were applied to the outputs of the HVSR analyses (f_0 and A_0).

4.4.1 Stanko & Markušić (2020)

Figure 69 shows the measured versus HVSR-based estimated values of V_{S30} using the Stanko and Markušić (2020) model. Several data points at measured V_{S30} values near about 800 to 1500 ft/s plot well above the 1:1 line, indicating overestimation, while other points at measured values around 2000 to 4000 ft/s fall well below the line, indicating underestimation. The spread was wide, and most of points lie outside the 1:1.3 and 1.3:1 bounds. Several estimated V_{S30} had the same value of 2000 ft/s, and this is due to the cut-off criteria in the equation for f_0 between 10 and 30 Hz. 7 out of 32 data points (18%) fall within the ±30% bounds recommended by AASHTO, indicating that most estimates fall outside the recommended tolerance. Of the four HVSR based methods, this had the most percentage of points outside the ±30% bounds.

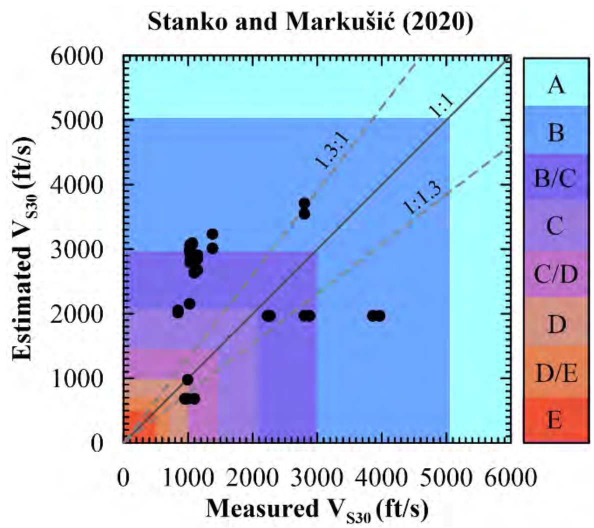

Figure 69. Comparisons of measured to HVSR-based estimated values of V_{S30} using Stanko and Markušić (2020)

4.4.2 McNamara et al. (2015)

Figure 70 shows the measured versus HVSR-based estimated values of V_{S30} using the McNamara et al. (2015) model. The data generally followed the increasing trend defined by the 1:1 line, although scatter is still present across the full velocity range. There are more data points falling close to the 1:1 trend and within the ±30% bounds, however, the distribution of points indicates a tendency toward overestimation for several sites. 16 out of 38 data points (42%) fall within the ±30% recommended by AASHTO, indicating moderate agreement between estimated and measured V_{S30} values.

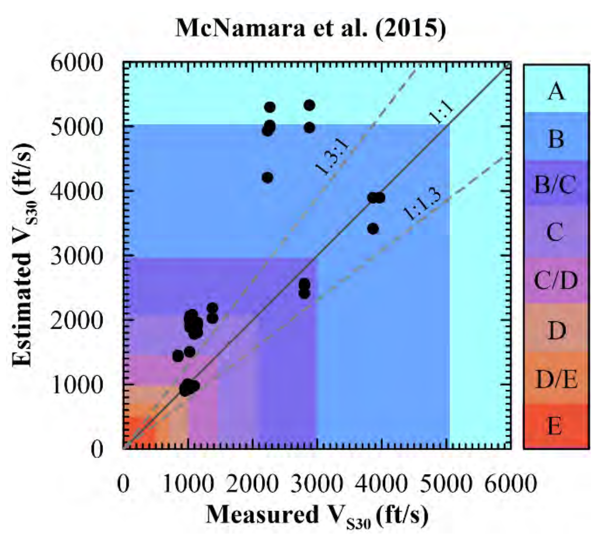

Figure 70. Comparisons of measured to HVSR-based estimated values of V_{S30} using McNamara et al. (2015)

4.4.3 Hassani and Atkinson (2016).

Figure 71 shows the relationship between measured V_{S30} and estimated V_{S30} using the Hassani and Atkinson (2016) model. The data generally followed the increasing trend defined by the 1:1 line, although scatter is still present across the full velocity range. 16 out of 38 data points (42%) fall within the ±30% recommended by AASHTO, also indicating moderate agreement between estimated and measured V_{S30} values, however, the overall distribution appears more balanced around the reference lines compared to the other correlations.

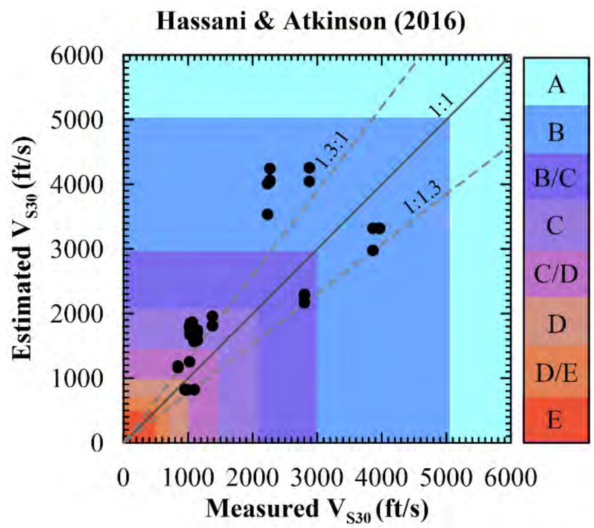

Figure 71. Comparisons of measured to HVSR-based estimated values of V_{S30} using Hassani and Atkinson (2016)

4.4.4 Ghofrani and Atkinson (2014)

Figure 72 presents the measured versus estimated V_{S30} values using the Ghofrani and Atkinson (2014) correlation. The data show a broad distribution across the velocity range, with both overestimation and underestimation observed at different measured V_{S30} levels. 19 out of 39 data points (48%) fell within the ±30% recommended by AASHTO, indicating moderate variability and a substantial portion of estimates outside the recommended tolerance.

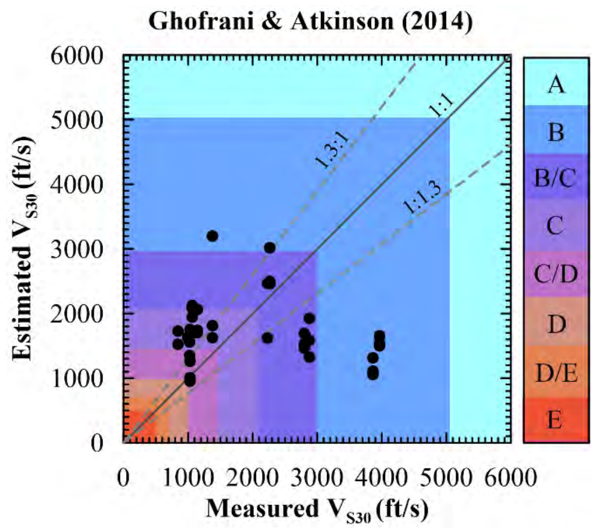

Figure 72. Comparisons of measured to HVSR-based estimated values of V_{S30} using Ghofrani and Atkinson (2014)

4.4.5 Sharma-Wagle et al. (2026)

Placeholder presents the measures versus estimated V_{S30} values using the four models presented in Sharma-Wagle et al. (2026). Low dimensional models provide similar performance with 20 and 27% of datapoints falling between the ±30% bound for the random forest (A) and gradient boosted (B) models respectively. Above a measured V_{S30} of approximately 1000 m/s both models tend to severely underpredict. High dimensional models perform similarly to low dimensional models with 18 and 28% of datapoints falling between the ±30% bound for the single (C) and dual artificial neural network (D) models, respectively. The high dimensional models do not perform as well at lower measured V_{S30} values where these two models have a tendency to overpredict.

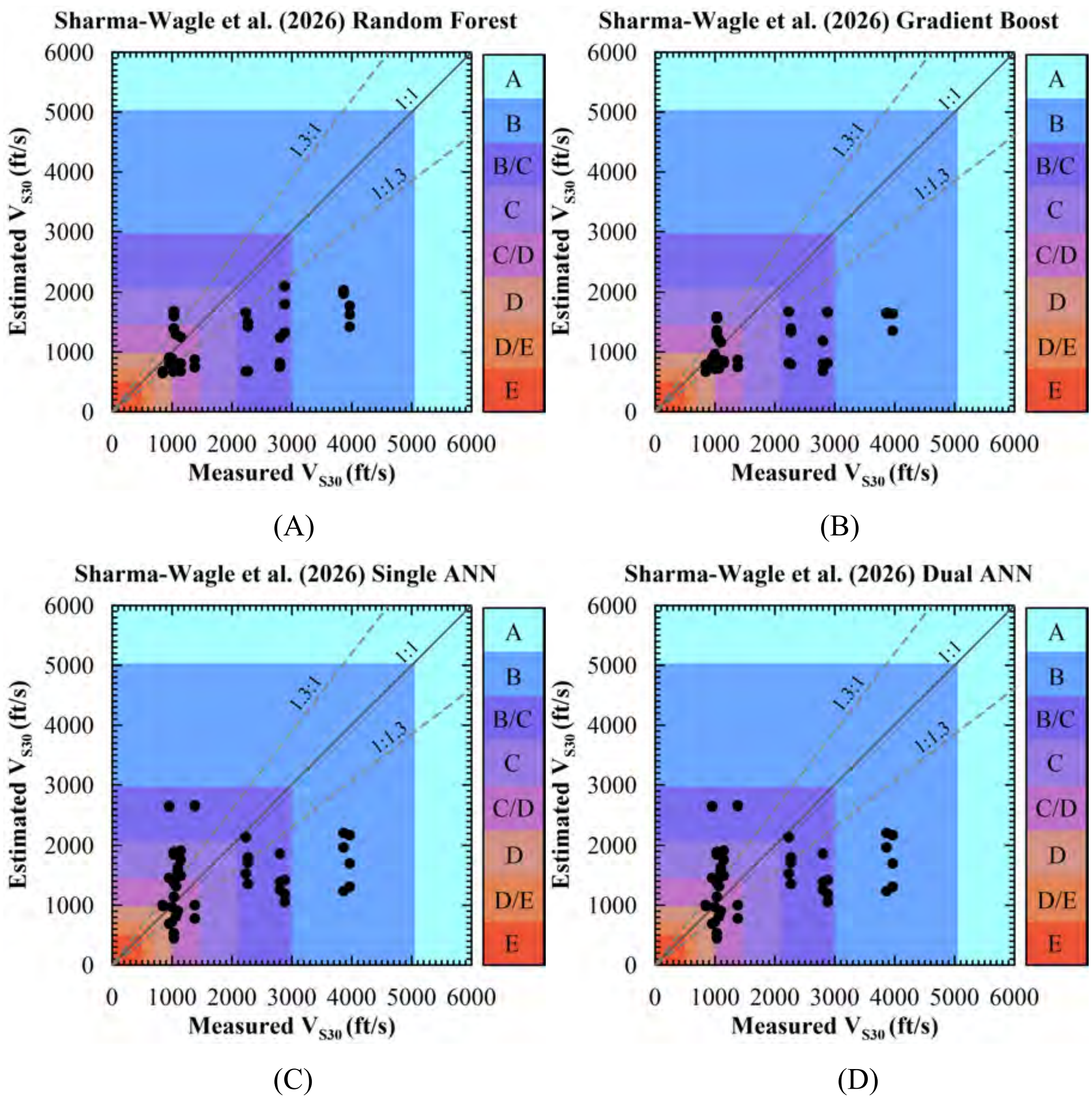

Figure 73. Comparisons of measured to HVSR-based estimated values of V_{S30} using the Sharma-Wagle et al. (2026) (A) random forest, (B) gradient boosted, (C) single artificial neural network, and (D) dual artificial neural network models

Based on NEHRP site class boundaries, the Hassani and Atkinson (2016) correlation produced the highest site class agreement with measured values (55%), followed by McNamara et al. (2015) (47%). Although the Ghofrani and Atkinson (2014) correlation produced a higher percentage of estimates within the ±30% bounds (38%) compared to the Stanko and Markušić (2020) correlation (18%), both methods resulted in nearly identical site class agreement rates of approximately 28%. This indicates that the higher numerical agreement observed for the Ghofrani and Atkinson (2014) model compared to the Stanko and Markušić (2020) did not correspond to improved site classification performance for these sites, likely due to the concentration of measured V_{S30} values near site class boundaries.

4.5 Geospatial Estimation Methods

Geospatial based estimation methods were applied to all sites from this study along with sites presented in Carcamo (2022). Values of V_{S30} were estimated using the models presented and residuals were calculated in natural log units. More detailed comparisons between the geospatial methods can be found in McLeod (2026). Of the methods presented in this study, the models from Geyin and Maurer (2023) and Gann-Phillips et al. (2024) performed the best.

4.5.1 *Geyin and Maurer (2023)*

The model presented in Geyin and Maurer (2023) was based on 17 geospatial factors and contains a database of 7,081 V_{S30} measurements. Estimated values are plotted 1:1 against measured values in Figure 74. Alongside the 1:1 line of a perfect fit of model to the data, additional lines of 1.3:1 and 1:1.3 represent the ±30% bounds recommended by AASHTO. For site classes C/D and below the model was most accurate. The model will tend to underpredict V_{S30} for stiffer sites.

4.5.2 *Gann-Phillips et al. (2024)*

The model presented in Gann-Phillips et al. (2024) was targeted exclusively for the Atlantic and Gulf coastal plains. The model was developed using 441 V_S profiles from the region. Estimated values are plotted 1:1 against measured values in Figure 75. Alongside the 1:1 line of a perfect fit of model to the data, additional lines of 1.3:1 and 1:1.3 represent the ±30% bounds recommended by AASHTO. The model is applicable only to coastal plain geology and therefore only to lower-velocity sites (classes CD and below). For these regions, the model was more effective than the model presented in Geyin and Maurer (2023), with a MSE of 0.0913. For sites within the coastal plain, the model provided the most accurate estimate of V_{S30} among the methods presented in this report.

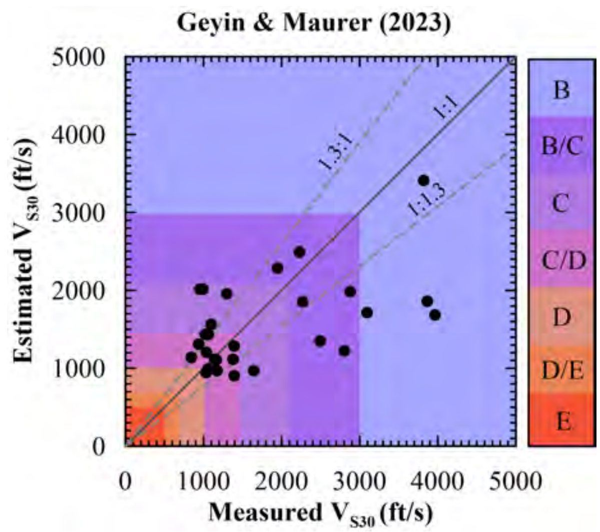

Figure 74: Comparisons of measured to estimated values of V_{S30} using Geyin and Maurer (2023) model

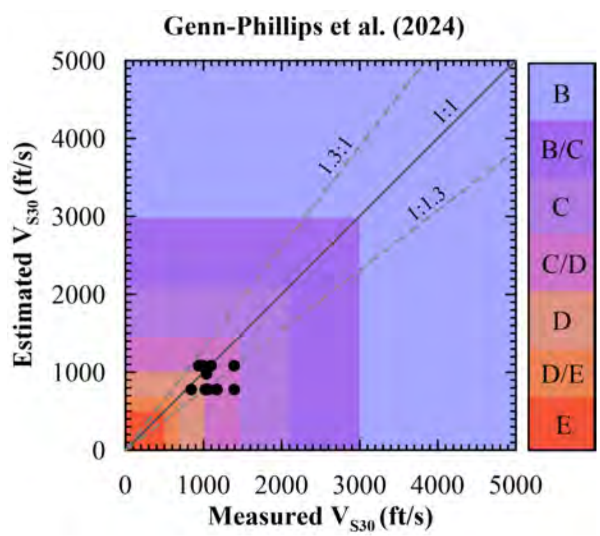

Figure 75: Comparisons of measured to estimated values of V_{S30} using Gann-Phillips et al. (2024) model

4.6 Summary

Of the SPT-based correlations evaluated as a part of this study, two performed best. The correlation presented in Imai and Tonouchi (1982) provided the best fit for SPT-based methods when applied to all soils with a MSE of 0.377. Despite the better fit indicated by MSE, the correlation tends to be unconservative at lower velocities. The second correlation was the "all soils" equation presented in Wair et al. (2012) with a MSE of 0.574. While the greater value of

MSE indicates a poorer fit, the correlation was more conservative than the one presented in Imai and Tonouchi (1982). More conservative estimates may be desirable but do have the possibility of artificially increasing the design hazard if SDC is overestimated. Considering best fit for individual soil types, the Imai and Tonouchi (1982) equation still provided the best fit for clays and silts with a MSE of 0.361. For sands the energy corrected blowcount equation for sands was the best fit with a MSE of 0.387.

RQD-based correlations generally were more scattered than SPT-based ones. The correlation presented in El-Naqa (1996) was a poor fit for the measured data of this study, reflected in the MSE value of 1.24. The equations presented in Biringen and Davie (2013) provide a better fit with MSE values of 0.416 and 0.221 for the Key Largo and Ft. Thompson equations respectively. Despite a lower MSE of 0.221 as compared to the lowest MSE of 0.286 from SPT-based methods, the equation tends to more greatly overpredict at lower velocities being potentially unconservative. This is of lower consequence as compared to SPT-based correlations as sites where rock is encountered the site class will likely be higher and not necessitate seismic considerations in design.

HVSR-based methods show more scatter when plotted on 1:1 plots as compared to other methods presented in this study. The best fit correlation in terms of 1:1 fit was Ghofrani and Atkinson (2014) which does not have the same agreement when considering site class. When considering agreement of site class, the best fit correlation was Hassani and Atkinson (2016).

Geospatial correlations provide better fit to the measured data compared to SPT, RQD, and HVSR-based correlations. For general use the Geyin and Maurer (2023) model provided the best fit and is applicable to more regions of the state. When used on sites within the coastal plain, the model presented in Gann-Phillips et al. (2024) provided the best fit of any of the methods presented in this study.

5 RECOMMENDATIONS FOR DETERMINING SEISMIC SITE CLASS AT ALABAMA BRIDGE SITES

5.1 Introduction

As discussed in Chapter 2, the seismic hazard level at a site is represented by the SDC in the AASHTO Guide Specifications, which determines the level of design that is required for a bridge. The seismic hazard will change based on the site class, but this change may or may not result in differences in the SDC depending on the location in the state. As discussed in the previous chapter, available correlations for V_S and V_{S30} are highly uncertain and tend to underestimate velocities for the stiffer materials and sites. It is therefore important to understand where these underestimations may affect the SDC and, in turn, lead to unnecessary design effort and increased construction costs. To address this, this chapter first presents SDC maps for the state of Alabama. These maps were then used in conjunction with the findings from the previous chapter to develop recommendations for estimating site class and SDC at bridge sites.

5.2 Development of SDC Maps

The SDC maps for Alabama were created based on the 2023 AASHTO Guide Specifications for LRFD Seismic Bridge Design and the gridded seismic hazard values provided by the USGS for different site classes. For each grid point, the S_{D1} value was calculated using different site classes. This S_{D1} value was then used with Table 2 to determine the SDC. The full suite of maps is shown in Appendix A. Figure 76 presents the Seismic Design Categories for Alabama for Site Classes A, B, and BC. These site classes represent rock and stiffer soil conditions, which generally lead to lower ground-motion amplification. Under these site conditions, all of Alabama remains within the lower seismic design category (SDC A).

Figure 77 shows the SDC for site class C conditions, which represent stiff soil. The softer site conditions lead to greater amplification of ground motion parameters and, consequently, higher S_{D1} values. This increase in S_{D1} leads to areas of Lauderdale and Colbert Counties moving into SDC B. As the site class continues to soften, the area of the state that falls into SDC B also expands until reaching site class D conditions (Figure 78), which represents the most conservative scenario for Alabama. For these conditions, approximately 1/3 of the state falls into SDC B, which, as discussed in Chapter 2, requires increased design work and potentially higher construction costs to account for the increased seismic demand.

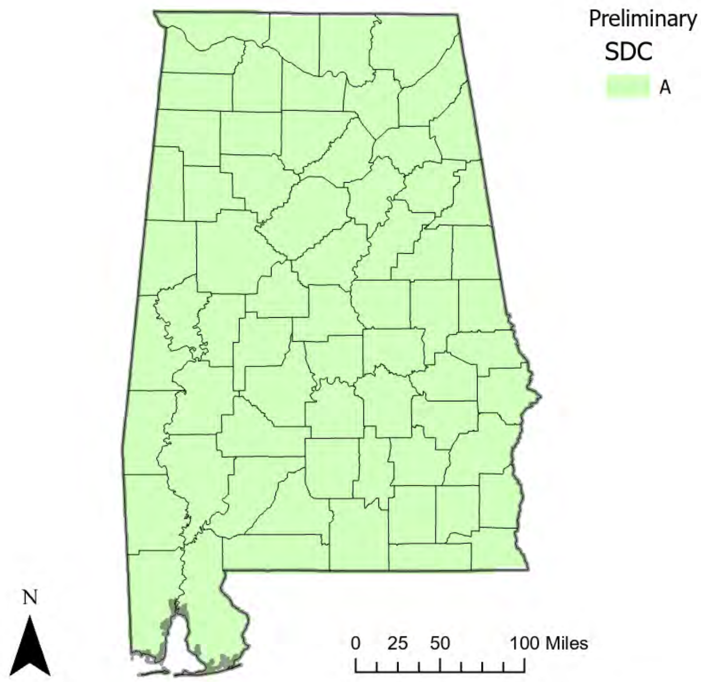

Figure 76: Alabama Seismic Design Categories (SDC) for Site Class A, B, BC

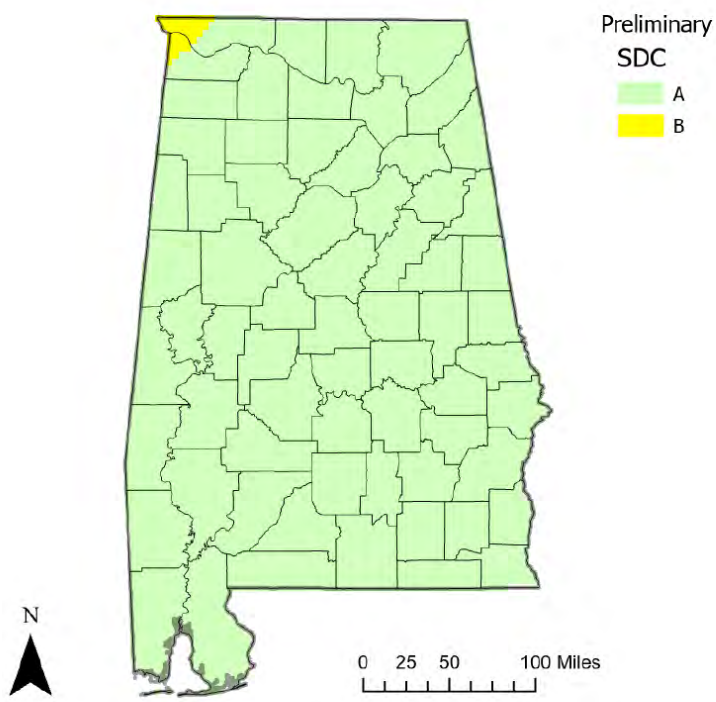

Figure 77: Alabama Seismic Design Categories (SDC) for Site Class C

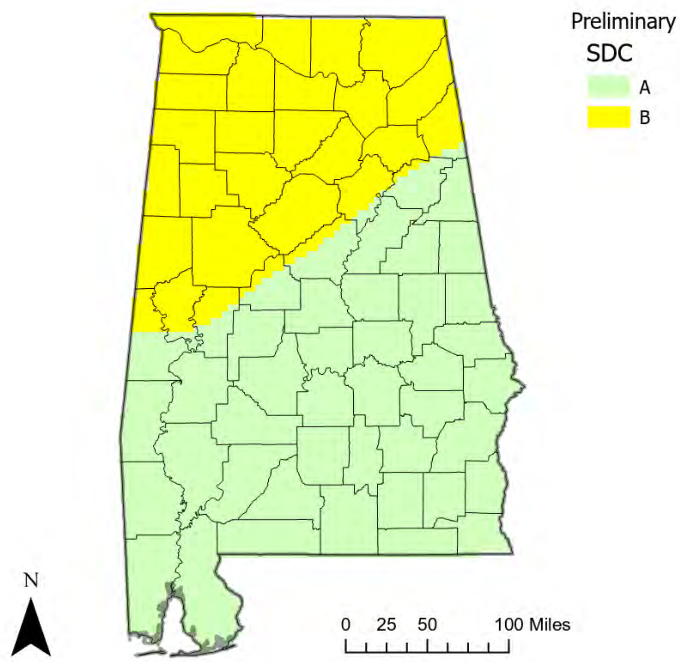

Figure 78: Alabama Seismic Design Categories (SDC) for Site Class D

In addition to the maps created as part of this study, ALDOT has developed and is testing a spreadsheet-based approach to directly estimate SDC using data from the USGS. This spreadsheet was still in the testing phase at the time this report was written, but is another good tool to estimate SDC based on the site class and location. While the spreadsheet and the maps use the same underlying data, the maps were created based on the gridded data and therefore have a coarser resolution than tools like the spreadsheet that pull interpolated data directly from the USGS. These differences are expected to be minor.

5.3 Recommended Procedure to Determine SDC

The AASHTO Guide Specifications have been reviewed to develop simplified flow charts for determining SDC for sites in Alabama based on the maps shown in the previous section. For rock sites (sites with less than 10 feet of soil), the Guide Specifications (Section 3.4.2.1) allow the engineer to assume site class BC for rock with moderate weathering or fracturing or site class C for sites with softer or more highly fractured and weathered rock. While the Guide Specifications do not provide definitions for these terms, Geotechnical Engineering Circular 5 (NHI 2017) does provide a table of rock weathering grades based on recommendations from the International

Society for Rock Mechanics. These grades are shown in Table 17. Based on this table, sites where the rock cores indicate only Grades I – III can be considered site class BC, while those with more than 10’ of Grades IV – VI can be considered site class C. Apart from Lauderdale and Colbert Counties, all rock sites, regardless of weathering, will fall into SDC A (Figure 77). Because of this, rock sites are not likely to benefit from shear wave velocity measurements unless they fall into this small region of the state where SDC B can be expected for weathered rock sites.

For soil sites (all sites that do not qualify as rock sites), the most conservative SDC can be estimated by assuming site class D. If an assumption of site class D leads to a site falling into SDC A (according to Figure 78), then there is likely no need for further analysis as changes in site class will not affect the SDC. For sites where assuming site class D would result in SDC B, a shear wave velocity profile should be estimated using either direct measurements or one of the correlations tested in Chapter 4. For direct measurements, the Guide Specification recommends considering at least 10% uncertainty in the V_{S30}. This increases to 30% for indirect methods. The most conservative SDC should then be selected, taking these uncertainties into account.

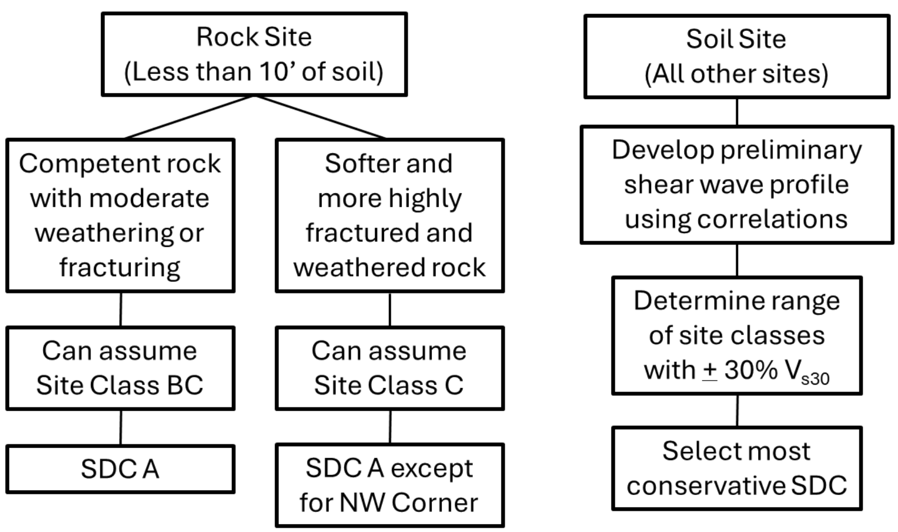

Figure 79. Flow chart showing recommended procedure for determining SDC in Alabama.

Table 17: Descriptions of different weathering grades for rock (after NHI 2017).

Term	**Description**	**Weathering Grade**
Fresh (F)	No visible sign of rock material weathering; slight discoloration on major discontinuity surfaces is possible.	I
Slightly Weathered (WS)	Discoloration indicates weathering of rock material and discontinuity surfaces. All rock material may be discolored by weathering and the external surface may be somewhat weaker than in its fresh condition.	II
Moderately Weathered (WM)	Less than half of the rock material is decomposed and/or disintegrated to a soil. Fresh or discolored rock is present either as a discontinuous framework or as corestones. A minimum 2 in. diameter sample cannot be broken readily by hand across the rock fabric.	III
Highly Weathered (WH)	More than half of the rock is decomposed and/or disintegrated to soil. Fresh or discolored rock is present either as a discontinuous framework or as corestones. A minimum 2 in. diameter sample can be broken readily by hand across the rock fabric.	IV
Completely Weathered (WC)	All rock material is decomposed and/or disintegrated to soil. The original mass structure is largely still intact. Material can by granulated by hand.	V
Residual Soil (RS)	All rock material is converted to soil. Material can be easily broken apart by hand.	VI

Based on the findings from Chapter 4, it is recommended that the Geyin and Maurer (2023) or Gann-Phillips et al. (2024) models be used first to develop a first estimate of site class. This can be completed even before borings are performed at the site. These estimates can then be confirmed through either in-situ testing or direct measurements during the site investigation phase of the project. To use these models, only the latitude and longitude and the surface geology is needed. The Geyin and Maurer (2023) is provided as a digital map and so the VS30 can be estimated directly based on the location. For the Gann-Phillips et al. (2024) model, geologic units in the coastal plain are binned and used to estimate V_{S30} (Table 18).

Table 18: Values for Median V_{S30} from Gann-Phillips et al. (2024) model

Geologic Group	Median Model V_{S30}
Quaternary Holocene	237
Quaternary Pliestocene	261
Tertiary	299
Cretaceous	331

The SPT-based correlations tested in this study had larger uncertainties than the recommended geospatial correlations and may be overly conservative for stiff sites. That does not mean they will not be useful in some situations, and a spreadsheet has been developed through this project to allow these correlations to be applied to boring log data. CPT-based correlations were not assessed in this project, but they are generally more reliable than SPT-based correlations and should be considered when CPT data are available. A second benefit of CPTs is that V_S profiles can often be measured simultaneously through downhole testing, which would eliminate the need for correlations or other tests.

5.4 Application to Sites from this Study

The recommended procedures for determining SDC were applied to the sites in this study to understand the distribution of SDC across the state. The results are shown in Figure 80. Almost all of the sites would fall in SDC A, but four of the sites in the western part of the state would fall into SDC B, even with direct measurements. This is due to the combination of relatively soft soil in those parts of the coastal plain and the higher seismic hazard in the northwestern part of the state. As discussed in Chapter 2, moving into SDC B increases the level of seismic design and the impacts of this on design approaches used by ALDOT will need to be examined.

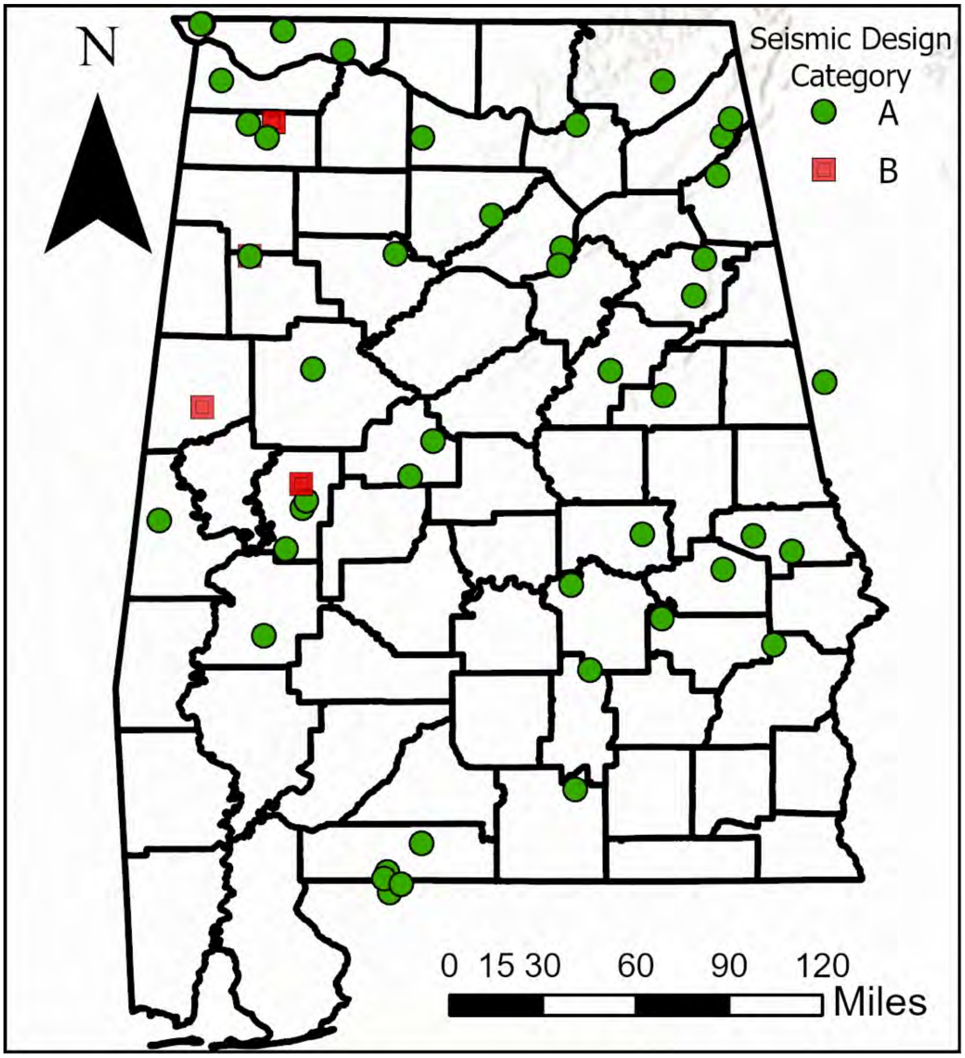

Figure 80: Map of Alabama showing the SDC of sites where V_S measurements were collected as part of this study.

For all sites visited as a part of this study, site class was also determined using the various correlations discussed in Chapter 4. For each, uncertainty was considered using either the ±30% recommended by AASHTO or a probabilistic distribution of inverted V_{S30} for direct measurements. The SDC for the direct and SPT-based methods are shown in Table 19 and for the HVSR and geospatial methods in

Table 20. The cell colors indicate whether the indirect methods are predicting site classes above (red) or below (orange) the range from the direct measurements. For most of the sites, the indirect methods capture the result from the direct methods when considering the uncertainties in each. The Imai and Tonouchi (1982) and geospatial methods have the best agreement, while the Wair et al. (2012) tends to provide a more conservative estimate as previously discussed. The HVSR results have more uncertainty and tend to overpredict site class.

Table 19. Range of site classes for visited sites using direct measurements and SPT-based estimation methods. Orange colors indicate the indirect method is giving a site class below the range indicated by direct measurements, while red indicates the indirect method is giving a site class above the range indicated by direct measurements.

Site	Direct Measurement			SPT (I&T82)			SPT (W12)		
	Lower Bound	Median	Upper Bound	Lower Bound	Median	Upper Bound	Lower Bound	Median	Upper Bound
Cedar Bluff	B/C	B/C	B	C/D	C	C	C/D	C/D	C
Beaver Creek	D	C/D	C/D	D	D	C/D	D/E	D/E	D
	D	C/D	C/D	D	C/D	C	D/E	D	C/D
Big Prairie Creek	D	C/D	C/D	D	C/D	C/D	D/E	D/E	D
Coldwell Creek	D	C/D	C/D	D	C/D	C/D	D/E	D	C/D
Moundville	D	D	C/D	D	C/D	C/D	D	D	C/D
	D	D	C/D	D	C/D	C/D	D/E	D	C/D
Greensboro	D	D	D	D	C/D	C/D	D/E	D/E	D
Duck River	B	B	B	B/C	B/C	B	C	B/C	B/C
Russellville High School	D	C/D	C/D	D/E	D/E	D	D/E	D/E	D
	C/D	C/D	C	D	C/D	C/D	D	C/D	C/D
Lauderdale County	C	B/C	B/C	B/C	B	B	B/C	B/C	B
	B/C	B/C	B	B/C	B/C	B	C	B/C	B/C
Bluewater Creek	C	B/C	B/C	B/C	B	B	C	B/C	B
Blount County	B	B	B	B/C	B/C	B	C	B/C	B

Table 20. Range of site classes for visited sites using HVSR and geospatial estimation methods. Orange colors indicate the indirect method is giving a site class below the range indicated by direct measurements, while red indicates the indirect method is giving a site class above the range indicated by direct measurements

<table>
<tr><th rowspan="2">Site</th><th colspan="3">HVSR</th><th colspan="3">Geospatial</th></tr>
<tr><th>Lower Bound</th><th>Median</th><th>Upper Bound</th><th>Lower Bound</th><th>Median</th><th>Upper Bound</th></tr>
<tr><td>Cedar Bluff</td><td>C/D</td><td>B/C</td><td>A</td><td>D</td><td>C/D</td><td>C</td></tr>
<tr><td rowspan="2">Beaver Creek</td><td>C/D</td><td>C</td><td>B/C</td><td>D/E</td><td>D</td><td>C/D</td></tr>
<tr><td>C/D</td><td>C</td><td>B/C</td><td>D/E</td><td>D</td><td>C/D</td></tr>
<tr><td rowspan="2">Big Prairie Creek</td><td>C/D</td><td>C</td><td>B/C</td><td rowspan="2">D/E</td><td rowspan="2">D</td><td rowspan="2">C/D</td></tr>
<tr><td>C/D</td><td>C</td><td>B/C</td></tr>
<tr><td rowspan="2">Coldwell Creek</td><td>D</td><td>C/D</td><td>B/C</td><td rowspan="2">D</td><td rowspan="2">C/D</td><td rowspan="2">C/D</td></tr>
<tr><td>D</td><td>D</td><td>C/D</td></tr>
<tr><td rowspan="2">Moundville</td><td>D</td><td>D</td><td>C</td><td>D</td><td>C/D</td><td>C/D</td></tr>
<tr><td>D</td><td>D</td><td>C/D</td><td>D</td><td>C/D</td><td>C/D</td></tr>
<tr><td>Greensboro</td><td>D</td><td>C/D</td><td>B</td><td>D/E</td><td>D</td><td>C/D</td></tr>
<tr><td>Duck River</td><td>B/C</td><td>B</td><td>B</td><td>C/D</td><td>C</td><td>B/C</td></tr>
<tr><td rowspan="2">Russellville High School</td><td>D</td><td>C</td><td>B</td><td>D</td><td>C/D</td><td>C</td></tr>
<tr><td>C/D</td><td>C</td><td>B/C</td><td>D</td><td>C/D</td><td>C</td></tr>
<tr><td rowspan="2">Lauderdale County</td><td>B/C</td><td>B</td><td>A</td><td>C</td><td>B/C</td><td>B</td></tr>
<tr><td>B/C</td><td>B</td><td>A</td><td>C/D</td><td>C</td><td>B/C</td></tr>
<tr><td>Bluewater Creek</td><td>B/C</td><td>B</td><td>A</td><td>C</td><td>C</td><td>B/C</td></tr>
<tr><td>Blount County</td><td>C</td><td>B</td><td>B</td><td>C/D</td><td>C</td><td>B/C</td></tr>
</table>

SDC was determined using the most conservative estimate of site class for each site and method (

Table 21). Generally, the most conservative estimate for each site is the classification with the lowest velocity with the exception of estimates of D/E or lower as site class D gives the most conservative SDC for Alabama. Virtually all of the approaches gave the same SDC at all sites, tith the exception of the geospatial estimates for the Cedar Bluff and Lauderdale County sites. For these locations, the geospatial correlations indicated SDC B, while the other methods returned A. This comparison validates the recommendations in this study to first apply the geospatial correlation to estimate SDC with consideration of uncertainty and then use either direct measurements or in situ-based correlations to sites that fall into SDC B

Table 21. SDC for all sites visited as a part of this study determined using the most conservative site classification. Highlighted cells show locations where that method overestimated the SDC.

Site	SDC (Direct Measurement)	SDC (SPT, I&T-82)	SDC (SPT, W-12)	SDC (HVSR)	SDC (Geospatial)
Cedar Bluff	A	A	A	A	B
Beaver Creek	A	A	A	A	A
	A	A	A	A	A
Big Prairie Creek	A	A	A	A	A
				A	
Coldwell Creek	A	A	A	A	A
				A	
Moundville	B	B	B	B	B
	B	B	B	B	B
Greensboro	A	A	A	A	A
Duck River	A	A	A	A	A
Russellville High School	B	B	B	B	B
	B	B	B	B	B
Lauderdale County	A	A	A	A	A
	A	A	A	A	B
Bluewater Creek	A	A	A	A	A
Blount County	A	A	A	A	A

5.5 Recommendations for Liquefaction Assessments

In addition to site class, it is also important to understand if liquefaction hazards may impact a site and require considerations in the design process. Liquefaction occurs when saturated, sandy soils lose their strength and stiffness during shaking due to generation of excess pore pressures. It primarily affects younger deposits (Holocene) below the water table. The AASHTO Guide Specifications suggests that liquefaction evaluations be performed for SDC B projects to determine if there are enough of these materials present to impact the bridge stability. To screen for potentially liquefiable materials, the Guide Specifications suggest using a peak ground acceleration threshold of 0.15 g, which is shown in Figure 81 based on an assumed site class of D (most conservative assumption for seismic hazard in Alabama). This map highlights the regions of the state where liquefaction analyses may be required. If a site falls into one of these regions, then a screening analysis should be performed to identify potentially liquefiable soils (normalized blow counts less than 10 or normalized cone tip resistances less than 75) and to determine if there are enough of these soils at the site to impact the bridge stability. If there are, then a triggering analysis is needed. The spreadsheet developed for this project, implements the liquefaction triggering procedures suggested by Boulanger and Idriss (2014) and can be used for preliminary analyses if required.

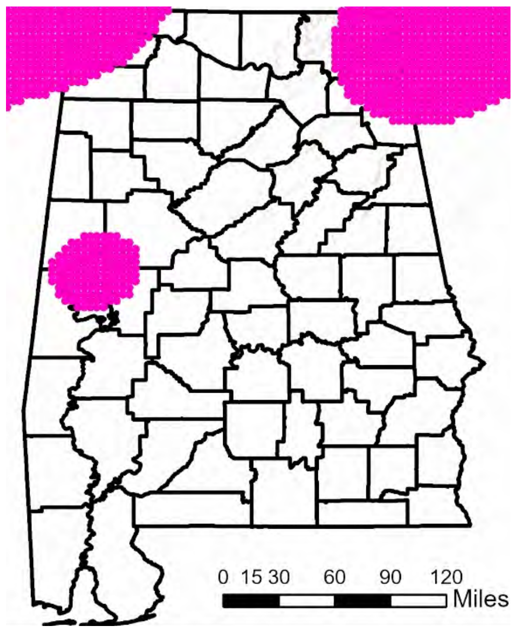

Figure 81: Locations in Alabama where the acceleration may be high enough to cause liquefaction to occur if loose, saturated sandy soils are present.

In locations where a liquefaction analysis may be required, it is recommended that CPT soundings be performed if possible. The CPT is generally considered the more reliable tool for measuring the properties of potentially liquefiable sands and it has the added benefit of being able to collect V_S data at the same time through downhole testing. SPT tests can also be used, but hollow stem augers should be avoided as they are susceptible to sample disturbance when trying to test sandy soils below the water table, which can lead to artificially low blowcounts (NASEM 2017). These artificially low blowcounts may lead to an incorrect assessment of liquefiable soils at a bridge site, greatly increasing the cost and complexity of the required foundations.

5.6 Summary

This study developed new SDC maps using the seismic hazard data provided by the USGS for the AASHTO Guide Specifications. These maps are shown in Appendix A and indicate that the entire state falls into SDC A for site classes A, B, or BC. For site class C, the entire state also falls into SDC A except Lauderdale and Colbert County. This represents the range of site classes that would be expected at rock sites (site with less than 10 feet of soil) regardless of weathering and so there will likely be no need for direct seismic measurements at most rock sites. The exception would be for the areas of Lauderdale and Colbert County that fall into SDC B for site class C, but would be SDC A for site class BC or greater. For projects falling into this category, direct measurements of shear wave velocity should be considered.

For soil sites, the most conservative site class for SDC determination is D, which makes it a good default assumption when planning a site investigation program for a new site. For sites that fall into SDC A using an assumption of site class D, there is likely no need for additional effort to estimate V_{S30} as it will not impact the design. For sites that fall into the region of the state where SDC B would apply, additional work should be performed to establish a reasonable estimate of V_{S30}. As discussed in Chapter 4, the SPT-based correlations have significant uncertainty and may be overly conservative for stiff sites, while the geospatial correlations are performing better for most sites examined in this study. For this reason, the geospatial models presented by Geyin and Maurer (2023) and Gann-Phillips et al. (2024) should be considered as a first option when estimating V_{S30}. These estimates can be used along with the 30% uncertainty to develop a new SDC. For sites that still fall into SDC B based on correlations, direct measurements of shear wave velocities would be beneficial. One good option for collecting this data would be to use seismic CPT soundings, which can collect both in situ test results for design and V_S profiles through downhole testing at the same time.

For sites falling into SDC B, a liquefaction evaluation should also be considered. This can be done by first checking the expected seismic loading to determine if accelerations are high enough to meet the AASHTO threshold for liquefaction evaluations (PGA > 0.15 g, Figure 81). If so, the site should be screened to identify loose, saturated sandy soils. If these are expected to be present, it is recommended the CPT soundings be performed to evaluate both the properties of these layers and to collect V_S profiles through downhole testing at the same time.

6 CONCLUSIONS AND RECOMMENDATIONS FOR IMPLEMENTATION

6.1 Summary

Alabama is a region with relatively low seismic hazard compared to the western US, but earthquakes are a real threat and design of critical infrastructure like bridges must consider potential performance during these potentially rare events. This requires having foundations and structural designs that can withstand the expected loading conditions. In seismic design the magnitude of the expected loading depends on the earthquake source and path, the site effects, and the response of the structure. In many code-based designs, including the *AASHTO Guide Specifications for LRFD Seismic Bridge Design (3rd Edition, 2023)*, V_{S30} (time-averaged shear wave velocity in the upper 100 ft) is used a proxy for site stiffness and other local site effects. Softer, soil sites will generally have more amplification than stiffer rock sites during shaking and may require more design effort to withstand this higher loading.

The most accurate method for determining V_{S30} is a direct measurement of V_S (shear wave velocity), but these may not always be feasible or economical. Indirect approaches can also be used to estimate V_S or in some cases V_{S30}. These include correlations based on in situ tests, correlations with other geophysical measurements such as HVSR, and geospatial models that seek to estimate V_{S30} based on regional characteristics like geology and topography. While these correlations and models have been shown to provide reasonable values for the regions in which they were developed, they may not be applicable to outside regions. Very few of the studies examined in this work had any measurements from sites in Alabama in their databases, which leads to additional uncertainty when applying those correlations to this region.

To address this gap, direct measurements of V_S were taken at fifteen sites around Alabama using MASW and refraction surveys along with passive HVSR surveys. The data collection for the MASW and refraction survey equipment was nearly identical with the only common difference being the fundamental frequency of geophones used. Recording parameters were also nearly identical with sampling frequency being the only parameter that differs between MASW and refraction surveys.

The surveys showed a wide range of site classes across Alabama ranging from site class D near Greensboro to Site Class B at rock sites in the northern part of the state. When used at the same site, MASW and refraction surveys provided very similar results. HVSR surveys for the sites yielded 46 unique HVSR curves. Of the 46 unique curves, only 6 did not meet the reliability requirements from SESAME.

The measured V_S and V_{S30} values from both this study and Carcamo (2022) were used to evaluate the correlations reviewed in Chapter 2. Of the SPT-based correlations evaluated as a part of this study, the correlation presented in Imai and Tonouchi (1982) provided the best fit for SPT-based methods. Despite the better fit, the correlation tends to be unconservative (i.e., overpredict measurements) at lower velocities. The second correlation is the "All Soils" correlation presented in Wair et al. (2012). While the greater value of MSE indicates a poorer fit, the correlation is more conservative than the one presented in Imai and Tonouchi (1982). More conservative estimates may be desirable to avoid underestimating the site class but do have the possibility of artificially increasing the design requirements. HVSR and RQD-based correlations were also evaluated but generally showed more scatter than SPT-based correlations.

Geospatial correlations provided better fit to the measured data compared to SPT, RQD, and HVSR-based correlations. The Geyin and Maurer (2023) model provided the best fit overall of the correlations examined in this study and its map-based format means it can easily be applied to all areas of the state. When used on sites within the coastal plain, the model presented in Gann-Phillips et al. (2024) provided the best fit of any of the methods presented in this study.

The findings from this study were used to develop SDC maps for Alabama and a set of recommended procedures to determine site class at bridge sites in Alabama. The procedure is meant to be flexible in order to allow for both default site class estimates to be used for sites where the SDC is unaffected by variations in site class and direct measurements at sites where SDC B may be expected. In addition to estimating SDC, recommendations were also developed to screen for potentially liquefiable soils, which would require further investigation.

6.2 Conclusions

This study has outlined a new approach to estimate site class at bridge sites in Alabama. The approach is grounded in the requirements and recommendations from the *AASHTO Guide Specifications for LRFD Seismic Bridge Design* (3rd Edition, 2023) but has been adapted to account for the low to moderate seismic hazard conditions in Alabama. The first step in applying the procedure is to develop a preliminary ground model for the site using information collected from geotechnical explorations, geologic maps, and site observations. Using this ground model, the location should be classified as either a rock site or a soil site based on the thickness of soil at the site. Rock sites must have less than 10 feet of soil overlying the rock. This thickness can be estimated using the bottom of the abutment as the starting depth and any surficial materials that will be removed during construction can be neglected. If the site is classified as a rock site, it will fall into SDC A in all parts of the state with the exception of Lauderdale and Colbert Counties (Figure 77). If the site is located in the region where SDC B is a possibility, the weathering grade of the rock should be assessed through geotechnical and geological explorations. For rocks with low or moderate weathering (Table 17), the default site class is BC and SDC A can be used. For more weathered rocks in these regions, direct measurements of V_{S30} should be obtained to determine the site class, SDC, and to use as inputs to future design calculations.

For soil sites (every site that does not qualify as a rock site), site class D can be assumed to obtain the most conservative estimate of SDC (Figure 78). If the most conservative SDC is A, then there is no need for further investigations of site class, and the design process can move forward with SDC A. If the site falls in the region of the state, where SDC B would apply, an initial estimate of V_{S30} can be obtained using the geospatial model by Geyin and Maurer (2023) or by Gann-Phillips et al. (2024) for sites in the coastal plain. This estimated V_{S30} should then be increased and decreased by a factor of 1.3 to account for the uncertainty in the models and used to determine the most conservative SDC based on the three site class estimates. If all three indicate SDC A, then the design can proceed with this SDC. If one or more indicates SDC B, then it is recommended that more refined estimates of V_{S30} are obtained using either direct measurements or correlations with in situ data. SPT-based correlations can be used, but are likely to be overly conservative for stiffer sites. Instead, it may be more economical to use CPTs at these sites, which can also provide direct V_S measurements through downhole testing at the same time.

For sites that do classify as SDC B, it is also recommended that screening be performed for potential liquefaction concerns. This requires identifying whether there are loose, saturated sandy soils that could lose strength and stiffness during a potential earthquake. Both SPT-based and CPT-based analyses are available to perform this screening, but it is recommended that CPT-based approaches be used when possible. CPT data is less susceptible to sample disturbance and other potential sources of measurement uncertainty than SPT data and as already mentioned, the CPT can also be used to obtain V_S profiles through downhole testing. When SPT data are used, the borings should be performed using mud rotary drilling rather than hollow stem augers to avoid potential disturbance of the soils that can lead to artificially low blowcounts.

6.3 Recommendations for Implementation

The SDC maps developed through this work are ready to be implemented as a compliment to the spreadsheet tool developed by ALDOT to estimate SDC. These maps are provided in Appendix A and as a digital map file. It is recommended that the maps or spreadsheet be used to determine which sites may fall into SDC B using either the maps for site class C (most conservative for rock sites) or site class D (most conservative for soil sites). The findings can then be used to guide next steps as discussed in the previous section.

The best performing SPT-based and geospatial correlations have also been provided to ALDOT for use when estimates of site class are needed. As discussed in the previous section, the geospatial models should be used to get an initial estimate of V_{S30}, which can then be used to estimate site class after considering potential uncertainties in the estimates. The SPT-based correlations can also be used, but have more uncertainty and may be overly conservative for stiff sites.

Direct measurements of shear wave velocity should be considered for sites where correlations indicate the site would fall into SDC B. These direct measurements can either be performed using surface-based methods like refraction or MASW for stiff sites or as part of CPT soundings for soil sites. HVSR tests can also be used but are unlikely to provide reliable V_{S30} estimates on their own. Instead, they can be used in conjunction with other information to better understand the site period and potential amplification.

Four of the sites tested in this study would fall into SDC B, even with direct measurements. All four sites were located in the northwestern part of the state where the combination of relatively soft soil in the coastal plain and higher seismic hazard pushed them into SDC B. While collecting V_S data at these sites would not change the answer for the SDC, it will provide important information for future design calculations.

Sites that fall into SDC B should also be evaluated for potential liquefaction concerns. This is unlikely to be an issue at most sites due to the expected level of shaking and the age of most deposits in Alabama, but the screening should still be performed to check. For sites where this screening may be needed (Figure 81), CPT data should be collected or SPT data should be collected using mud rotary drilling. Hollow stem augers should not be used for borings that may be needed for liquefaction evaluations because of the potential for disturbance of sandy soils below the water table. This disturbance can artificially lower the blowcount and may lead to an indication of liquefaction problems when none are present. As it may not be known ahead of time whether a liquefaction analysis is needed, it may be good practice to avoid using hollow stem auger drilling when sandy soils are expected to be present below the water table to avoid potential disturbance issues.

6.4 Recommendations for Future Research

This research has developed a new set of approaches to estimate site class at Alabama bridge sites. While the approaches are complete, additional work is needed to test and refine them during implementation into ALDOT's design practice. Potential improvements to the recommended procedures could include developing integrated approaches to estimate site class that could use inputs from both geospatial correlations and in situ data to reduce uncertainty. The geospatial models tested in this study could also be recalibrated to provide more accurate estimates for Alabama. These were beyond the scope of the current study, but could be considered in the future if the current uncertainty levels are determined to be too high.

This study has focused on estimating site class and SDC, but there is also a need to understand how current seismic design practice in Alabama may need to change to fit with the latest guidelines. This study has shown that the changes have led to more of the state potentially falling into SDC B, but the impact of this change on bridge design practice is unknown. This remains an important area for future research.

The current study has focused on design of new bridges, but the inspection and evaluation of existing bridges is also a key aspect. The SDC maps in this study could be used as a first estimate of areas of the state where existing bridges may have higher seismic demands. This information could be used along with the site class estimates from the geospatial models to prioritize locations for evaluation.

An additional area for future research is post-earthquake inspections. While earthquakes in Alabama are rare, even relatively small earthquakes may trigger a need for bridge inspections in a large region of the state. Currently, there is no system in place to understand which of these bridges may be more or less likely to experience damage, which may make prioritizing inspections more difficult. The findings of this study could be used along with generic fragility curves for bridges to create an alert tool that could assess the likelihood of damage at a bridge for a given earthquake and assist ALDOT with understanding which bridges are most critical to inspect first.

REFERENCES

AASHTO (American Association of State Highway and Transportation Officials). 2023. *AASHTO LRFD Bridge Design Specifications, 3rd Edition*. Washington, D.C.: AASHTO.

Abrahamson, N., Atkinson, G., Boore, D., Bozorgnia, Y., Campbell, K., Chiou, B., Idriss, I. M., Silva, W., and Youngs, R. 2008. "Comparisons of the NGA Ground-Motion Relations." *Earthquake Spectra*, 24(1), 45-66. https://doi.org/10.1193/1.2924363

Ahdi, S. K. (2018) "An improved framework for the analysis and dissemination of seismic site characterization data at varying resolutions". (Ph.D. Dissertation, Dept. of Civil and Environmental Engineering, University of California Los Angeles).

Allen, T. I., and Wald, D. J. 2009. "On the use of high-resolution topographic data as a proxy for seismic site conditions (V_S 30)." *Bulletin of the Seismological Society of America*, 99(2A), 935-943.

Anbazhagan, P., Bajaj, K., Reddy, G. R., Phanikanth, V. S., and Yadav, D. N. 2016. "Quantitative assessment of shear wave velocity correlations in the shallow bedrock sites." *Indian Geotechnical Journal*, 46(4), 381–397. https://doi.org/10.1007/s40098-016-0181-y

Andrus, R. D., Mohanan, N. P., Piratheepan, P., Ellis, B. S., and Holzer, T. L. 2007. "Predicting shear-wave velocity from cone penetration resistance." *Proc., 4th Inter. Conf. on Earthq. Geotech. Eng*., Thessaloniki, Greece.

ASTM. 2011. *Standard Test Method for Electronic Friction Cone and Piezocone Penetration Testing of Soils*. ASTM D 6066-11. West Conshohocken, PA: ASTM.

ASTM. 2020. ASTM. 2020. *Standard Test Method for Electronic Friction Cone and Piezocone Penetration Testing of Soils*. ASTM D 5778-20. West Conshohocken, PA: ASTM.

Baldi, G., Bellotti, R. Ghionna, V. N., Jamiolkowski, M., and LoPresti, D. C. F. 1989. "Modulus of sands from CPTs and DMTs." *Proc., 12th Inter. Conf. Soil Mech. and Foundation Eng*., Vol. 1, Rio de Janeiro, pp. 165–170.

Ballard, R. F. 1976. "Method for Crosshole Seismic Testing." *Journal of the Geotechnical Engineering Division*, 102(12), 1261-1273. https://doi.org/10.1061/AJGEB6.0000355

Bard, P. Y., and Participants, S. E. S. A. M. E. 2004. "The SESAME project: an overview and main results." *In Proc. of 13th World Conf. on Earthquake Engineering*, Vancouver, BC, Canada, August (pp. 1-6).

Biringen, E. and Davie, J. 2013. “Correlation Between V_S and RQD for Different Rock Types” *International Conference on Case Histories in Geotechnical Engineering*. 11. https://scholarsmine.mst.edu/icchge/7icchge/session_06/11

Boulanger, R. W., and Idriss, I. M. (2014). *CPT and SPT based liquefaction triggering procedures* (Report No. UCD/CGM-14/01). Center for Geotechnical Modeling, Department of Civil and Environmental Engineering, University of California, Davis.

Butler, D. K., and Curro, J. R. 1981. “Crosshole seismic testing—Procedures and Pitfalls.” *Geophysics*, 46(1), 23-29. https://doi.org/10.1190/1.1441134

Carcamo, P. 2022. “Application of Methods to Characterize V_{S30} in Alabama.” (Ph.D. Dissertation, Dept. of Civil and Environmental Engineering, Auburn University).

El-Naqa, A. 1996. “Assessment of geomechanical characterization of a rock mass using a seismic geophysical technique.” *Geotech Geol Eng* 14, 291–305. https://doi.org/10.1007/BF00421945

Farr, T. G., and Kobrick, M. 2000. “Shuttle Radar Topography Mission produces a wealth of data.” *Eos, Transactions American Geophysical Union*, 81(48), 583-585.

Fatehnia, M., Hayden, M. and Landschoot, M. 2015. “Correlation between Shear Wave Velocity and SPT-N Values for North Florida Soils.” *EJGE*. 20. 12421-12430.

Fletcher, G.F., 1965. “Standard penetration test: its uses and abuses.” *Journal of the Soil Mechanics and Foundations Division*, *91*(4), pp.67-75.

Foti, S., Hollender, F., Garofalo, F. *et al.* 2018. ”Guidelines for the good practice of surface wave analysis: a product of the InterPACIFIC project.” *Bull Earthquake Eng* **16**, 2367–2420. https://doi.org/10.1007/s10518-017-0206-7

Gann-Phillips, C., Cabas, A., Ji, C., Cramer, C., Kaklamanos, J., and Boyd, O. 2024. “Regional seismic velocity model for the US Atlantic and Gulf Coastal Plains based on measured shear wave velocity, sediment thickness, and surface geology.” *Earthquake Spectra*, 40(2), 1269-1300.

Garofalo, F., Foti, S., Hollender, F., Bard, P.Y., Cornou, C., Cox, B.R., Ohrnberger, M., Sicilia, D., Asten, M., Di Giulio, G. and Forbriger, T., 2016. “InterPACIFIC project: Comparison of invasive and non-invasive methods for seismic site characterization. Part I: Intra-comparison of surface wave methods.” *Soil Dynamics and Earthquake Engineering*, *82*, pp.222-240.

GEObit Instruments. 2023. *GEOtinyMK3 Low Power Compact Digital Seismometer: User Manual, Revision 12.6, Firmware Version 13.0.0.* GEObit Instruments.

Geometrics, I. 2009. *SeisImager/2D Seismic Refraction Data Analysis Software Manual and Examples Booklet* (ver 3.3).

Geyin, M., and Maurer, B.W. 2023. "U.S. National V_S30 Models and Maps Informed by Remote Sensing and Machine Learning." *Seismol. Res. Lett. 94*, 1467–1477, doi: 10.1785/0220220181.

Ghofrani, H., and Atkinson, G. M. 2014. "Site condition evaluation using horizontal-to-vertical response spectral ratios of earthquakes in the NGA-West 2 and Japanese databases." *Soil Dynamics and Earthquake Engineering*, 67, 30-43, https://doi.org/10.1016/j.soildyn.2014.08.015

Green, R. 1974. "The seismic refraction method—a review." *Geoexploration*, 12(4), 259-284.

Grelle, G., and Guadagno, F. M. 2009. "Seismic refraction methodology for groundwater level determination: "Water seismic index"." *Journal of Applied Geophysics*, 68(3), 301-320. https://doi.org/10.1016/j.jappgeo.2009.02.001

Hasancebi, N., and Ulusay, R. 2007. "Empirical correlations between shear wave velocity and penetration resistance for ground shaking assessments." *Bull. Eng. Geology and the Environment*, 66:203–213.

Hassani, B., and Atkinson, G. M. 2016. "Applicability of the site fundamental frequency as a V_S 30 proxy for central and eastern North America." *Bulletin of the Seismological Society of America*, 106(2), 653-664.

Hegazy, Y. A., and Mayne, P. W. 1995. "Statistical correlations between VS and cone penetration data for different soil types." *Proc., Inter. Symp. on Cone Penetration Testing, CPT '95*, Linkoping, Sweden, Vol. 2, pp. 173–178.

Hepton, P. 1988. "Shear wave velocity measurements during penetration testing." *Penetration Testing in the UK.* Thomas Telford, London, 275-278.

Herath, P., Stern, T., Savage, M., Bassett, D., Henrys, S., Barker, D., Avendonk, H. V., Bangs, N., Arnulf, A., Arai, R., Kodaira, S., and Mochizuki, K. 2020. "Using P- to S- wave conversions from controlled sources to determine the shear-wave velocity structure along Hikurangi Margin Forearc, New Zealand (N.° EGU2020-11940)." *EGU2020. Copernicus Meetings*. https://doi.org/10.5194/egusphere-egu2020-11940

Imai, T. and Tonouchi, K. 1982. “Correlation of N-value with S-wave velocity and shear modulus.” *Proc. 2nd European Symp. Of Penetration Testing* (Amsterdam), 57–72.

Iwahashi, J., and Pike, R. J. 2007. “Automated classifications of topography from DEMs by an unsupervised nested-means algorithm and a three-part geometric signature.” *Geomorphology* 86, 409–440.

Jinan, Z. 1987. “Correlation between seismic wave velocity and the number of blow of SPT and depth.” *Selected Papers from the Chinese J. Geotech. Eng*., ASCE, pp. 92–100.

Kahraman, S. 2001 “A Correlation Between P-wave Velocity, Number of Joints and Schmidt Hammer Rebound Number.” *International Journal of Rock Mechanics and Mining Sciences*, 38(5), pp.729–733.

Kaneko, F., Kanemori, T., and Tonouchi, K. 1990. “Low-Frequency Shear Wave Logging in Unconsolidated Formations for Geotechnical Applications.” *ASTM Special Technical Publication* 1101, ASTM, 79-98.

Kramer, S. L. 1996. *Geotechnical Earthquake Engineering*. Upper Saddle River, New Jersey. Prentice-Hall.

Lee, S. H. H. 1992. “Analysis of the multicollinearity of regression equations of shear wave velocities.” *Soils and Foundations*, 32(1):205–214.

Lermo, J., and Chávez-García, F. J. 1993. “Site effect evaluation using spectral ratios with only one station.” *Bulletin of the seismological society of America*, 83(5), 1574-1594.

Mayne, P. W. 2006. “In situ test calibrations for evaluating soil parameters.” *Proc., Characterization and Engineering Properties of Natural Soils II*, Singapore.

Mayne, P. W., and Rix, G. J. 1995. “Correlations between shear wave velocity and cone tip resistance in natural clays.” *Soils and Foundations*, 35(2):107–110.

McDonald, F. J., Angona, F. A., Mills, R. L., Sengbush, R. L., Van Nostrand, R. G., and White, J.E. 1958. “Attenuation of Shear and Compressional Waves in Pierre Shale.” 23(3), 421 439.

McNamara, D. E., Stephenson, W. J., Odum, J. K., Williams, R. A., and Gee, L. 2015. "Site response in the eastern United States: A comparison of V_S30 measurements with estimates from horizontal: vertical spectral ratios", The 2011 Mineral, Virginia, Earthquake, and Its Significance for Seismic Hazards in Eastern North America, J. Wright Horton, Jr., Martin C. Chapman, Russell A. Green

Miller, R. D., Pullan, S. E., Waldner, J. S. and Haeni, F. P. 1986. “Field comparison of shallow seismic sources.” *Geophysics*, 51: 2067–2092.

Miller, R. D., Pullan, S. E., Steeples, D. W. and Hunter, J. A. 1992. “Field comparison of shallow seismic sources near Chino, California.” *Geophysics*, 57: 693–709.

Miller, R. D., Pullan, S. E., Steeples, D. W. and Hunter, J. A. 1994. “Field comparison of shallow P-wave seismic sources near Houston, Texas.” *Geophysics*, 59: 1713–1728.

Mucciarelli, M., and Gallipoli, M. R. 2001. “A critical review of 10 years of microtremor HVSR technique.” *Boll. Geof. Teor. Appl*, 42(3-4), 255-266.

Mussett, A.E., and Khan, M.A. 2000. “Looking into The Earth: An Introduction to Geological Geophysics.” New York, Cambridge University Press, 470 p

Nakamura, Y. 1989. “A method for dynamic characteristics estimation of subsurface using microtremor on the ground surface”. *Railway Technical Research Institute*, Quarterly Reports, 30(1).

Nakamura, Y. 2009. “Basic Structure of QTS (HVSR) and Examples of Applications.” In: Mucciarelli, M., Herak, M., Cassidy, J. (eds) Increasing Seismic Safety by Combining Engineering Technologies and Seismological Data. NATO Science for Peace and Security Series C: Environmental Security. Springer, Dordrecht. https://doi.org/10.1007/978-1-4020-9196-4_4

Nakamura, Y. 2019. “What Is the Nakamura Method?” *Seismological Research Letters*. https://doi.org/10.1785/0220180376

National Academies of Sciences, Engineering, and Medicine. 2021. State of the Art and Practice in the Assessment of Earthquake-Induced Soil Liquefaction and Its Consequences. Washington, DC: The National Academies Press. https://doi.org/10.17226/23474.

Ohta, Y, and Goto, N. 1978. “Empirical shear wave velocity equations in terms of characteristic soil indexes.” *Earthquake Engineering and Structural Dynamics*, 6:167–187.

Ohya, S., Ogura, K., and Imai, T. 1984. “The Suspension PS Velocity Logging System.” *Offshore Technology Conference*. https://doi.org/10.4043/4680-MS

Osborne, W. E., Szabo, E. W., Copeland, C. W., Jr., and Neathery, T. L. 1989. Geologic map of Alabama: Special Map 221. Geological Survey of Alabama.

Park, S., and Elrick, S. 1998. “Predictions of shear-wave velocities in southern California using surface geology.” *Bull. Seism. Soc. Am*. 88, 677–685.

Park, C. B., Miller, R. D., and Xia, J. 1999. “Multichannel analysis of surface waves (MASW).” *Geophysics*, 64, 800-808.

Parker, G. A., Harmon, J. A., Stewart, J. P., Hashash, Y. M., Kottke, A. R., Rathje, E. M., and Campbell, K. W. 2017. “Proxy-based V_S 30 estimation in central and eastern North America.” *Bulletin of the Seismological Society of America,* 107(1), 117-131.

PASI. 2013. *HVSR Data Acquisition Unit GEMINI-2: User Manual, 2013 Edition, Revision 2.0.1.* P.A.S.I. srl, Torino, Italy.

Pickett, G. R. 1963. “Acoustic Character Logs and their Applications in Formation Evaluation.” *Journal of Petroleum Technology*, 15, 659-667.

Piratheepan, P. 2002. “Estimating Shear-Wave Velocity from SPT and CPT Data.” M. S. thesis, Dept. of Civil Engineering, Clemson University.

Raikes, S. A., and White, R. E. 1984. “Measurements of Earth Attenuation from Downhole and Surface Seismic Recordings.” *Geophysical Prospecting,* 32(5), 892-919. https://doi.org/10.1111/j.1365-2478.1984.tb00745.x

Reynolds, J. M. 2011. *An Introduction to Applied and Environmental Geophysics*. John Wiley & Sons.

Robertson, P. K. 2009. “Interpretation of cone penetration tests – a unified approach.” *Canadian Geotech. J.*, 46(11):1337–1355.

Robertson, P. K., Campanella, R. G., Gillespie, D., and Rice, A. 1986. “Seismic CPT to Measure in Situ Shear Wave Velocity.” 112(8), 791-803.

Salaamah, A. F., Fathani, T. F., and Wilopo, W. 2019. “Correlation of P-wave velocity with rock quality designation (RQD) in Volcanic Rocks.” *Journal of Applied Geology*, 3(2), 11. https://doi.org/10.22146/jag.48594

Schmertmann, J.H., 1978. “Guidelines for cone penetration test: performance and design.”

Seed, H. B., Idriss, I. M., and Arango, I. 1983. “Evaluation of Liquefaction Potential Using Field Performance Data.” *J. Geotech. Eng.,* 109(3):458–482.

Seed, H. B., Tokimatsu, K., Harder, L. F., and Chung, R. M. 1985. “Influence of SPT procedures in soil liquefaction resistance evaluations.” *Journal of geotechnical engineering*, 111(12), 1425-1445.

SESAME 2004. "Guidelines for the implementation of the H/V spectral ratio technique on ambient vibrations: Measurements, processing and interpretation." European Commission Research Project EVG1-CT-2000-00026.

Sharma Wagle, K., Vantassel, J. P., Rodriguez-Marek, A., & Anbazhagan, B. (2026). "A Set of Data-Driven Models to Predict VS 30 from the Horizontal-to-Vertical Spectral Ratio of Microtremors." *Bulletin of the Seismological Society of America*.Stanko, D., and Markušić, S. 2020. "An empirical relationship between resonance frequency, bedrock depth and V_S30 for Croatia based on HVSR forward modelling." *Natural Hazards*, 103(3), 3715-3743. https://doi.org/10.1007/s11069-020-04152-z

Stümpel, H., Kähler, S., Meissner, R., and Milkereit, B. 1984. "The Use of Seismic Shear Waves and Compressional Waves for Lithological Problems of Shallow Sediments." *Geophysical Prospecting*, 32(4), 662-675. https://doi.org/10.1111/j.1365-2478.1984.tb01712.x

Sykora, D. E., and Stokoe, K. H. 1983. "Correlations of in-situ measurements in sands of shear wave velocity." *Soil Dynamics and Earthquake Engineering*, 20:125–36.

Teague, D., Cox, B. 2016. "Site response implications associated with using non-unique Vs profiles from surface wave inversion in comparison with other commonly used methods of accounting for Vs uncertainty." *Soil Dynamics and Earthquake Engineering*, 91:87-103, https://doi.org/10.1016/j.soildyn.2016.07.028.

Wair, B. R., DeJong, J. T., and Shantz, T. 2012. "Guidelines for Estimation of Shear Wave Velocity Profiles." Berkley, California: Pacific Earthquake Engineering Research Center.

Wald, D. J., and Allen, T. I. 2007. "Topographic slope as a proxy for seismic site conditions and amplification." *Bull. Seismol. Soc. Am*. 97, no. 5, 1379–1395.

Wathelet, M. 2008. "An improved neighborhood algorithm: Parameter conditions and dynamic scaling." *Geophysical Research Letters* 35(9), L09301. https://doi.org/10.1029/2008GL033256

Wathelet, M., Chatelain, J., Cornou, C., Giulio, G. D., Guillier, B., Ohrnberger, M., and Savvaidis, A. 2020a. "Geopsy: A User-Friendly Open-Source Tool Set for Ambient Vibration Processing." *Seismological Research Letters*, 91(3), 1878-1889. https://doi.org/10.1785/0220190360

Yong, A., Hough, S. E., Iwahashi, J., and Braverman, A. 2012. “A Terrain-Based Site-Conditions Map of California with Implications for the Contiguous United States.” *Bulletin of the Seismological Society of America,* 102(1), 114-128. https://doi.org/10.1785/0120100262

Vantassel, J. P. 2025. “hvsrpy: An Open-Source Python Package for Microtremor and Earthquake Horizontal-to-Vertical Spectral Ratio Processing.” *Seismological Research Letters*. 96 (4): 2671–2682, https://doi.org/10.1785/0220240395

APPENDIX A: SEISMIC DESIGN CATEGORY MAPS

Alabama Seismic Design Categories (SDC)
Site Class A

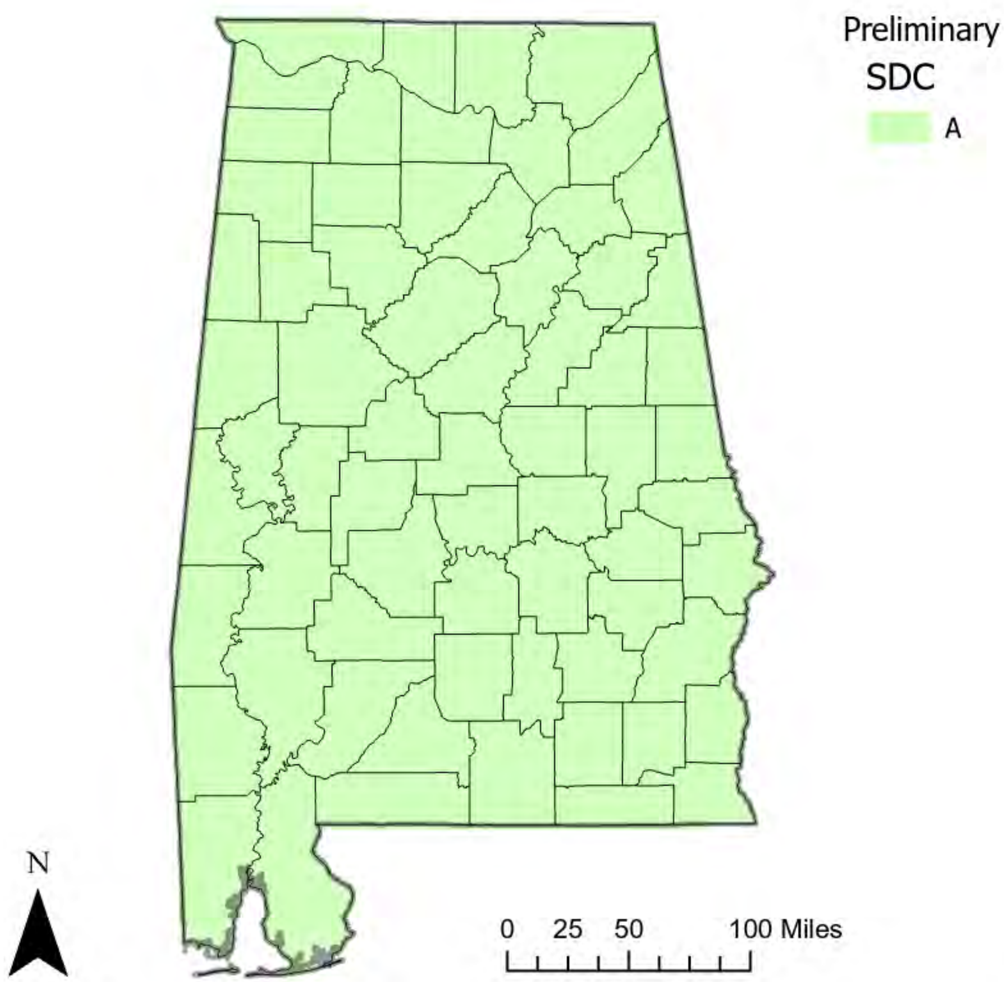

References

AASHTO Guide Specifications for LRFD Seismic Bridge Design 3rd ed.

United States Geological Survey (USGS) Earthquake Ground Motions, 2023.

Alabama Seismic Design Categories (SDC)
Site Class B

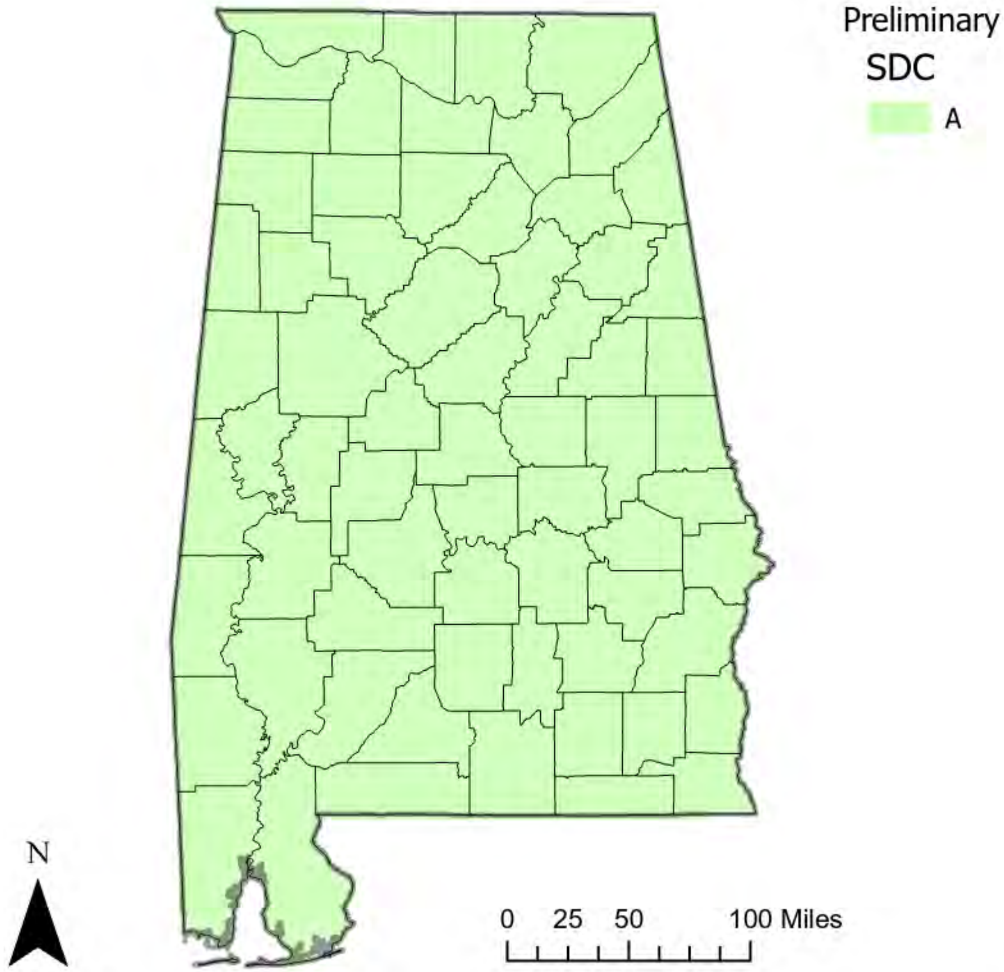

References

AASHTO Guide Specifications for LRFD Seismic Bridge Design 3rd ed.

United States Geological Survey (USGS) Earthquake Ground Motions, 2023.

Alabama Seismic Design Categories (SDC)
Site Class BC

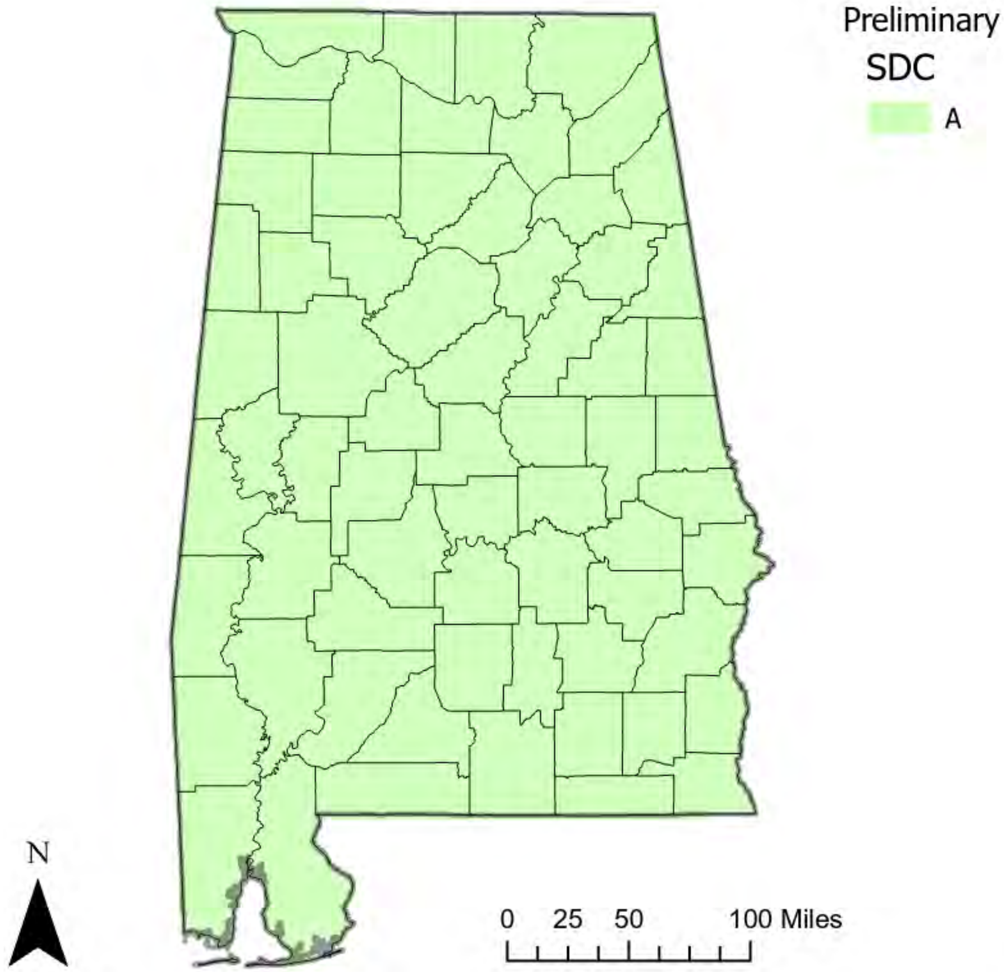

References
AASHTO Guide Specifications for LRFD Seismic Bridge Design 3rd ed.

United States Geological Survey (USGS) Earthquake Ground Motions, 2023.

Alabama Seismic Design Categories (SDC)
Site Class C

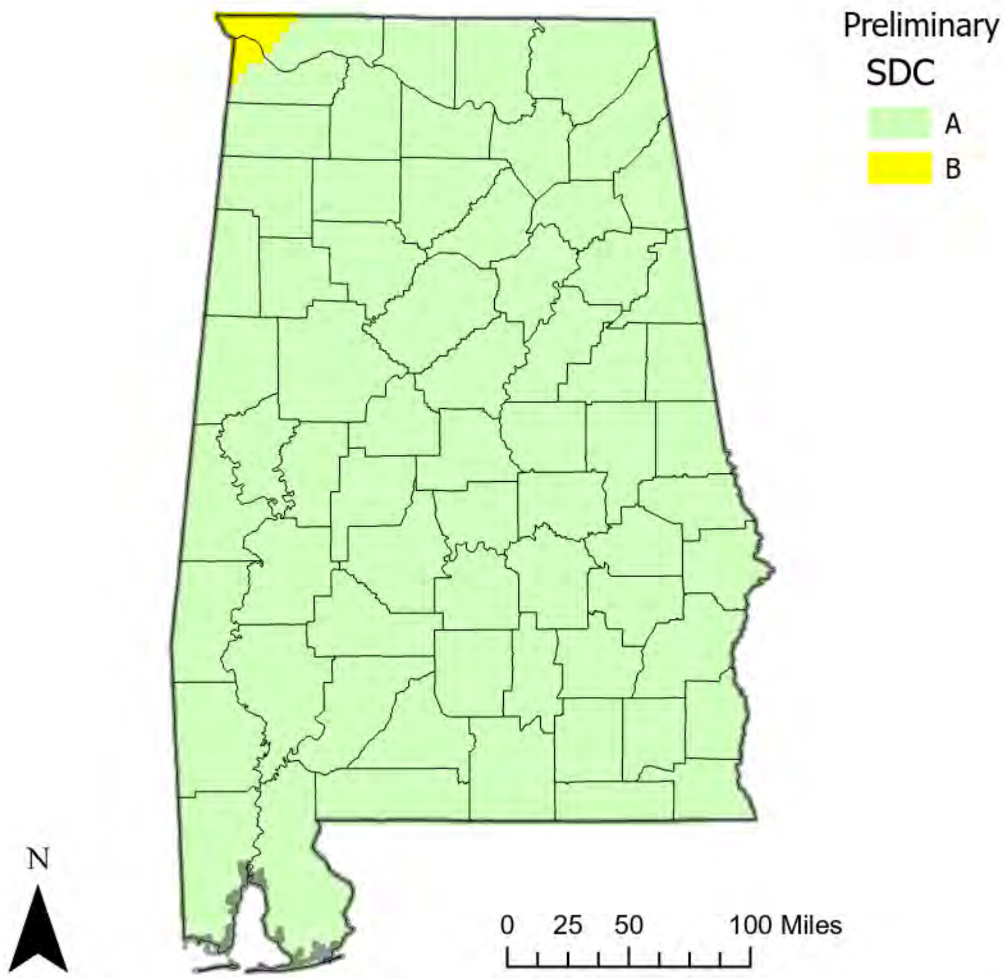

References

AASHTO Guide Specifications for LRFD Seismic Bridge Design 3rd ed.

United States Geological Survey (USGS) Earthquake Ground Motions, 2023.

Alabama Seismic Design Categories (SDC)
Site Class CD

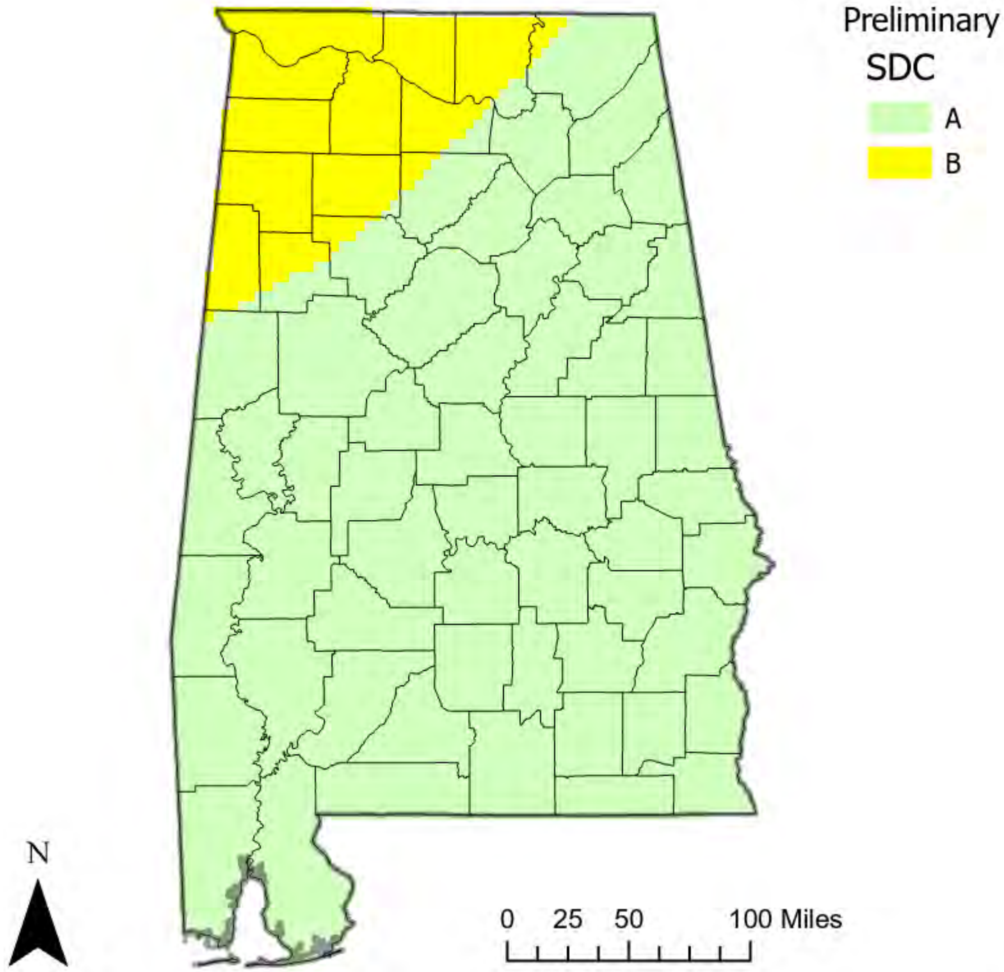

References

AASHTO Guide Specifications for LRFD Seismic Bridge Design 3rd ed.

United States Geological Survey (USGS) Earthquake Ground Motions, 2023.

Alabama Seismic Design Categories (SDC)
Site Class D

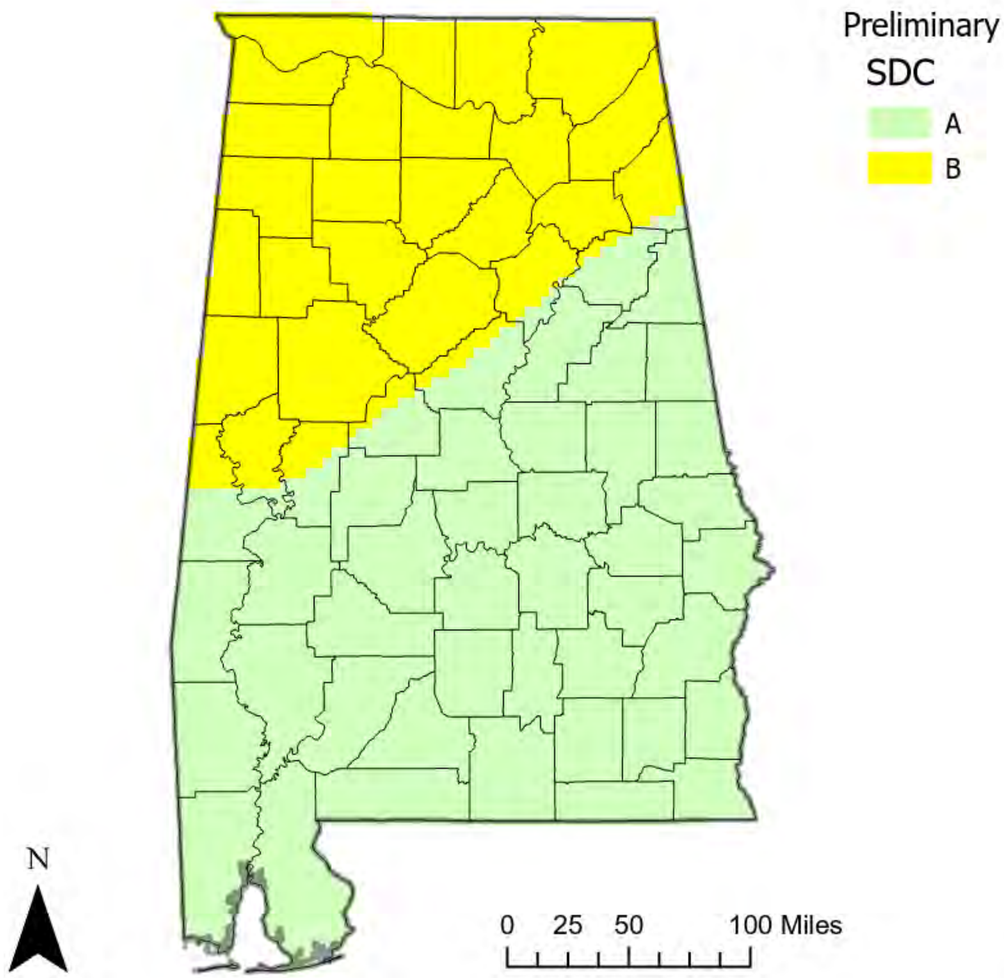

References
AASHTO Guide Specifications for LRFD Seismic Bridge Design 3rd ed.

United States Geological Survey (USGS) Earthquake Ground Motions, 2023.

Alabama Seismic Design Categories (SDC)
Site Class DE

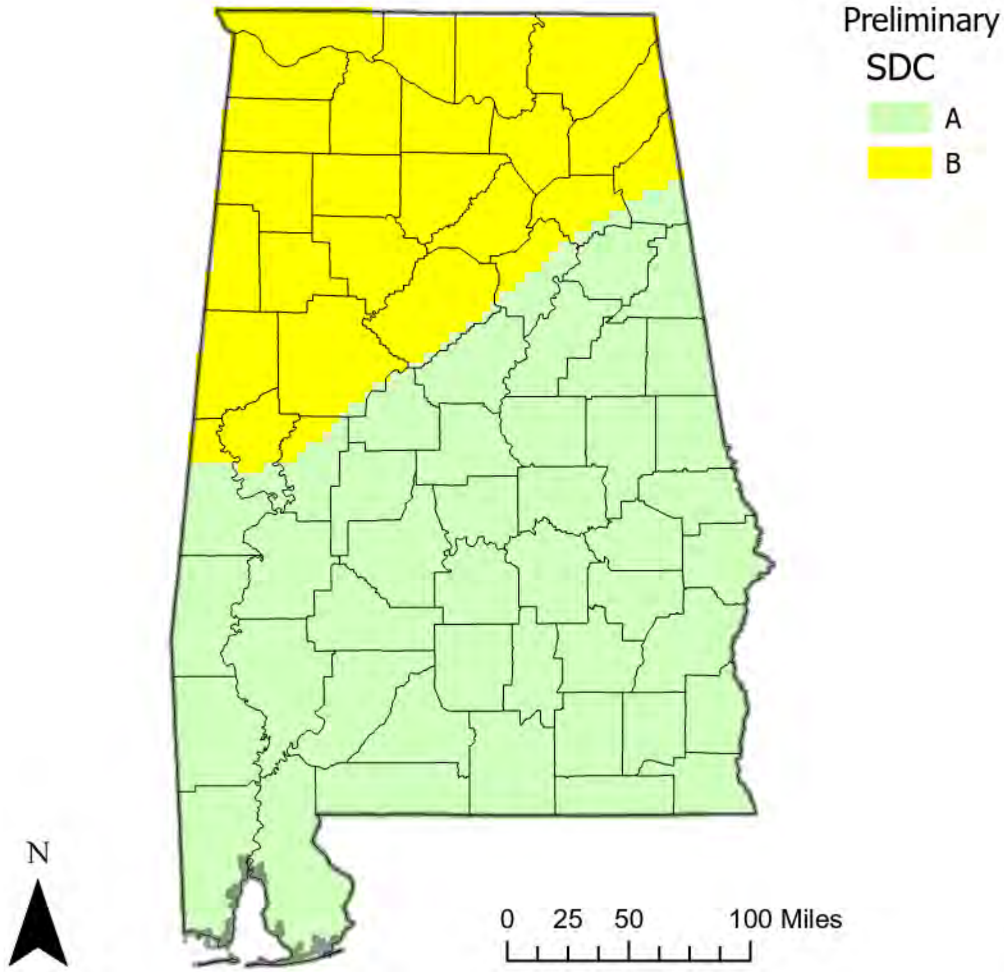

References

AASHTO Guide Specifications for LRFD Seismic Bridge Design 3rd ed.

United States Geological Survey (USGS) Earthquake Ground Motions, 2023.

Alabama Seismic Design Categories (SDC)
Site Class E

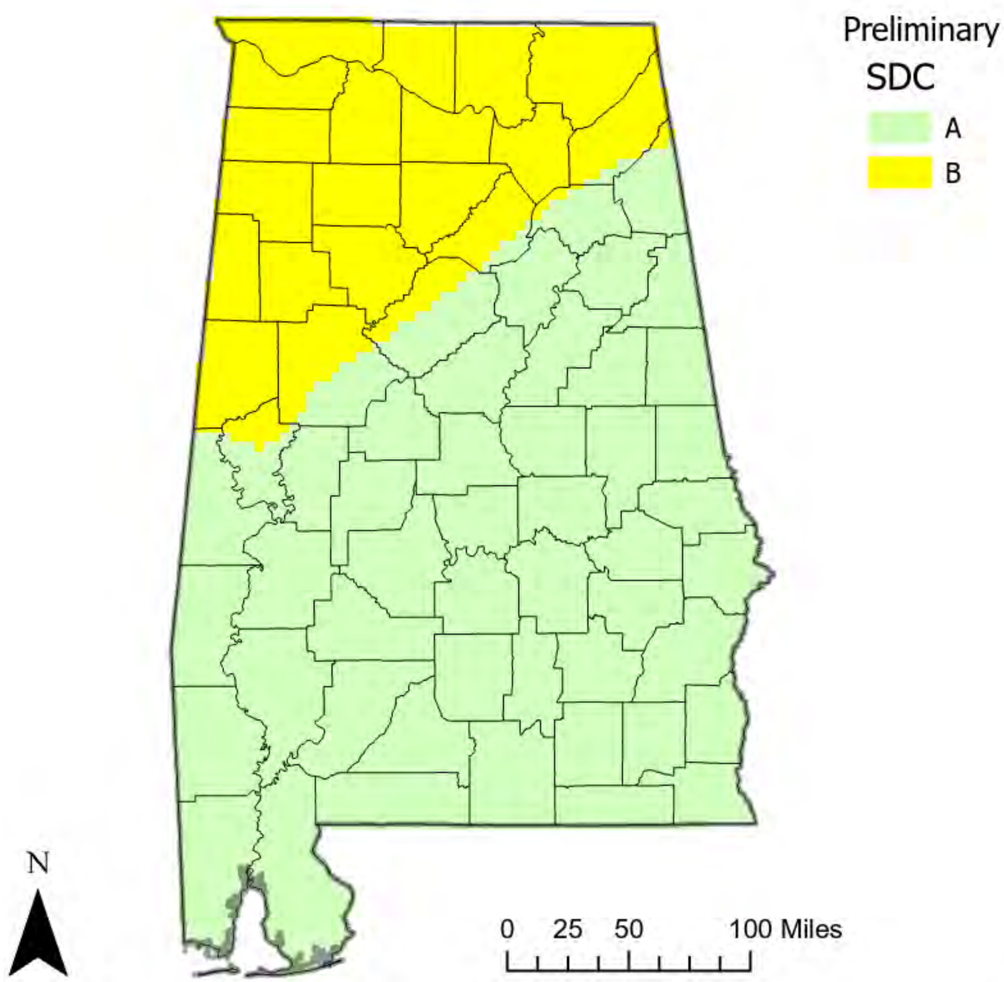

References

AASHTO Guide Specifications for LRFD Seismic Bridge Design 3rd ed.

United States Geological Survey (USGS) Earthquake Ground Motions, 2023.